CENTER FOR CONNECTED AND AUTOMATED TRANSPORTATION

Final Report #22
June 2022

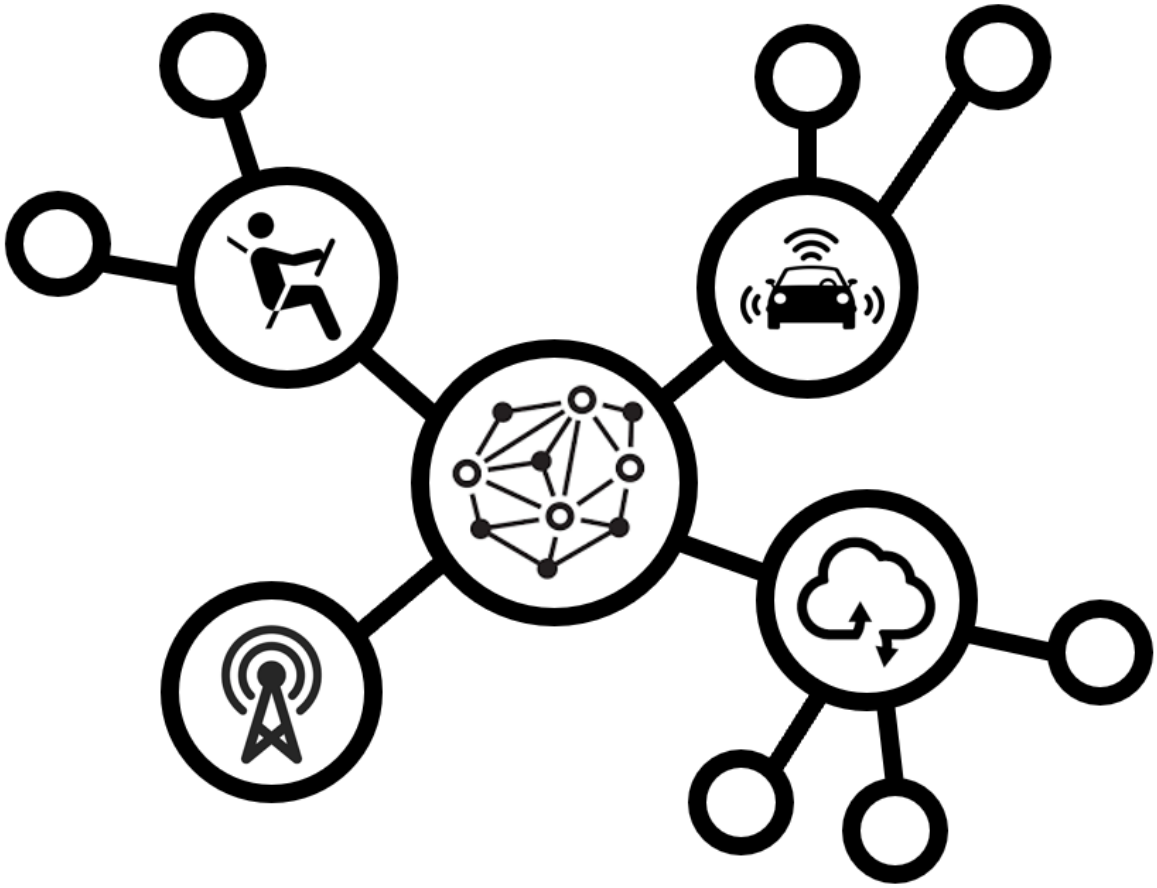

Development of Dynamic Network Traffic Simulator for Mixed Traffic Flow under Connected and Autonomous Vehicle Technologies

Chaojie Wang
Yu Wang
Srinivas Peeta

PURDUE UNIVERSITY®

CENTER FOR CONNECTED AND AUTOMATED TRANSPORTATION

Report No. 22
Report Date: June 2022
Project Start Date: 1/1/2018
Project End Date: 04/14/2021

Development of Dynamic Network Traffic Simulator for Mixed Traffic Flow under Connected and Autonomous Vehicles Technologies

Chaojie Wang
Ph.D. Candidate

Yu Wang
Postdoctoral Fellow

Srinivas Peeta
Frederick R. Dickerson Chair & Professor

Georgia Institute of Technology

CENTER FOR CONNECTED AND AUTOMATED TRANSPORTATION

ACKNOWLEDGEMENTS AND DISCLAIMER

Funding for this research was provided by the Center for Connected and Automated Transportation under Grant No. 69A3551747105 of the U.S. Department of Transportation, Office of the Assistant Secretary for Research and Technology (OST-R), University Transportation Centers Program. The contents of this report reflect the views of the authors, who are responsible for the facts and the accuracy of the information presented herein. This document is disseminated under the sponsorship of the Department of Transportation, University Transportation Centers Program, in the interest of information exchange. The U.S. Government assumes no liability for the contents or use thereof.

Suggested APA Format Citation:

Wang, C., Wang, Y., & Peeta, S. (2022). Development of Dynamic Network Traffic Simulator for Mixed Traffic Flow under Connected and Autonomous Vehicles Technologies, CCAT Report #22, Center for Connected and Automated Transportation, Purdue University, W. Lafayette, IN.

Contact Information

Samuel Labi
3000 Kent Ave, West Lafayette, IN
Phone: 7654945926
Email: labi@purdue.edu

Srinivas Peeta
3000 Kent Ave, West Lafayette, IN
Phone: 4048942300
Email: peeta@gatech.edu

CCAT
University of Michigan Transportation Research Institute
2901 Baxter Road
Ann Arbor, MI 48152

uumtri-ccat@umich.edu
(734) 763-2498
www.ccat.umtri.umich.edu

UMTRI | The University of Akron | Illinois Center for Transportation | Purdue University | Washtenaw Community College | Central State University

CENTER FOR CONNECTED AND AUTOMATED TRANSPORTATION

Technical Report Documentation Page

1. Report No. CCAT Report #22	**2. Government Accession No.** N/A	**3. Recipient's Catalog No.** N/A
4. Title and Subtitle Development of Dynamic Network Traffic Simulator for Mixed Traffic Flow under Connected and Autonomous Vehicles Technologies		**5. Report Date** June 2022 **6. Performing Organization Code** N/A
7. Author(s) Chaojie Wang, Yu Wang, Srinivas Peeta		**8. Performing Organization Report No.** N/A
9. Performing Organization Name and Address Center for Connected and Automated Transportation Purdue University, 550 Stadium Mall Drive, W. Lafayette, IN 47907; and University of Michigan Ann Arbor, 2901 Baxter Road, Ann Arbor, MI 48109		**10. Work Unit No.** **11. Contract or Grant No.** Contract No. 69A3551747105
12. Sponsoring Agency Name and Address U.S. Department of Transportation Office of the Assistant Secretary for Research and Technology 1200 New Jersey Avenue, SE, Washington, DC 20590		**13. Type of Report and Period Covered** Final Report. 8/15/2017 - 04/30/2021 **14. Sponsoring Agency Code** OST-R
15. Supplementary Notes Conducted under the U.S. DOT Office of the Assistant Secretary for Research and Technology's (OST-R) University Transportation Centers (UTC) program.		

16. Abstract

Connected and autonomous vehicles (CAVs) will generate a revolution in the transportation system, with great potential to improve traffic safety, efficiency, and environmental sustainability. However, the transition to CAVs will occur over time and, during it, CAVs will coexist with human-driven vehicles (HDVs) in the traffic flow. While several studies have examined the potential impact of CAVs on the driving environment, there is a key need for modeling approaches that can characterize network level evolution of information flow propagation and traffic flow dynamics and their impacts on stability under mixed traffic streams. There is the need for a comprehensive traffic flow modeling framework that incorporates different levels of connectivity and automation as well as different market penetration rates. This study first develops a multiclass information flow propagation model to describe and control the interactions between information flow dynamics and traffic flow dynamics. A two-layer model is developed to characterize the information flow propagation wave (IFPW) under the designed queuing strategy with solution methods under homogenous and heterogeneous conditions. This study also proposes a multiclass traffic assignment model, where HDV users and CAV users follow different route choice principles, characterized by the cross-nested logit (CNL) model and user equilibrium (UE) model, respectively. Combining two models, traffic managers can control the propagation of information of different information classes under V2V communications and design effective planning and operational strategies to leverage the advantages of CAVs and manage traffic congestion under mixed traffic flows.

17. Key Words Connected and Autonomous Vehicles, Traffic Simulator, Traffic Network, Mixed Traffic	**18. Distribution Statement** No restrictions.		
19. Security Classif. (of this report) Unclassified	**20. Security Classif. (of this page)** Unclassified	**21. No. of Pages** 106 pages	**22. Price** Leave blank – not used

Form DOT F 1700.7 (8-72) Reproduction of completed page authorized

Table of Contents

List of Figures

List of Tables

1. Introduction

Advances in connectivity and automation technologies have brought the upsurge of connected and autonomous vehicles (CAVs) research. However, during the transition from a human-driven vehicle (HDV) environment to a CAV environment, mixed traffic streams will coexist and interact, leading to network flow impacts. First, the connectivity ability of CAVs introduces information dynamics to the network, which will interact during the information propagation process. Existing information propagation models lack capabilities to control information flow, which may preclude their ability to meet application needs, including the need to propagate different information types simultaneously to different target locations within corresponding time delay bounds. Second, CAVs' differential behaviors can influence the network flow patterns. Compared to existing HDVs, CAVs offer users the potential for reduced value of time, enhanced quality of travel experience, and seamless situational awareness and connectivity. Hence, CAV users can differ in their route choice behavior compared to HDV users, leading to mixed traffic flows that can significantly deviate from the single-class HDV traffic pattern. To address the aforementioned gaps, this project investigates CAVs' impacts on flow dynamics and flow patterns in traffic networks.

Chapter 2 of this study is devoted to the analysis of the interactions between information flow dynamics and traffic flow dynamics. In doing this, we propose a queuing-based modeling approach to control the propagation of information flow of multiple classes. Two control parameters associated with a vehicle, the number of communication servers and the mean communication service rate, are leveraged to control the propagation performance of different information classes. A two-layer model is developed to characterize the information flow propagation wave (IFPW) under the designed queuing strategy. The upper layer is formulated as integro-differential equations to characterize the spatiotemporal information dissemination due to V2V communication. The lower layer characterizes the traffic flow dynamics using the Lighthill-Whitham-Richards model. The analytical solution of the asymptotic density of informed vehicles and the necessary condition for existence of the IFPW are derived for homogeneous traffic conditions. Numerical experiments provide insights on the impact of the mean communication service rate on information spread and its spatial coverage. Further, a numerical solution method is developed to solve the two-layer model, which aids in estimating the impacts of the control parameters in the queuing strategy on the IFPW speed under homogenous and heterogeneous conditions. The proposed modeling approach enables controlling the propagation of information of different information classes to meet application needs, which can assist traffic managers to design effective and efficient traffic management and control strategies under V2V communications. Chapter 2 is a collaborative work with Jian Wang, Ningbo University, China, and Lili Lu, Ningbo University, China.

Aiming to quantitively investigate the evolution of mixed traffic flows in a traffic network, Chapter 3 of this study proposes a multiclass traffic assignment model, where HDV users and CAV users follow different route choice principles, characterized by the cross-nested logit (CNL) model and user equilibrium (UE) model, respectively. The CNL model captures HDV users' uncertainty associated with limited knowledge of traffic conditions while overcoming the route overlap issue of logit-based stochastic user equilibrium. The UE model characterizes the CAV's capability for acquiring accurate information on traffic conditions. In addition, the multiclass model can capture the characteristics of mixed traffic flow such as the difference in value of time between HDVs and

CAVs and the asymmetry in their driving interactions, thereby enhancing behavioral realism in the modeling. The study develops a new solution algorithm labeled RSRS-MSRA, in which a route-swapping based strategy is embedded with a self-regulated step size choice technique, to solve the proposed model efficiently. Sensitivity analysis of the proposed model is performed to gain insights into the effects of perturbations on the mixed traffic equilibrium, which facilitates the estimation of equilibrium traffic flow and identification of critical elements under expected or unexpected events. The results of Chapter 3 can assist transportation decision-makers to design effective planning and operational strategies to leverage the advantages of CAVs and manage traffic congestion under mixed traffic flows. Chapter 3 is a collaborative work with Jian Wang, Ningbo University, China, and Xiaozheng He, Rensselaer Polytechnic Institute, United States.

2. Deployment of Roadside Units to Overcome Connectivity Gap in Transportation Networks with Mixed Traffic

2.1 Introduction

The rapid development of vehicle-to-vehicle (V2V) communication technologies has motivated their use for a wide spectrum of innovative solutions to enhance transportation safety, efficiency, and sustainability. A V2V communications-based traffic system can potentially be leveraged to enhance traffic safety by more effectively detecting emerging conflict situations, improve traffic efficiency through information-based and other control strategies, and reduce energy consumption and emissions. For example, this entails the communication of a vehicle's status to other vehicles and/or the surrounding infrastructure, and thereby the exchange of information on travel/traffic conditions. Hence, vehicles equipped with such a capability for two-way communications can potentially gain spatio-temporal knowledge on travel-related conditions, which can be used to develop vehicle-level travel strategies and/or network-level traffic management strategies. Further, V2V-based traffic systems enable decentralized information generation and dissemination. Vehicles in a V2V-based system can generate information and relay it to other vehicles through multi-hop processes. Unlike centralized information systems, a V2V-based traffic system can potentially provide timely information in emergency/disaster situations by avoiding delays associated with data collection and communication with control center.

Understanding the characteristics of spatiotemporal information flow propagation in a V2V-based traffic system is important as most applications require timely and reliable information delivery. However, modeling information flow propagation in space and time is challenging. Factors from both traffic flow domain and communications domain significantly affect the reliability of V2V communication and information propagation. The traffic flow dynamics affect occurrence of V2V communications. Communication constraints, such as communication frequency, channel capacity, and communication power, significantly affect the reliability of V2V communications.

In the literature, various models have been proposed to characterize information flow propagation in different traffic flow and communication environments. These models can be classified into microscopic and macroscopic. Microscopic models address information flow propagation by considering the spatial distribution of traffic flow. They factor the effects of the random positions of equipped vehicles in the traffic stream on information flow propagation. Simulation and analytical models have been developed to analyze V2V propagation performance in terms of the expected information propagation distance (Wang, 2007; Wang et al., 2010; Wang et al., 2011; Wang et al., 2012; Yin et al., 2013; Wang et al., 2015; Du and Dao, 2015; Du et al., 2016), under different traffic flow scenarios. However, these models oversimplify the effects of communication constraints by assuming that information can be retransmitted instantaneously. This assumption neglects the time latency of information flow propagation. Thereby, these models only characterize information dissemination in the space domain, but not in the time domain.

To address the aforementioned gaps, some recent studies have sought to characterize information flow propagation at a macroscopic level (Kim et al. 2017; Wang et al. 2018; Kim et al., 2018) by introducing the concept of information flow propagation wave (IFPW). They use the notion that when information spreads through multi-hop broadcasting communications, from a macroscopic perspective, there is a moving boundary that separates traffic flow into informed and uninformed regions, and moves towards the uninformed region like a wave. By leveraging the analogy of the IFPW with disease spread in epidemiology, analytical models are developed to characterize the IFPW. These macroscopic models relax the assumption of instantaneous information propagation and can describe the spatiotemporal spread of information in the traffic flow. In addition, these models capture the effects of V2V communication constraints realistically using a communication kernel. Further, interactions between V2V communications and traffic flow dynamics are captured by incorporating the effects of congested traffic, such as the backward propagating traffic wave, on information flow propagation.

The models discussed heretofore are descriptive, and seek to describe the spatiotemporal propagation of information to address effects of traffic flow dynamics and/or communication constraints. However, they lack a capability to control the propagation of information flow, which is necessary for traffic management applications in a V2V-based traffic system. For example, real-time traffic/routing information can help travelers choose better routes to reduce travel time. However, congestion can worsen if all travelers receive the same information and choose the same (or similar) routes in an uncoordinated V2V-based system or receive and choose the same routing suggestions. Hence, the propagation of information flow needs to be controlled so that the spatiotemporal access to information varies across vehicles in such a way as to improve system performance. Similarly, under emergency evacuation, the propagation speed of evacuation information needs to be controlled so that it can reach different areas in the affected region with different impact levels at the desired times to reduce the severe traffic congestion or gridlock that would otherwise occur due to the simultaneous evacuation of all evacuees.

Another common characteristic of previous studies is that they only consider the propagation of a specific information packet of interest or one type of information. In practical applications, information can belong to different classes (e.g., safety information, routing information, work zone information). Hence, a V2V-based system may need to propagate information from different information classes simultaneously. However, the application needs of information from different information classes can be different, in terms of three performance measures: (i) information spread, defined here as the proportion of vehicles informed with a specific information packet, (ii) bounds on time delays for this information to reach specific locations, and (iii) spatial coverage, defined here as the distance this information can be propagated from its point of origin. For example, urgent traffic accident information (e.g., road is blocked by an accident) needs to be delivered to all vehicles in the impacted area with low latency. By comparison, routing information needs to reach only a certain proportion of vehicles to avoid possible congestion arising from the provision of information on the suggested route. Work zone information may need to be propagated in a small area in the vicinity of where these information are generated.

Similar to previous studies (e.g., Wang, 2007; Wang et al., 2010; Wang et al., 2011; Wang et al., 2012; Yin et al., 2013; Wang et al., 2015; Du and Dao, 2015; Du et al., 2016; Kim et al., 2017; Kim et al., 2018; Wang et al., 2018), this study seeks to capture the effects of traffic flow dynamics on information flow propagation, but not vice versa. Further, this study only considers event-driven information triggered by a specific event, such as accident or congestion which requires multi-hop dissemination (Wang et al., 2018). To meet application needs related to information spread, time delay bounds, and spatial coverage, it designs a queuing-based modeling approach to control the propagation of information of different information classes. An information class is defined as a type of information which has similar application needs in terms of the three propagation performance measures. To enable control for multiclass information flow propagation, this study assumes that the size of each information packet is the same and the channel capacity is shared equally with all equipped vehicles within communication range of that vehicle (Wang et al., 2018). Under this assumption, an equipped vehicle can send data containing multiple information packets during one transmission, whose number is determined by the size of one information packet, channel capacity, communication frequency, and the number of equipped vehicles within communication range of that vehicle. This implies that an equipped vehicle can serve (send) multiple information packets simultaneously. It should be noted that the word "multiclass" only refers to different types of information, and not classes of vehicles, while the queuing system discussed in this study only applies to information packets, and not vehicles. To better characterize the information service (sending) process in our queuing-based approach, we denote a "virtual communication server" (hereafter, referred to as "communication server") as the storage amount in the transmitted data that is equal to the size of an information packet. A communication server can serve at most one information packet at a time. The total number of communication servers is equal to the maximum number of information packets that an equipped vehicle can send simultaneously during one transmission, which is labeled the transmission capacity. We denote communication service time as the time duration an information packet is in the communication server. During the communication service time, the information packet will be repeatedly sent by the equipped vehicle where the number of transmissions depends on the communication frequency which is the number of data transmissions per unit time enabled by the V2V device characteristics of the vehicle. We denote the mean communication service rate for a server as the inverse of the mean communication service time of all information packets served by that server.

To enable control for multiclass information flow propagation, for the first time in the literature, a queuing strategy is developed for each V2V-equipped vehicle to propagate the information packets of different information classes that it receives or generates. We assume information packets in different information classes will form different queues. Thereby, when an information packet is received by an equipped vehicle, it will be forwarded to the queue for the information class it belongs to. After being in the queue, the information packet will enter a communication server for this information class to be disseminated. It will be deleted from the server after its assigned communication service time is reached. Based on this conceptual queuing strategy, information propagation control is enabled by assigning different number of communication servers and mean communication service rates to different information classes to send the information. It

should be noted that the mean communication service rate for an information class determines the mean communication service time of each information packet in the information class, which impacts the number of transmissions of each information packet in this class. Due to existence of communication failure, an information packet cannot be guaranteed to be received by other vehicles if it is just sent once by an equipped vehicle. The queuing strategy allows an equipped vehicle to control the number of transmissions of an information packet by leveraging the mean communication service rate so as to control the number of vehicles within communication range of this vehicle that can receive the information packet. Thereby, while the mean communication service rate does not impact the success rate of one V2V communication, it significantly impacts the total success rate of V2V communications by allowing an equipped vehicle to transmit information multiple times. Also, the number of communication servers assigned to an information class significantly impacts the mean waiting time in the queue for information packets in that class, which impacts the information flow propagation speed. Thereby, two control parameters, the number of assigned communication servers and mean communication service rate, can be determined for each information class to achieve the desired propagation performance related to information spread, time delay bounds, and spatial coverage.

This study conceptually extends the macroscopic models developed by Kim et al. (2017) and Wang et al. (2018), and proposes a new two-layer analytical modeling approach to characterize the IFPW under the proposed queuing strategy. An integro-differential equation (IDE) model is derived to characterize the spatiotemporal information propagation flow under the designed queuing strategy in the upper layer. The lower layer adopts the Lighthill-Whitham-Richards (LWR) model (Lighthill and Whitham, 1955; Richards, 1956) to characterize the traffic flow dynamics. The two-layer model enables investigation of the following three questions. First, what is the density of equipped vehicles that can receive a specific information packet under given values of the two control parameters? This question seeks to provide insights on controlling information spread. Second, how do the two control parameters in the queuing system impact the propagation speeds of specific information packets of interest belonging to different information classes? Addressing this question is useful for controlling the time delay of information packets of different information classes in reaching desired locations. Third, what are the conditions that can ensure the specific information packet can form a wave to be propagated over the traffic stream, and how the two control parameters impact the propagation distance of an information packet? This question addresses the necessary conditions for the formation of an IFPW which is related to the spatial coverage of information.

The contributions of this study are fivefold. First, unlike previous studies that describe how information propagates in space and time, this study newly proposes to control the spatiotemporal propagation of information to generate prescriptive solutions that can be leveraged for performance enhancement and management of V2V-based traffic systems. Second, the study addresses, for the first time, the more general case of multiple information classes that are inherent to traffic systems. To do so, it develops a queuing-based modeling approach for an equipped vehicle to propagate different types of information simultaneously. Thereby, it enables effective and efficient control for

multiclass information flow propagation under different traffic and communication environments by determining the values of the two control parameters in the queuing strategy. Third, the study develops a new nonlinear IDE system to characterize the information dissemination wave. The necessary conditions for the existence of IFPW and the analytical solution for the asymptotic density of informed vehicle are derived under homogenous conditions. To the best of our knowledge, the solution of the IDE system analogy to the proposed IDE system has not been studied before, even in the epidemiology literature. These analytical expositions quantify the impacts of the two control parameters on the density of informed vehicles and the spatial coverage. Fourth, the study designs numerical solutions to solve the two-layer model under homogeneous as well as heterogeneous conditions while considering multiple performance measures. They provide valuable insights for controlling multiclass information flow propagation to achieve the desired performance in terms of information spread, the time delay to reach the target locations, and spatial coverage under heterogeneous conditions. Fifth, the study calibrates and validates the proposed model using NS-3 simulations. NS-3 is a discrete network simulator that implements the IEEE 802.11p protocol (the standard protocol for V2V and V2I communications) (Talebpour et al. 2016). It can simulate real-world communication environments and test a spectrum of communication protocols efficiently. The NS-3 simulation shows that under homogeneous traffic flow conditions, the analytical and numerical solutions of information flow propagation performance (e.g., information spread, IFPW speed) are very close to those of the simulated results. This indicates that the proposed method can be applied to control the multiclass information propagation effectively.

The remainder of the paper is organized as follows. The next section discusses the designed queuing strategy and the framework of the proposed model to characterize the IFPW. Section 2.3 formulates a two-layer model to characterize the IFPW in space and time under the proposed queuing strategy. In Section 2.4, the analytical solution for the asymptotic density of informed vehicles and the condition for existence of IFPW under homogeneous traffic conditions are discussed. In addition, the numerical solution method is presented to solve the proposed two-layer model for heterogeneous conditions. Results from numerical experiments are discussed in Section 2.5, to demonstrate the effectiveness of the proposed model to control the propagation performance of different information classes. Section 2.6 provides some concluding comments.

2.2 Preliminaries

Consider a highway with a traffic flow stream consisting of V2V-equipped and V2V-unequipped vehicles. Information is generated and broadcasted to other equipped vehicles through multi-hop V2V communications. Each equipped vehicle receives information from other equipped vehicles and broadcasts such information and the information it generates to all other equipped vehicles within communication range. Let information packets relayed in the traffic flow be divided into s classes, each of which has different requirements in terms of information spread, time delay bounds and spatial coverage. Let $\mathcal{L} = \{1,2,\cdots s\}$ denotes the set of information classes. When an equipped vehicle receives multiple packets, it filters the information packets to identify those that have not been

received before. It then moves such unduplicated information packets (labeled effective information packets) into the queues for the corresponding information classes to wait to be propagated according to the information class they belong to. The effective information arrival rate is affected by unsuccessful V2V communication and removal of duplicated information packets. Because such events are random and independent, following Wang et al. (2018) and Zhang et al. (2016), this study assumes that the arrival of effective information packets to different information classes follows a Poisson process. Let $\lambda_1, \lambda_2 \cdots, \lambda_s$ be the arrival rate of information packets for information classes $1,2 \cdots, s$, respectively.

Suppose that the size of all information packets disseminated over the traffic flow is identical. Each information packet can contain different event-driven information. Suppose channel capacity is shared equally with all equipped vehicles within communication range. This assumption trades off the need to enable the dissemination of every information packet as fast as possible against the congestion effects that accrue because the aggregated data transmitted by all vehicles within communication range of an equipped vehicle in unit time exceeds channel capacity. It is also used in Wang et al. (2018). Let N denote the transmission capacity, which describes the number of information packets that can be delivered by an equipped vehicle through one V2V communication. In this study, we assume the transmission capacity for all equipped vehicles to be the same. It should be noted that to prevent the effects of information congestion, N has an upper bound (denoted as N_{max}) determined by the size of an information packet, the density of the traffic flow, the communication frequency and the channel capacity (Wang et al., 2018).

To control propagation performance for each information class, a queuing strategy for relaying information of different information classes is designed in this study, as shown in Figure 1. Note that an equipped vehicle can transmit N information packets during one communication. To better illustrate the queuing strategy, we assume an equipped vehicle has N communication servers each of which can serve one information packet. A communication server represents the storage amount in the transmitted data that is equal to the size of one information packet (see Figure 1). The number of the communication servers assigned to a particular information class determines the maximum number of information packets in this information class that can be transmitted simultaneously by an equipped vehicle. Let n_j be the number of communication servers assigned to information class j, $j \in \mathcal{L}$. To control multiclass information flow propagation, information packets in different classes will form different queues (see Figure 1). If one communication server for information class j is empty, the first information packet in the queue for information class j will enter into the server to be sent out. Let u_j be the mean communication service rate (packets/second) for information packets in information class j. The inverse of u_j (i.e., $1/u_j$) is the mean communication service time (i.e., transmission duration) for an information packet in information class j. The information packet in the communication server will be transmitted repetitively until the communication service time is reached. Thereby, the communication service time significantly impact the number of vehicles that can receive the specific information of interest of information class j.

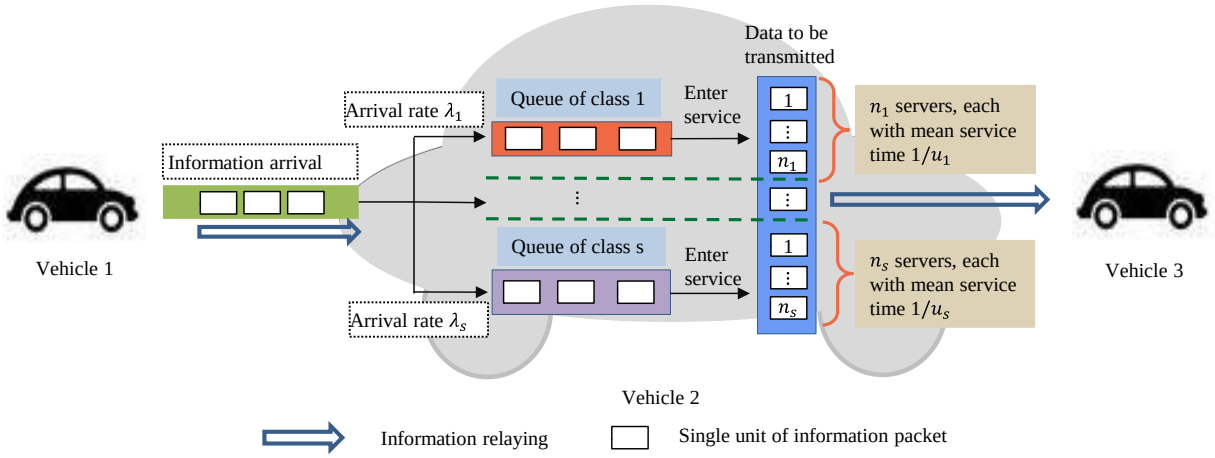

Figure 2.1: Queuing strategy for relaying information of different classes

To facilitate modeling, we assume that the communication service time of each information packet in an arbitrary class j, $j \in \mathcal{L}$ follows an exponential distribution with mean $1/u_j$. The communication service time can be generated randomly in advance according to the exponential distribution with mean $1/u_j$. An information packet is removed from the system if its assigned communication service time is reached. Note that for an arbitrary information class j, the arrival of information packets follows a Poisson process with parameter λ_j and the corresponding communication service time follows an exponential distribution with mean $1/u_j$. Thereby, propagation of information packets in information class j follows a $M/M/n_j$ queuing process.

Note that the mean communication service rate for information packets in an arbitrary information class j (i.e., u_j) impacts the number of vehicles that can receive information packets from this information class. Further, according to the queueing theory, the mean communication service rate (u_j) and the number of assigned communication servers (i.e., n_j) for information class j determine the mean waiting time of an information packet in the queue. Thereby, the propagation performance of an information packet of information class j in terms of information spread, time delay bounds, and spatial coverage can be controlled by assigning various values to n_j and u_j. It should be noted that the propagation performance of information of different information classes is constrained by the total number of communication servers in an equipped vehicle.

Under the designed queuing strategy, equipped vehicles are divided into four vehicle classes, the susceptible vehicles (labeled S), the information-holding vehicles (labeled H), the information-relay vehicles (labeled R) and the information-excluded vehicles (labeled E). Susceptible vehicles are equipped vehicles that have not received the specific information packet of interest. They become information-holding vehicles if they receive that information packet and are holding it in the queue for transmittal. The information-holding vehicles become information-relaying vehicles if that information packet enters a communication server to be disseminated to the other vehicles. Once the communication service time is reached for that information packet, it will be removed from the vehicle.

The information-relaying vehicle then becomes an information-excluded vehicle. It is worth noting that the susceptible vehicles can become information-relaying vehicles directly if the specific information packet of interest enters into a communication server without waiting in a queue; that is, when this information packet is received/generated, there is no queue for the corresponding information class.

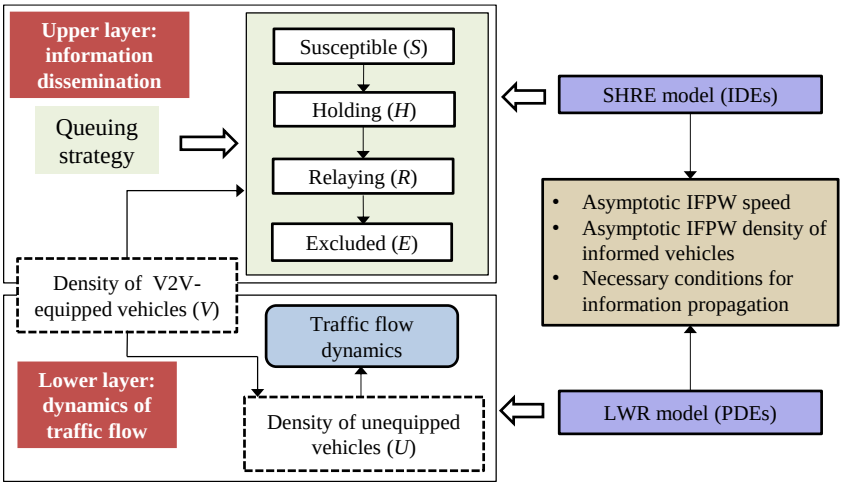

Figure 2.2: Queuing strategy for relaying information of different classes

Similar to Wang et al. (2018), the IFPW is defined as the moving boundary which separates traffic flow into informed and completely uninformed regions. It consists of two waves: the information dissemination wave in the information flow domain and the traffic flow propagation wave in the traffic flow domain. A two-layer model is developed in this study to model the IFPW. The modeling framework is shown in Figure 2. In the upper-layer, integro-differential equations (IDEs) will be derived to characterize the information dissemination waves. This layer describes how vehicle densities by vehicle class will change instantaneously through V2V communications under the designed queuing strategy. The lower layer describes the traffic flow dynamics. In this study, the LWR model will be used to characterize traffic flow dynamics. Based on the two-layer model, the asymptotic IFPW speed, the asymptotic density of informed vehicles and the conditions for existence of IFPW will be investigated in this study.

It should be noted that while the starting point for the modeling framework in this study is similar to those of Kim et al. (2017) and Wang et al. (2018), it differs from them fundamentally in four key aspects. First, while Kim et al. (2017) and Wang et al. (2018) only descriptively quantify the impacts of traffic flow and communication constraints on information flow propagation, this study seeks to control information flow propagation to ensure that performance in terms of information spread, time delay bounds and spatial converge can meet the application needs of information under different traffic flow and communication environments. Second, this study proposes a queuing strategy for multiclass information flow propagation that enables distribution of limited communication resources in an equipped vehicle (i.e., number of communication servers, and mean communication service time) for sending information of different classes. This

improves information propagation efficiency by coordinating the communication resources with dynamic information arrival rates. However, the communication service time, which is critical for V2V communication reliability, is not controlled in Kim et al. (2017) and Wang et al. (2018). For example, the communication service time may be too short when information arrival rate is high, precluding reliable propagation of that information. Third, this study develops a new nonlinear IDE system to characterize the information flow dissemination wave in the upper layer, and analytically derives its solution. This IDE system has not been studied before even in epidemiology, unlike the IDE systems developed in Kim et al. (2017) and Wang et al. (2018) which have been extensively studied in epidemiology. Fourth, unlike those studies, this study verifies the success rate of V2V communications and calibrates parameters using NS-3 simulations. This enhances the applicability of the proposed model by better capturing the impacts of traffic flow and communication constraints on V2V communications.

2.3 Modeling the multiclass information flow propagation wave

2.3.1 Modeling the information flow dissemination wave in the upper layer

Assume the specific information packet of interest belongs to an arbitrary information class j, $j \in \mathcal{L}$. This section seeks to model the information dissemination wave in the upper layer under the designed queuing strategy. It describes the instantaneous change in the density (veh/km) of equipped vehicles by vehicle class (i.e., S, H, R, E for information packets in class j) due to V2V communications. The impacts of communication constraints (communication power, communication frequency, signal interference, etc.) on the success of V2V communications is explicitly factored in this model.

Let t be the current time. Divide the time horizon of interest uniformly into consecutive time windows of length w each. Denote $S_j(x,t)$ and $I_j(x,t)$ as the densities of the susceptible vehicles and the vehicles informed with the specific information packet of interest in information class j, respectively, at time t and location x. Note that the informed vehicles consist of vehicles from classes H, R and E which have received this information packet. Let $\Delta S_j(x,t) = S_j(x,t) - S_j(x,t-w)$ be the density of vehicles informed with the specific information packet of interest during time $[t-w, t]$. Denote $\Delta I_j(y, t-w) = I_j(x,t) - I_j(x,t-w)$ as the density change of informed vehicles at location x during time interval $[t-w, t]$. Note $\Delta I_j(y, t-w) = -\Delta S_j(x, t-w)$ as an equipped vehicle is either susceptible or informed. Let the current time be $t = m \cdot w$; m is a positive integer. Conceptually adapting from epidemiology and modifying, $\Delta S_j(x,t)$ is formulated as:

$$\Delta S_j(x,t) = -S_j(x,t-w) \cdot \int_{\Omega} K(x,y) \cdot w\beta \cdot R_j(y,t)dy \tag{2.1}$$

where Ω denotes the domain of space, β is communication frequency, and $w\beta$ denotes the expected number of transmissions occurring in time length w. Also, $R_j(y,t)$ is the density of vehicles relaying the specific information packet of interest in information class j at time t and location y. Function $K(x,y)$ is a communication kernel which represents the probability that a susceptible vehicle at location y can successfully receive the specific information packet sent from a vehicle at location x under a given communication environment (communication frequency, channel capacity, communication power, etc.) and traffic flow environment (traffic density, etc.). It characterizes the reliability of V2V communication realistically by capturing the impact of factors in both the communication and traffic flow domains. In the study experiments in Section 2.5, function $K(x,y)$ is calibrated using NS-3 simulation. $\int_\Omega K(x,y)\cdot w\beta \cdot R_j(y,t)dy$ denotes the probability that a susceptible vehicle at location x receives the specific information packet of information class j sent by an informed vehicle over the space domain Ω.

Suppose the mean arrival rate of information packets in information class j, $j \in \mathcal{L}$ is λ_j packets/second. Let n_j and u_j be the number of communication servers and the mean communication service rate (packets/second) assigned to information class j, respectively. n_j and u_j are controllable parameters which will be leveraged to control the propagation of the specific information packet of interest of information class j. To ensure the information packets in information class j can be propagated by an equipped vehicle, n_j and u_j are selected such that $\lambda_j < n_j u_j$, $\forall j \in \mathcal{L}$.

As discussed earlier, under the designed queuing strategy, the arrival and service process of information packets in information class j follow $M/M/n_j$ queue process. Thereby, at current time t, the vehicles that are relaying the specific information packet of interest of information class j consist of two groups: (2.1) the vehicles relaying the specific information packet without the information-holding process (i.e., queuing process). This implies when these vehicles receive the specific information packet, there is no queue for information class j in these vehicles. Thereby, the specific information packet of interest can enter into the communication server to be disseminated out directly; and (2.2) the vehicles relaying the specific information packet with an information-holding process (queue process), i.e., the specific information packet of interest experiences a queuing process before entering into the communication server.

Let T_j^q be the waiting time for the specific information packet of interest of information class j, and $W_j^q(v_j) = \Pr\{T_j^q \le v\}$ be the probability that the waiting time of this information packet in the queue is less than v. According to Gross et al. (2008, page 71), we have

$$W_j^q(v) = \Pr\{T_j^q \le v\} = 1 - \frac{{r_j}^{n_j} P_j^0}{n_j!\,(1-\rho_j)}\, e^{-(n_j u_j - \lambda_j)v_j} \tag{2.2}$$

where $r_j = \lambda_j / u_j$; $\rho_j = \lambda_j / (n_j u_j)$; and P_j^0 is the probability that there is no information packet of information class j in the system, formulated as

$$P_j^0 = \left(\frac{{r_j}^{n_j}}{n_j!\,(1-\rho_j)} + \sum_{l=0}^{n_j-1} \frac{{r_j}^{l}}{l!} \right)^{-1} \tag{2.3}$$

According to Eq. (2.2),

$$W_j^q(0) = \Pr\{T_j^q \le 0\} = \Pr\{T_j^q = 0\} = 1 - \frac{{r_j}^{n_j} P_j^0}{n_j!\,(1-\rho_j)} \tag{2.4}$$

where W_j^0 is the probability that the specific information packet is received by a vehicle at a time instant when there is no queue for information class j. Let

$$\xi_j = \frac{{r_j}^{n_j} P_j^0}{n_j!\,(1-\rho_j)} \tag{2.5}$$

Then

$$W_j^q(0) = 1 - \xi_j \tag{2.6}$$

From Eq. (2.2), we have

$$\Pr\{T_j^q > v\} = 1 - W_j^q(v) = \frac{{r_j}^{n_j} P_0}{n_j!\,(1-\rho_j)}\, e^{-(n_j u_j - \lambda_j) v_j} \tag{2.7}$$

Let T_j^s be the service time of the specific information packet of interest in the communication server, and $\Pr\{T_j^q \le \theta\}$ be the probability that the communication service time is less than θ. Recall the communication service time follows exponential distribution with mean $1/u_j$, then

$$\Pr\{T_j^q \le \theta\} = 1 - e^{-u_j \theta} \tag{2.8}$$

This implies

$$\Pr\{T_j^q > \theta\} = e^{-u_j \theta} \tag{2.9}$$

$R_j(y,t)$ can then be formulated as

$$R_j(y,t) = A_j(y,t) + B_j(y,t) \tag{2.10}$$

where

$$A_j(y,t) = W_j^q(0) \cdot \sum_{i=1}^{t/w} \Delta I_j(y, t-iw) \cdot \Pr\{T_j^s > iw\}$$

$$= (1-\xi_j) \cdot \sum_{i=1}^{t/w} \Delta I_j(y, t-iw) \cdot e^{-u_j \cdot iw}$$

$$B_j(y,t) = \sum_{i=1}^{t/w} \int_0^{iw} \Delta I_j(y, t-iw) \cdot \frac{\partial\left(\Pr\{T_j^q > v\}\right)}{\partial v} \cdot \Pr\{T_j^s > iw - v\}\, dv$$

$$= \sum_{i=1}^{t/w} \int_0^{iw} \Delta I_j(y, t-iw) \cdot (n_j u_j - \lambda_j) \cdot \xi_j \cdot e^{-(n_j u_j - \lambda_j)v} \cdot e^{-u_j \cdot (iw - v)}\, dv$$

where $A_j(y,t)$ is the accumulated density of vehicles relaying the specific information packet of interest of information class j without queuing process at location y and current time t. $\Delta I_j(y, t-iw) \cdot \Pr\{T_j^s > iw\}$ is the density of vehicles informed at time $t-iw$ and relaying the specific information packet at location y and current time t. $B_j(y,t)$ is the accumulated density of vehicles relaying the specific information packet after queuing process at location y and current time t. The term $\int_0^{iw} \Delta I_j(y, t-iw) \cdot \frac{\partial\left(\Pr\{T_j^q > v\}\right)}{\partial v} \cdot \Pr\{T_j^s > iw - v_j\}\, dv$ denotes the density of vehicles at location y that become informed iw time units ago and are propagating the specific information at current time t after experiencing the queuing process.

To derive the continuous model, let $w \to 0$; dividing both sides of Eq. (2.1) by w, we have

$$\lim_{w\to 0} \frac{\Delta S_j(x,t)}{w} = \frac{\partial S_j(x,t)}{\partial t} = \lim_{w\to 0} -\beta S_j(x, t-w) \cdot \int_\Omega K(x,y) \cdot w \frac{(A_j(y,t) + B_j(y,t))}{w} dy \tag{2.11}$$

Note

$$\Delta I_j(y, t-iw) = I_j(y, t-(i-1)w) - I_j(y, t-iw) \approx \frac{\partial I_j(y, t-iw)}{\partial t} w. \tag{2.12}$$

Then

$$\lim_{w\to 0} -\beta S_j(x,t-w)\cdot\int_{\Omega} K(x,y)\cdot w\cdot A_j(y,t)dy$$

$$= \lim_{w\to 0} -\beta(1-\xi_j)S_j(x,t-w) \cdot\sum_{i=1}^{t/w}\int_{\Omega}\frac{\partial I_j(y,t-iw)}{\partial t}\cdot K(x,y)\cdot w\cdot e^{-u_j\cdot iw}dy. \tag{2.13a}$$

and

$$\lim_{w\to 0} -\beta S_j(x,t-w)\cdot\int_{\Omega} K(x,y)\cdot w\cdot B_j(y,t)dy$$

$$= \lim_{w\to 0} -\beta S_j(x,t-w)\cdot\int_{\Omega} K(x,y)\cdot f_j(y,iw)dy \tag{2.13b}$$

where

$$f_j(y,iw)=\sum_{i=1}^{t/w}\int_0^{iw}\frac{\partial I_j(y,t-iw)}{\partial t} w\cdot(n_j u_j-\lambda_j)\xi_j \cdot e^{-(n_j u_j-\lambda_j)v}\cdot e^{-u_j\cdot(iw-v)}\,dv \tag{2.13c}$$

Note the terms $\left(\partial I_j(y,t-\tau)/\partial t\right)K(x,y)e^{-\lambda\tau}$ and $\int_0^{\tau}\frac{\partial I(y,t-\tau)}{\partial t}\cdot(n_j u_j-\lambda_j)\cdot\xi_j\cdot e^{-(n_j u_j-\lambda_j)v}\cdot e^{-u_j\cdot(\tau-v)}dv$ are continuous and bounded in the time domain. Both of them are Riemann integrable. Thereby, Eq. (2.13a) and Eq. (2.13b) can be written, respectively, as:

$$\lim_{w\to 0} -\beta\left(1-\xi_j\right)S_j(x,t-w) \cdot\sum_{i=1}^{t/w}\int_{\Omega}\frac{\partial I_j(y,t-iw)}{\partial t}\cdot K(x,y)\cdot w\cdot e^{-u_j\cdot iw}dy$$

$$= -\beta\cdot\left(1-\xi_j\right)\cdot S_j(x,t) \cdot\int_{\Omega}\int_0^{t}\frac{\partial I_j(y,t-\tau)}{\partial t}\cdot K(x,y)\cdot e^{-u_j\tau}d\tau\cdot dy \tag{2.14a}$$

$$\lim_{w\to 0} -\beta S_j(x,t-w)\cdot\int_{\Omega} K(x,y)\cdot f_j(y,iw)dy$$

(2.14b)

$$= \beta S_j(x,t) \cdot \int_\Omega \int_0^t \int_0^\tau \frac{\partial I_j(y,t-\tau)}{\partial t} K(x,y)(n_j u_j - \lambda_j)\xi_j \cdot e^{-(n_j u_j - \lambda_j)v} e^{-u_j \cdot (\tau - v)} dv \cdot d\tau \cdot dy$$

Note $\partial I_j(x,t-\tau)/\partial t = -\partial S_j(x,t-\tau)/\partial t$; substituting Eq. (2.14) into Eq. (2.11), we have

$$\frac{\partial S_j(x,t)}{\partial t} = \beta \cdot (1-\xi_j) \cdot S_j(x,t) \cdot \int_\Omega \int_0^t \frac{\partial S_j(y,t-\tau)}{\partial t} \cdot K(x,y) \cdot e^{-u_j \tau} d\tau dy + \beta S_j(x,t) \cdot \int_\Omega \int_0^t \int_0^\tau \frac{\partial I_j(y,t-\tau)}{\partial t} K(x,y)(n_j u_j - \lambda_j)\xi_j \cdot e^{-(n_j u_j - \lambda_j)v} e^{-u_j \cdot (\tau - v)} dv \cdot d\tau \cdot dy \quad (2.15)$$

According to Eq. (2.10) and Eq. (2.12), in continuous space, the density of information-relaying vehicles can be written as

$$R_j(y,t) = -(1-\xi_j) \int_0^t \frac{\partial S_j(y,t-\tau)}{\partial t} \cdot e^{-u_j \tau} d\tau - \int_0^t \int_0^\tau \frac{\partial S_j(y,t-\tau)}{\partial t} \cdot (n_j u_j - \lambda_j)\xi_j \cdot e^{-(n_j u_j - \lambda_j)v} \cdot e^{-u_j \cdot (\tau - v)} dv \cdot d\tau \quad (2.16)$$

The terms $-(1-\xi_j)\int_0^t \frac{\partial S_j(y,t-\tau)}{\partial t} \cdot e^{-u_j \tau} d\tau dy$ and $-\int_0^t \int_0^\tau \frac{\partial S_j(y,t-\tau)}{\partial t} \cdot (n_j u_j - \lambda_j)\xi_j \cdot e^{-(n_j u_j - \lambda_j)v} \cdot e^{-u_j \cdot (\tau - v)} dv \cdot d\tau$ denote the density of information-relaying vehicles without queuing process and with queuing process, respectively. Let $\eta = t - \tau$, then

$$R_j(y,t) = f_{j,1}(y,t) + f_{j,2}(y,t) \quad (2.17a)$$

where

$$f_{j,1}(y,t) = -(1-\xi_j) \int_0^t \frac{\partial S_j(y,\eta)}{\partial \eta} \cdot e^{-u_j (t-\eta)} d\eta \quad (2.17b)$$

$$f_{j,2}(y,t) = -\int_0^t \int_0^{t-\eta} \frac{\partial S_j(y,\eta)}{\partial \eta} \cdot (n_j u_j - \lambda_j)\xi_j \cdot e^{-(n_j u_j - \lambda_j)v} \cdot e^{-u_j \cdot (t-\eta-v)} dv \cdot d\eta \quad (2.17c)$$

The derivative of $R_j(y,t)$ with respect to t is

$$\frac{\partial R_j(y,t)}{\partial t} = \frac{\partial f_{j,1}(y,t)}{\partial t} + \frac{\partial f_{j,2}(y,t)}{\partial t} \tag{2.18a}$$

where

$$\begin{aligned}\frac{\partial f_{j,1}(y,t)}{\partial t} &= -(1-\xi_j)\frac{\partial S_j(y,t)}{\partial t} \\ &\quad + u_j(1-\xi_j)\int_0^t \frac{\partial S_j(y,\eta)}{\partial \eta}\cdot e^{-u_j(t-\eta)}d\eta \\ &= -(1-\xi_j)\frac{\partial S_j(y,\eta)}{\partial t} - u_j f_{j,1}(y,t) - u_j R_j(y,t)\end{aligned} \tag{2.18b}$$

$$\begin{aligned}\frac{\partial f_{j,2}(y,t)}{\partial t} &= -\int_0^t \frac{\partial S_j(y,\eta)}{\partial \eta}\cdot(n_j u_j - \lambda_j)\xi_j e^{-(n_j u_j-\lambda_j)(t-\eta)}d\eta \\ &\quad + u_j f_{j,1}(y,t)\end{aligned} \tag{2.18c}$$

Thereby,

$$\begin{aligned}\frac{\partial R_j(y,t)}{\partial t} &= -(1-\xi_j)\frac{\partial S_j(y,\eta)}{\partial t} \\ &\quad - \int_0^t \frac{\partial S_j(y,\eta)}{\partial \eta}\cdot(n_j u_j - \lambda_j)\xi_j \cdot e^{-(n_j u_j-\lambda_j)(t-\eta)}d\eta \\ &\quad - u_j R_j(y,t)\end{aligned} \tag{2.19}$$

Let $H_j(y,t) = -\int_0^t \frac{\partial S_j(y,\eta)}{\partial \eta}\cdot \xi_j \cdot e^{-(n_j u_j-\lambda_j)(t-\eta)}d\eta$. According to Eq. (2.7), the probability that an information packet in information class j is received by a vehicle at time η and is waiting in the queue at current time t $(t > \eta)$ is $\xi_j \cdot e^{-(n_j u_j-\lambda_j)(t-\eta)}$. This implies that $H_j(y,t)$ is the density of information-holding vehicles at location y and time t. Differentiating $H_j(y,t)$ with respect to t, we have

$$\frac{\partial H_j(y,t)}{\partial t} = -\xi_j \frac{\partial S_j(y,t)}{\partial t} - (n_j u_j - \lambda_j)H_j(y,t) \tag{2.20}$$

Let $E_j(x,t)$ denote the density of information-excluded vehicles at location x at time t. As informed vehicles consist of the information-holding, information-relaying and information-excluded vehicles, $I_j(x,t) = H_j(x,t) + R_j(x,t) + E_j(x,t)$. Thereby, we have

$$\frac{\partial H_j(x,t)}{\partial t} + \frac{\partial R_j(x,t)}{\partial t} + \frac{\partial E_j(x,t)}{\partial t} = \frac{\partial I_j(x,t)}{\partial t} = -\frac{\partial S_j(x,t)}{\partial t}. \tag{2.21}$$

Substituting Eq. (2.19) and Eq. (2.20) into Eq. (2.21), yields

$$\frac{\partial E_j(x,t)}{\partial t} = u_j R_j(x,t) \tag{2.22}$$

According to the above analysis, we have the following IDE system:

$$\frac{\partial S_j(x,t)}{\partial t} = -\beta S_j(x,t) \int_\Omega R_j(y,t) \cdot K(x,y)dy \tag{2.23a}$$

$$\frac{\partial H_j(x,t)}{\partial t} = \beta \cdot \xi_j \cdot S_j(x,t) \int_\Omega R_j(y,t) \cdot K(x,y)dy - \left(n_j u_j - \lambda_j\right) \cdot H_j(x,t) \tag{2.23b}$$

$$\frac{\partial R_j(x,t)}{\partial t} = \left(1-\xi_j\right) \cdot \beta S_j(x,t) \int_\Omega R_j(y,t) \cdot K(x,y)dy + \left(n_j u_j - \lambda_j\right) \cdot H_j(y,t) - u_j \cdot R_j(x,t) \tag{2.23c}$$

$$\frac{\partial E_j(x,t)}{\partial t} = u_j \cdot R_j(x,t) \tag{2.23d}$$

For simplicity, we will label the IDE system (2.23) as the susceptible-holding-relaying-excluded (SHRE) model. It describes the instantaneous change in densities of vehicles by vehicle class for dissemination of an information packet in information class j. Eq. (2.23) shows that susceptible vehicles become informed vehicles at a rate proportional to the densities of susceptible vehicles and information-relaying vehicles (see Eq. (2.23a)). According to Eq. (2.23b), information-holding vehicles become information-relaying vehicles at a rate inversely proportional to $\left(n_j u_j - \lambda_j\right)$. Thereby, if the assigned number of communication servers (n_j) and the mean communication service rate (u_j) are increased, information-holding vehicles would become information-relaying vehicles faster. This implies that the specific information packet of interest experiences less waiting time in the queue. Hence, it can be propagated in the traffic stream at a higher speed. Eq. (2.23c) indicates that the density change of information-relaying vehicle increases monotonically with respect to number of communication servers (n_j) and the mean communication service rate (u_j). According to Eq. (2.23d), the density change of information-excluded vehicles is proportional to u_j. Note $1/u_j$ denotes the mean communication service time of information packets of information class j. If u_j is smaller, the information packet would stay in the commination server for a longer time, implying that it can be disseminated more times using the repetitive broadcast process. This will impact both the IFPW speed and asymptotic density of informed vehicles. Thereby, we can control n_j and u_j to meet the application needs of information packets in information class j.

It is worth noting that Eq. (2.23d) can be used to characterize the dissemination wave of information packets in an arbitrary information class j, $j \in \mathcal{L}$. As $\sum_{i=1}^{s} n_i = N$, we can assign different number of communication servers and mean communication service rates for different information classes appropriately to meet their application needs simultaneously. Eq. (2.23) also implies that if $\xi_j \equiv 0$ (i.e., the probability that an arriving information packet in information class j has to wait in queue is 0), then there exists no queue for information class j, and the SHRE model becomes the susceptible-relaying-excluded model studied by Wang et al. (2018). It models the information flow

dissemination wave under an information-relay control strategy where there is no queuing delay (i.e., no information-holding vehicles).

2.3.2 Modeling the traffic flow dynamics in the lower layer

The upper-layer SHRE model describes how the density of vehicles by vehicle class changes instantaneously due to V2V communications. It captures the impacts of communication constraints on success rate of V2V communications, and also factors the effects of the queuing strategy and the distribution of information-relaying vehicles on the IFPW formation. As mentioned before, the IFPW is a combination of the information flow dissemination wave and the traffic flow propagation wave. This section models the traffic flow dynamics to determine the traffic flow propagation wave. The effects of traffic flow dynamics on IFPW are threefold. First, they impact the success rate of V2V communications (i.e., $K(x,y)$) by determining the number of equipped vehicles within communication range of an information-relaying vehicle. Second, the number of the vehicles sending the specific information depends on the spatial distribution of information-relaying vehicles which evolves with the traffic flow dynamics. Third, the traffic flow speed significantly contributes to the IFPW speed. It adds to the IFPW speed in the direction of vehicular traversal and reduces the IFPW speed in direction opposite to that of vehicular traversal.

In this study, the first-order LWR model is used to describe the traffic flow dynamics. It can reproduce some essential features of traffic flow, such as the formation and propagation of traffic flow waves. The model consists of the flow conservation law and an explicit density-flow relationship known as the fundamental diagram of traffic flow. The flow conservation law and the fundamental diagram can be expressed as the following PDE model:

$$\frac{\partial k(x,t)}{\partial t} + \frac{\partial q(x,t)}{\partial x} = 0 \tag{2.24}$$

$$q(x,t) = F(k,x,t) \tag{2.25}$$

where $k(x,t)$ is the traffic flow density at location x at time t, $q(x,t)$ is the instantaneous flow, and $F(k,x,t)$ is the fundamental diagram in which the flow and density are related by a continuous and piecewise differentiable equation.

2.4 Analytical and numerical solutions for the two-layer model

This section discusses the analytical and numerical solutions for the two-layer model under homogeneous and heterogeneous traffic conditions, respectively. Homogeneous traffic conditions refer to unidirectional traffic flow with uniform traffic flow density and the heterogeneous traffic conditions refer to the other traffic flow situations (e.g., bi-directional flow). It should be noted that under both homogeneous and heterogeneous traffic flow conditions, the driving behaviors of all drivers are assumed to be identical. Under homogeneous traffic conditions, the traffic flow dynamics only shift the IFPW

towards the direction of traffic flow and do not change the densities of vehicles of different classes. Thereby, the impacts of traffic flow dynamics on the IFPW speed are uniform in space and time. The asymptotic density of informed vehicles and the condition for existence of IFPW can be derived analytically using only the upper-layer SHRE model.

Under heterogeneous traffic flow conditions, the traffic flow dynamics change the densities of vehicles of different classes spatiotemporally. Thereby, the impacts of the traffic flow dynamics on the IFPW speed are non-uniform in space and time. To obtain the solutions of the two-layer model under heterogeneous conditions, the change in density of vehicles of each vehicle class due to V2V communications (in the upper layer) and the traffic flow dynamics (in the lower layer) need to be tracked simultaneously. To do so, a numerical solution method is proposed here to capture the interactions between the upper and lower layers sequentially under discrete time and space settings.

2.4.1 Analytical solution of the two-layer model under homogeneous traffic conditions

The proposed SHRE model conceptually adapts the idea of susceptible-exposed-infected-recovered (SEIR) model that is extensively studied in epidemiology (see McCluskey, 2012; Li and Muldowney, 1995; Li et al., 1999; Smith et al., 2001). The equilibrium solution and conditions for local stability of the SEIR model are analyzed in these studies. However, the classical SEIR only address the temporal spread of a disease among the population at one location. By comparison, the designed SHRE model is a spatial model that seeks to determine how a specific information packet of interest will be propagated in both space and time. Thereby, the solutions of SEIR model in previous epidemiological studies cannot be applied to the SHRE model. To the best of our knowledge, the solution of the IDE system analogy to the SHRE model has not been studied before. Here, we derive analytical solution for the asymptotic density of vehicles by vehicle class of the SHRE model and study the conditions for the existence of the IFPW.

Let σ be the density of equipped vehicles. Suppose at time 0, all equipped vehicles are susceptible vehicles in the highway. Thereby, the initial conditions for the SHRE model are $S_j(x,0) = \sigma$, $H_j(x,0) = R_j(x,0) = E_j(x,0) = 0$. Assume the specific information packet of interest of information class j is generated and propagated by an equipped vehicle at location 0 and time 0. Similar to Kim et al. (2017) and Wang et al., (2017), under homogeneous traffic conditions, the information under the designed queuing strategy will quickly form a wave (if it exists) to propagate backward and forward at a uniform speed. The asymptotic density of vehicles of each vehicle class is the same beyond the location where the wave speed is stable. However, we cannot derive the analytical solutions for asymptotic speed of the IFPW. The IFPW speed will be solved for using the numerical method introduced in Section 2.4.2.

As discussed in Section 2.3.1, the communication kernel $K(x,y)$ characterizes the one-hop success rate of V2V communications. It significantly impacts the traveling wave

solutions. In this study, the Gaussian communication kernel in Eq. (2.26) proposed by Kim et al. (2017) will be used to characterize the one-hop success rate of V2V communications, in which the parameters a and b are calibrated using V2V communication data obtained through NS-3 simulation. It shows that the communication is subject to attenuation over distance. Also, it can be noted that the communication kernel satisfies $\int_{\Omega} K(x,y)dy = \int_{-\infty}^{+\infty} K(x,y)dy = b$.

$$K(x,y) = \frac{b}{a\sqrt{\pi}} e^{\frac{-(x-y)^2}{a^2}}, a > 0,\ 0 < b \leq 1, \tag{2.26}$$

The asymptotic density of vehicles by vehicle class and asymptotic density of informed vehicles are defined as follows.

Definition 1 (asymptotic density of vehicles by vehicle class): the asymptotic density of vehicles of vehicle class $z_j^*(x)$, $\mathrm{z}_j \in \{S_j, H_j, R_j, E_j\}$ at location x is defined as $z_j^*(x) = \lim_{t\to\infty} \mathrm{z}(x,t)$.

Definition 2 (asymptotic density of informed vehicles): let $I_j^*(x)$ be the asymptotic density of informed vehicles at location x, it is defined as $I_j^*(x) = \lim_{t\to\infty} I_j(x,t)$.

The following two theorems will be useful to analyze the asymptotic density of informed vehicles.

Theorem 1 (asymptotic density of information-holding vehicles): if $n_j u_j > \lambda_j$, then $H_j^*(x) = \lim_{t\to+\infty} H_j(x,t) = 0$

Proof: Let $\omega_j = n_j u_j - \lambda_j$; multiplying both sides of Eq. (2.23b) by $e^{\omega_j t}$, we have

$$e^{\omega_j t}\frac{\partial H_j(x,t)}{\partial t} + e^{\omega_j t}\cdot H_j(x,t) = e^{\omega_j t}\beta\cdot\xi_j\cdot S_j(x,t)\int_{\Omega} R_j(y,t)\cdot K(x,y)dy \tag{2.27}$$

This implies

$$\frac{\partial\left(e^{\omega_j t}H_j(x,t)\right)}{\partial t} = e^{\omega_j t}\beta\cdot\xi_j\cdot S_j(x,t)\int_{\Omega} R_j(y,t)\cdot K(x,y)dy \tag{2.28}$$

Then

$$e^{\omega_j t}H_j(x,t) - e^{\omega_j t}H_j(x,0) = \int_0^t e^{\omega_j \tau}\beta\cdot\xi_j\cdot S_j(x,\tau)\int_{\Omega} R_j(y,\tau)\cdot K(x,y)dy \cdot d\tau \tag{2.29}$$

Note $H_j(x,0) \equiv 0$. According to Eq. (2.23d), Eq. (2.29) can be written as

$$\begin{aligned} H_j(x,t) &= e^{-\omega_j t}\beta \cdot \xi_j \cdot \int_0^t e^{\omega_j \tau} S_j(x,\tau) \int_\Omega \frac{1}{u_j} \frac{\partial E_j(y,\tau)}{\partial \tau} \cdot K(x,y) dy \cdot d\tau \\ &= \frac{e^{-\omega_j t}\beta \cdot \xi_j}{u_j} \int_\Omega K(x,y) \int_0^t S_j(x,\tau)\, e^{\omega_j \tau} \frac{\partial E_j(y,\tau)}{\partial \tau} d\tau \cdot dy \end{aligned} \tag{2.30}$$

Note that as $t \to +\infty$, the densities of vehicles of different vehicle classes at each location y become stable. Thereby, $\lim_{t\to+\infty} \partial E_j(y,\tau)/\partial t \to 0$. For an arbitrarily small positive value ε, let $g(g < +\infty)$ be the value such that $\partial E_j(y,\tau)/\partial \tau < \varepsilon$ for $\tau > g$. Then

$$\begin{aligned} \lim_{t\to+\infty} H_j(x,t) &= \lim_{t\to+\infty} \frac{e^{-\omega_j t}\beta \cdot \xi_j}{u_j} \int_\Omega K(x,y) \int_0^t S_j(x,\tau)\, e^{\omega_j \tau} \frac{\partial E_j(y,\tau)}{\partial \tau} d\tau \cdot dy \\ &= \lim_{t\to+\infty} \frac{e^{-\omega_j t}\beta \cdot \xi_j}{u_j} \int_\Omega K(x,y) \int_0^g S_j(x,\tau)\, e^{\omega_j \tau} \frac{\partial E_j(y,\tau)}{\partial \tau} d\tau \cdot dy \\ &+ \lim_{t\to+\infty} \frac{e^{-\omega_j t}\beta \cdot \xi_j}{u_j} \int_\Omega K(x,y) \int_g^{+\infty} S_j(x,\tau)\, e^{\omega_j \tau} \frac{\partial E_j(y,\tau)}{\partial \tau} d\tau \cdot dy \end{aligned} \tag{2.31}$$

Note that $S_j(x,\tau)\, e^{\omega_j \tau} \frac{\partial E_j(y,\tau)}{\partial \tau}$ is bounded when $\tau \in [0,g]$. Thereby, $\int_0^g S_j(x,\tau)\, e^{\omega_j \tau} \frac{\partial E_j(y,\tau)}{\partial \tau} d\tau$ is bounded. This implies

$$\lim_{t\to+\infty} \frac{e^{-\omega_j t}\beta \cdot \xi_j}{u_j} \int_\Omega K(x,y) \int_0^g S_j(x,\tau)\, e^{\omega_j \tau} \frac{\partial E_j(y,\tau)}{\partial \tau} d\tau \cdot dy \to 0 \tag{2.32}$$

As $\partial E_j(y,\tau)/\partial \tau < \varepsilon$ for $\tau > g$. Then

$$\begin{aligned} &\lim_{t\to+\infty} \frac{e^{-\omega_j t}\beta \cdot \xi_j}{u_j} \int_\Omega K(x,y) \int_g^{+\infty} S_j(x,\tau)\, e^{\omega_j \tau} \frac{\partial E_j(y,\tau)}{\partial \tau} d\tau \cdot dy \\ &\le \lim_{t\to+\infty} \frac{e^{-\omega_j t}\beta \cdot \xi_j}{u_j} \sigma\, e^{\omega_j t} \cdot \varepsilon \\ &= \frac{\beta \cdot \xi_j}{u_j} \sigma \cdot \varepsilon \end{aligned} \tag{2.33}$$

Note that ε is an arbitrarily small positive value. Thereby,

$$H_j^*(x) = \lim_{t\to+\infty} H_j(x,t) = 0 \tag{2.34}$$

Theorem 2 (asymptotic density of information-relaying vehicles): if $n_j u_j > \lambda_j$, then $R_j^*(x) = \lim_{t \to +\infty} R_j(x,t) = 0$.

Theorem 2 can be proved using the same method used to prove Theorem 1; it is omitted here to avoid duplication.

Theorems 1 and 2 indicate that if $n_j u_j > \lambda_j$, there would be no information-holding and information-relaying vehicles at each location eventually. This is because when $n_j u_j > \lambda_j$, the specific information packet of interest waiting in the queue for information class j will have finite waiting time and finite communication service time. It will enter into the communication server for propagation and is removed from it eventually.

Let $\gamma_j = \beta b \sigma / u_j$, the following theorem discusses the asymptotic density of information-excluded vehicles.

Theorem 3 (asymptotic density of information-excluded vehicles): if $n_j u_j > \lambda_j$, and $\gamma_j > 1$, then $R_j^*(x) = \lim_{t \to +\infty} R_j(x,t) = \sigma \cdot \alpha_j^*$, where $\alpha_j^* \in (0,1)$ is the unique solution of the following nonlinear equation

$$e^{-\gamma_j \alpha_j} + \alpha_j - 1 = 0 \tag{2.35}$$

Proof: Under homogeneous traffic conditions, the traffic flow density is uniform. Hence, for arbitrary time t and location x, we have

$$S_j(x,t) + H_j(x,t) + R_j(x,t) + E_j(x,t) = \sigma \tag{2.36}$$

Note that $E_j(x,0) = 0$; according to Eq. (2.23d):

$$E_j(x,t) = \int_0^t u_j \cdot R_j(y,t) dt \tag{2.37}$$

Eq. (2.23a) implies that

$$\frac{\partial \left(ln\left(S_j(x,t) \right) \right)}{\partial t} = -\beta \int_\Omega R_j(y,t) \cdot K(x,y) dy \tag{2.38}$$

Integrating both sides of Eq. (2.38) from 0 to t, we have

$$ln\left(S_j(x,t) \right) - ln(\sigma) = -\beta \int_\Omega \left[\int_0^t R_j(y,\tau)\, d\tau \right] \cdot K(x,y) dy \tag{2.39}$$

Substituting Eq. (2.37) into Eq. (2.39), yields

$$ln\left(S_j(x,t) \right) - ln(\sigma) = -\frac{\beta}{u_j} \int_\Omega \left[\int_0^t u_j R_j(y,\tau)\, d\tau \right] \cdot K(x,y) dy \tag{2.40}$$

$$= -\frac{\beta}{u_j}\int_{\Omega} E_j(x,t)\cdot K(x,y)dy$$

Thereby,

$$S_j(x,t) = \sigma \cdot e^{-\frac{\beta}{u_j}\int_{\Omega} E_j(x,t)\cdot K(x,y)dy} \tag{2.41}$$

Substituting Eq. (2.41) into Eq. (2.36), we have

$$\sigma \cdot e^{-\frac{\beta}{u_j}\int_{\Omega} E_j(x,t)\cdot K(x,y)dy} + H_j(x,t) + R_j(x,t) + E_j(x,t) = \sigma \tag{2.42}$$

Let $t \to +\infty$, then

$$\sigma \cdot e^{-\frac{\beta}{u_j}\int_{\Omega} E_j^*(x)\cdot K(x,y)dy} + H_j^*(x) + R_j^*(x) + E_j^*(x) = \sigma \tag{2.43}$$

Note that $\int_{\Omega} E_j^*(x)\cdot K(x,y)dy = b\cdot E_j^*(x)$, and according to Theorems 1 and 2, $H_j^*(x) = R_j^*(x) = 0$. Then

$$\sigma \cdot e^{-\frac{\beta b}{u_j}E_j^*(x)} + E_j^*(x) = \sigma \tag{2.44}$$

Let $\alpha_j = (1/\sigma)\cdot E_j^*(x)$. As $E_j^*(x) \in [0,\sigma]$, $\alpha_j \in (0,1)$. Eq. (2.44) can be rewritten as

$$e^{-\gamma_j\alpha_j} + \alpha_j = 1 \tag{2.45}$$

For simplicity, denote the function $\varphi(\alpha_j)$ as

$$\varphi(\alpha_j) = e^{-\gamma_j\alpha_j} + \alpha_j - 1 \tag{2.46}$$

Note that

$$\varphi'(\alpha_j) = d\varphi(\alpha_j)/d\alpha_j = -\gamma_j e^{-\gamma_j\alpha_j} + 1 \tag{2.47}$$

According to Eq. (2.47), $d\varphi(\alpha_j)/d\alpha_j\big|_{\alpha_j=0} = -\gamma_j + 1 < 0$ for $\gamma_j > 1$. As $\varphi(0) = 0$, this implies that $\varphi(\alpha_j) < 0$ for α_j sufficiently close to 0. Note that $\varphi(1) = e^{-\gamma_j} > 0$. Hence, there must exist a solution to Eq. (2.45) for $\alpha_j \in (0,1)$. The second-order derivative of $\varphi(\alpha_j)$ with respect to α_j is $\varphi''(\alpha_j) = d^2\varphi(\alpha_j)/d{\alpha_j}^2 = (\gamma_j)^2 e^{-\gamma_j\alpha_j} > 0$. Thereby, $\varphi(\alpha_j)$ is a convex function. There exists at most two solutions for $\varphi(\alpha_j) = 0$. $\alpha_j = 0$ is a solution to $\varphi(\alpha_j) = 0$. This implies that there exists a unique solution to $\varphi(\alpha_j) = 0$ for $\alpha_j \in (0,1)$. Let α_j^* be the corresponding solution. We have $E_j^*(x) = \sigma\cdot\alpha_j^*$. Theorem 3 is proved.

Recall $I_j^*(x) = H_j^*(x) + R_j^*(x) + E_j^*(x)$, and $H_j^*(x) = R_j^*(x) = 0$. We have the following corollary.

Corollary 1: The asymptotic density of informed vehicles is $I_j^*(x) = E_j^*(x) = \sigma \cdot \alpha_j^*$.

According to Eq. (2.34), α_j^* is determined only by the value of γ_j which equals $\beta b\sigma/u_j$. Thereby, when the communication frequency (β), the parameter b in the communication kernel and the initial density of equipped vehicles (σ) are fixed, the service rate u_j can be leveraged by transportation operators to propagate the specific information in information class j to control the proportion of vehicles that can receive the specific information. Let $P_{I_j}^*$ be the information spread (i.e., proportion of informed vehicles) for the specific information packet of interest in information class j; we have $P_{I_j}^* = \sigma \cdot \alpha_j^*/\sigma = \alpha_j^*$.

The following theorem discusses the existence of the IFPW.

Theorem 4 (conditions for existence of IFPW): The IFPW does not exist when $\gamma_j < 1$.

Proof: Note for $\alpha \in [0,1]$,

$$\varphi'(\alpha_j) = d\varphi(\alpha_j)/d\alpha_j = -\gamma_j e^{-\gamma_j \alpha_j} + 1 > -\gamma_j + 1 > 0 \tag{2.48}$$

Thereby, $\varphi(\alpha_j)$ increases monotonically with respect to α_j for $\alpha_j \in (0,1)$. As $\varphi(0) = 0$, there exists no solution to $\varphi(\alpha_j) = 0$ for $\alpha_j \in (0,1)$. This implies that the vehicles are far from the location (location is labeled as x) where the information packet is generated, and the asymptotic solution of $E_j(x,t)$ is 0. As all informed vehicles will become information-excluded vehicles, this result indicates that no vehicle can receive the specific information packet of interest of information class j if they are far from the location where the information is generated in this case. Thereby, the IFPW does not exist for $\gamma_j < 1$.

Theorem 4 shows that if the initial density of equipped vehicles and the service rate are high, the specific information packet of interest can only be propagated locally. Vehicles that are far from the location where the specific information is generated cannot receive it. This property can be used by transportation operators to design effective control strategies to propagate information within a small vicinity (e.g., sudden braking information, lane merge information). It should be noted that u_j will impact the propagation distance of the specific information of interest when the IFPW does not exist. Through a numerical example, we will show that if u_j is set such that γ_j is closer to 1 ($\gamma_j < 1$), the specific information of interest will be propagated further away. If $\gamma_j > 1$, the specific information packet will form a wave to be propagated in the network.

As discussed earlier, we cannot derive an analytical solution for the asymptotic IFPW speed even if it exists. The IFPW speed will be computed using the numerical method introduced in the next section. Note that the asymptotic IFPW speed is significantly

impacted by the queuing delay which is determined by the two control parameters (i.e., n_j and u_j) simultaneously. To meet the application needs of information in an arbitrary information class j related to information spread, time delay to reach a target location and spatial coverage, the values for the two control parameters n_j and u_j can be determined as follows: first, choose u_j appropriately according to Theorem 4 if the information needs to be only propagated locally. If the information needs to be propagated in the network, then determine u_j appropriately according to Theorem 4 and corollary 1 so that information spread can be satisfied. Third, determine n_j appropriately to control the IFPW speed so that it can reach the target location in the desired time.

2.4.2 Numerical solution method

The analytical solutions for the various information classes introduced in previous section only apply to homogeneous traffic conditions. Under heterogeneous conditions, the IFPW may not be stable due to the non-uniform impact of traffic flow dynamics on information dissemination. To analyze how information is spread in space and time under heterogeneous conditions, this section proposes a numerical solution method based on Kim et al. (2017) to solve the two-layer model. The numerical solution method helps to: (1) estimate the IFPW speed under both homogeneous and heterogeneous traffic conditions, and (2) estimate the distance the specific information can be propagated when the IFPW does not exist, under both homogeneous and heterogeneous traffic conditions, and (3) estimate the density of informed vehicles under heterogeneous conditions.

The numerical solution method discretizes space and time into cells of length Δx and time interval Δt, respectively. Let $1,2,3\cdots$ denote the cells in the highway sequentially. The fourth-order Runge-Kutta method will be used to approximate the densities of vehicles by vehicle class (i.e., $S_j(x,t)$, $H_j(x,t), R_j(x,t)$ and $X_j(x,t)$) changed according to the SHRE model in the upper layer. To solve the LWR model in the lower layer, the generalized cell transmission finite difference method proposed by Daganzo (1995) is used to approximate Eq. (2.24) and Eq. (2.25) as follows

$$[k(x,t+\Delta t)-k(x,t)]/\Delta t = [q(x-\Delta x,t)-q(x,t)]/\Delta x \tag{2.49}$$

$$q(x,t) = \min\left\{T\big(k(x,t)\big), Q\left(k_{jam}-k(x+\Delta x,t)\right)\right\}, \tag{2.50}$$

where T specifies the maximum flow that can be sent by the upstream cell and Q specifies the maximum flow that can be received by the downstream cell. k_{jam} is the jam traffic density. Let U denote the unequipped vehicles. The steps to solve the two-layer model numerically are as follows:

Step 1: At time 0 ($t=0$), obtain the initial number of vehicles of each class $z, z \in \{S_j, H_j, R_j, E_j, U\}$ and corresponding density of vehicles of each vehicle class in each cell. Let $t = t + \Delta t$.

Step 2: Solve the lower-layer model to determine the flow in each cell x (i.e., $q(x,t)$) that advances to the downstream cell according to Eq. (2.49) and Eq. (2.50). Update the number of vehicles in each cell.

Step 3: Calculate the number of vehicles of each class $z \in \{S_j, H_j, R_j, E_j, U\}$ that advance to the downstream as follows:

$$q_z(x,t) = \frac{k_z(x,t-\Delta t)}{k(x,t-\Delta t)} \cdot q(x,t), \quad z \in \{S_j, H_j, R_j, E_j, U\}, \tag{2.51}$$

where $q_z(x,t)$ is the traffic flow of class z leaving cell x at time interval t and $k_z(x,t-\Delta t)$ is the density of class z in cell x and time $t-\Delta t$.

Step 4: Update the density of vehicles by vehicle class in each cell of the upper layer using the discrete multiclass flow conservation law, as follows:

$$[k_z(x,t) - k_z(x,t-\Delta t)]/\Delta t = [q_z(x-\Delta x,t) - q_z(x,t)]/\Delta x\,, z \in \{S_j, H_j, R_j, E_j, U\}. \tag{2.52}$$

where $k_{s_j}(x,t)$, $k_{H_j}(x,t)$, $k_{R_j}(x,t)$ and $k_{E_j}(x,t)$ represents $S_j(x,t)$, $H_j(x,t)$,$R_j(x,t)$ and $E_j(x,t)$, respectively that describe the density of vehicles of each class in the upper layer.

Step 5: Approximate the density of vehicles by vehicle class (i.e., $S_j(x,t)$, $H_j(x,t)$, $R_j(x,t)$ and $E_j(x,t)$) that are changed according to the SHRE model in the upper layer.

Step 6: If the predetermined time length is reached, then stop. Otherwise, let $t = t + \Delta t$, and go to Step 2.

The numerical method solves the discretized LWR model and the SHRE model sequentially to capture the effects of traffic flow dynamics on information dissemination. It is worth noting that to reduce computational load, the convolution term ($\int_\Omega R_j(y,t) \cdot K(x,y)dy$) in Eq. (2.23) can be approximated using the Fast Fourier Transform (FFT) method. More details of the numerical method and the FFT method can be found in Kim et al. (2017). The numerical method can provide the density of vehicles by vehicle class at each cell and time interval.

The numerical method can also be used to verify the analytical solutions of density of informed vehicles and to approximate the IFPW speed under both homogeneous and heterogeneous traffic conditions. Note that IFPW consists of two waves: the forward wave which travels in the direction of vehicular traversal and the backward wave which travels opposite to the direction of vehicular traversal. Correspondingly, there exist two IFPW speeds, the forward and backward IFPW speeds. The method to estimate the two IFPW speeds is as follows. Let t_1 and t_2 be two arbitrary time intervals. Without loss of generality, let $t_1 > t_2$. Let $z_{j,0}$ be the density of vehicles in an arbitrary vehicle class z_j. $z_{j,0}$ is set between the minimum and maximum density of vehicle class z_j. Then, at the two time intervals $t_h, h = 1,2$, there exist two cells on the two wave fronts, respectively,

for which the density of vehicle class z_j is most close to $z_{j,0}$. Denote the two cells as l_{B,t_h} and l_{F,t_h} $(h = 1,2)$, respectively. Without loss of generality, let l_{B,t_h} be the cell in the backward IFPW and the l_{F,t_h} be the cell in the forward IFPW. Then, the forward IFPW (labeled as c_F) and the backward IFPW (labeled as c_B) can be approximated as

$$c_F = \frac{(l_{F,t_2} - l_{F,t_1})\Delta x}{t_2 - t_1} \tag{2.53}$$

$$c_B = \frac{|(l_{B,t_2} - l_{B,t_1})\Delta x|}{t_2 - t_1} \tag{2.54}$$

2.5 Numerical experiments

This section discusses several numerical experiments to illustrate the application of the proposed method to control multiclass information flow propagation. Consider a highway with 30 km length. Discretize the highway uniformly into 2000 cells. Table 2.1 shows other inputs in the experiment.

Table 2.1: Experiment parameters

Traffic flow parameters	Value
Free flow speed (u_f)	108 km/h
Time interval (Δt)	0.5 seconds
Cell length (Δx)	15 meters
Number of lanes	1
Market penetration rate (W)	50%

2.5.1 Calibration of the communication kernel

Table 2.2 presents the inputs for NS-3 parameters.

Table 2.2: Inputs for NS-3 parameters

Parameters	Value
IEEE 802.11p channel capacity	6 Mbps
Band	5.9 GHz
Communication frequency	10 Hz
Communication power/distance	300 m
Minimum contention window	15 slots
Energy detection threshold	-96 dBm
Noise floor	-99 dBm
SINR threshold	5 dB

To calibrate the communication kernel function in Eq. (2.26), NS-3 will be used to simulate the success rate of one-hop V2V communications under different traffic flow densities. Recently, NS-3 has been used to simulate V2V communications and evaluate the performance of communication protocols for vehicular ad hoc networks (see e.g., Dey et al., 2016; Noori and Olyaei., 2013; Talebpour et al., 2016). The inputs for the V2V communication related parameters in NS-3 are shown in Table 2.2. The simulation is operated based on IEEE 802.11p protocol in 5.9 GHz band with channel capacity 6 Mbps (Li, 2010) and communication power 300 m (Torrent-Moreno et al., 2009; Yu and Biswas, 2007). In V2V communications, whether a receiver vehicle can successfully receive an information packet from a sender vehicle is primarily decided by two factors: the reception signal power, and the noise and interference. The reception signal power determines whether the receiver vehicle can receive the signals from the sender vehicles, and the level of noise and interference determines the probability of reception error. In this simulation, the Friis propagation loss model (Benin et al., 2012) is used in NS-3 to calculate the reception signal power. It characterizes the impacts of transmission power, distance between receiver and sender, transmission gain, and reception gain on reception signal power. The receiver vehicle receives the information packet only if the reception signal power is larger than the energy detection threshold -96 dBm. To estimate the noise and interference, the signal to (interference and) noise ratio (SINR) model is used in NS-3 simulation. The SINR is the ratio of the power of a certain signal of interest over the sum of the interference power (from all the other interfering signals) and the power of some background noise (for details, see Wang et al. 2018). The threshold of SINR is set as 5 dB (Hisham et al., 2016; Hisham et al., 2017), indicating that the V2V communication is considered to be successful if SINR is larger than 5 dB; otherwise, it will be considered as a communication failure.

Table 2.3: Maximum number of communication servers, and calibrated parameters in communication kernel using NS-3 simulation

Density (veh/km)	10	20	30	40	50	60	70	80	90	100
a	0.177	0.172	0.163	0.145	0.138	0.122	0.107	0.094	0.087	0.078
b	0.311	0.295	0.273	0.242	0.221	0.185	0.164	0.141	0.126	0.11
N_{max}	66	33	22	16	13	11	9	8	7	6

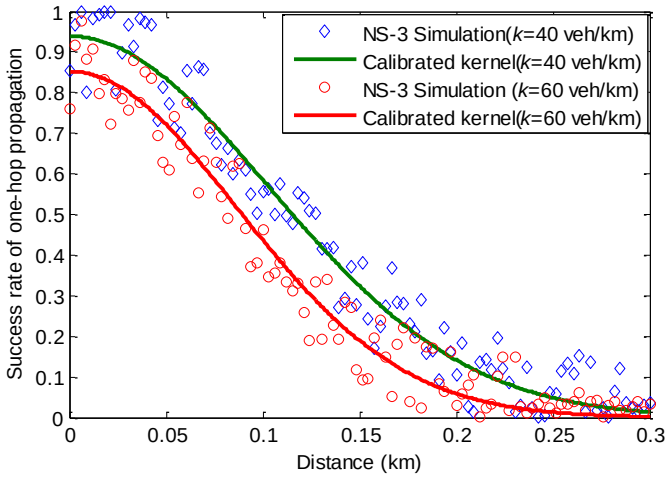

Figure 2.3: Calibrated communication kernel for $k = 40$ veh/km and $k = 60$ veh/km

Recall that all equipped vehicles within communication range are assumed to share the channel capacity equally. Suppose that a single unit of information packet has a size 500 (Torrent-Moreno et al., 2009; Bilstrup et al., 2009). To prevent information congestion effects that would occur if the channel capacity is full, the maximum number of communication servers can be calculated as follows

$$N_{max} = \left[\frac{C}{2 \cdot k \cdot \beta \cdot R \cdot W \cdot \chi}\right].$$

where R is the communication range, C is the channel capacity (6 Mbps), and W is the market penetration rate of V2V-equipped vehicles (50% in this study). χ is the information packet size (500 bytes), and k is the traffic flow density. The operator $[h]$ denotes the largest integer less than h. The calculated N_{max} values for different traffic flow densities are shown in Table 2.3. They will be used as the total number of communication servers under the corresponding traffic flow densities. To account for the impacts of positions of vehicles on success rate of V2V communications, vehicles are assumed to be randomly distributed along the 30 km highway. The simulation is conducted for 30 minutes, and is repeated 100 times. The calibrated parameters in the communication kernel are presented in Table 2.3. Figure 2.3 illustrates the simulated success rate of one-hop propagation and calibrated communication kernels at $k = 40$ veh/km and $k = 60$ veh/km. The R-squared values of the calibrated communication kernel at $k = 40$ veh/km and $k = 60$ veh/km are 0.97 and 0.93, respectively, indicating that the calibrated communication kernel robustly captures the relationship between success rate of one-hop propagation and the distance of the sender vehicle to the receiver vehicle. In addition, for the same distance, the success rate of one-hop propagation at $k = 60$ veh/km is less than it is at $k = 40$ veh/km. This because the communication interference increases if more vehicles are located within the communication range of a sender vehicle, causing greater communication failure.

2.5.2 IFPW under homogeneous conditions

2.5.2.1 Asymptotic density of informed vehicles and IFPW speed

The following example shows how to calculate the asymptotic density of informed vehicles analytically under homogeneous conditions. Suppose the traffic flow density is 40 veh/km, and the market penetration rate of equipped vehicles is 40%. Then, for each cell, the number of equipped vehicles is 0.24 veh/cell (σ). According to Table 2.3, the parameters a and b in Eq. (2.26) are 0.145 and 0.242, respectively. Suppose the specific information of interest is from information class j. Assume the information arrival rate is 2 packets/second, the number of communication servers (n_j) assigned to send the information packets in information class j is 11 and the corresponding mean communication service rate u_j is 0.2 packet/seconds (i.e., mean service time is 20 seconds). Note $n_j u_j - \lambda_j = 11 \times 0.2 - 2 = 0.2 > 0$ and $\gamma_j = \beta b \sigma / u_j = 10 \times 0.242 \times 0.5 * \frac{0.6}{0.2} = 3.630 > 1$. According to Theorem 4 and Corollary 1, the asymptotic density of informed vehicles exists. Corollary 1 indicates that $I_j^*(x) = 0.24 \cdot \alpha_j^*$, where α_j^* is the unique solution of the nonlinear solution $e^{-2.904\alpha_j} + \alpha_j - 1 = 0$ for $\alpha_j \in [0,1]$. Using Newton method to solve the nonlinear equation, we have $\alpha_j^* = 0.971$. Thereby, the asymptotic density of informed vehicles is $I_j^*(x) = 0.24 \cdot 0.971 = 0.233$ vehicle/cell $= 15.53$ veh/km. The information spread (proportion of informed vehicles) is $P_{I_j}^* = \alpha_j^* = 0.971$.

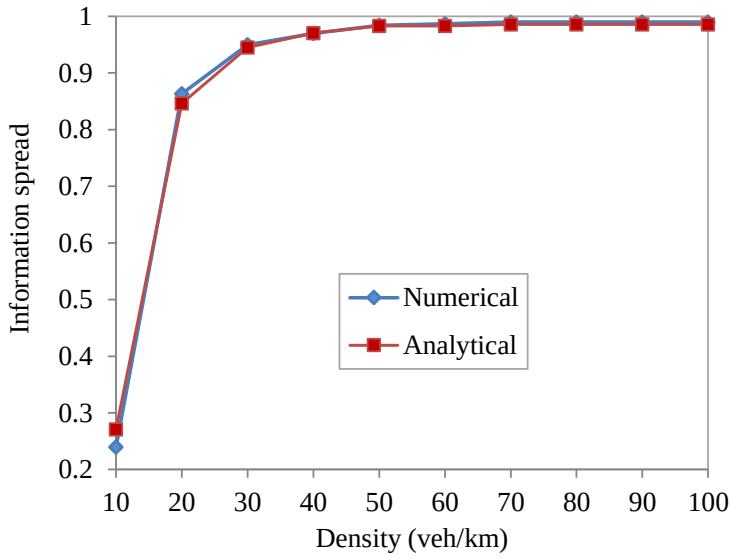

Figure 2.4: Information spread at $n_j = 11$ and $u_j = 0.2$ under different traffic densities

Figure 2.4 compares the information spread of the specific information packet of information class j under different traffic flow densities at $n_j = 11$ and $u_j = 0.2$ packets/second. It shows that the numerical solutions overlap with the analytical solutions, implying that the numerical algorithm proposed in Section 2.4.2 can effectively solve the two-layer model. Figure 2.4 also demonstrates that when traffic flow density increases, the information spread also increases as more vehicles will propagate it in an unit of time. This indicates that under higher traffic flow density scenarios, the mean communication service rate of information packets of class j can be reduced for the same information spread.

Suppose the traffic flow density is 40 veh/km and the specific information packet of interest in information class j is generated by a vehicle at time 0 and location 0. Let $\lambda_j = 1$ packets/second, $n_j = 11$ and $u_j = 0.12$ packets/second. Figure 2.5 shows the spatial distribution of density of vehicles by vehicle classes at $t = 120$ seconds and $t = 180$ seconds. It indicates that the IFPW can form the same shape to move forward and backward. Most of the information-holding and information-relaying vehicles are located close to the wave front. This is because when $\lambda_j < n_j u_j$ and $u_j > 0$, the information packet in information class j will experience finite queuing delay and communication service time. Thereby, the vehicles that receive the specific information packet of interest a long time ago will exclude it from the system. The information-holding and information-relaying vehicles will become information-excluded vehicles eventually.

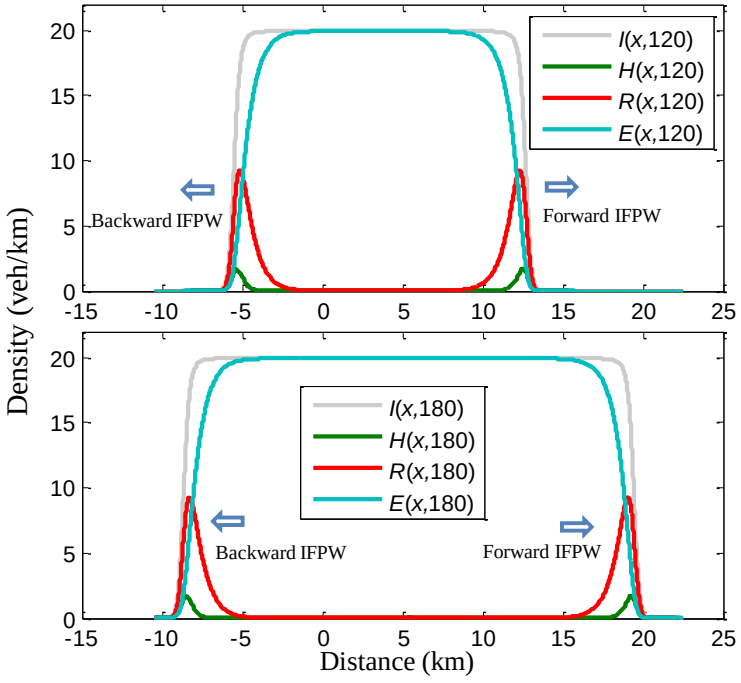

Figure 2.5: Density of vehicles by vehicle class at $t = 120$ seconds and $t = 180$

seconds

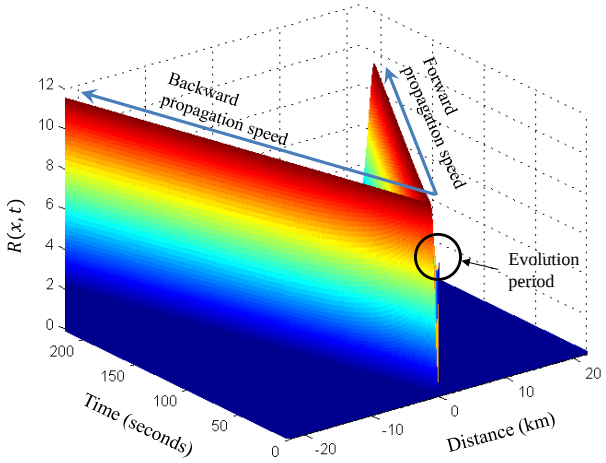

Figure 2.6: Density of information-relaying vehicles in space and time at $k = 40\ veh/km$

To analyze the asymptotic IFPW speed, Figure 2.6 shows the spatiotemporal distribution of density of information-relaying vehicles. It illustrates that the specific information packet of interest of information class j is propagated backward and forward at a uniform speed reached only a few seconds after it is generated. To numerically estimate the IFPW speed, Figure 2.7 shows the spatial distribution of density of information-excluded vehicles at $t = 120$ seconds and $t = 180$ seconds. Let $R_0 = 12\ veh/km$ be the reference density in Eq. (2.53) and Eq. (2.54). According to Figure 7, the cells whose densities of information-relaying vehicles in the backward and forward IFPWs are most close to R_0 at $t = 120$ seconds are located at -4.725 km and 11.925 km, respectively. The cells whose densities of information-relaying vehicles in the backward and forward IFPWs are most close to R_0 at $t = 180$ seconds are located at -7.860 km and 18.66 km, respectively. According to Eq. (2.53) and Eq. (2.54), the forward and backward IFPW speeds can be estimated as:

$$c_F = \frac{\left(l_{F,t_2} - l_{F,t_1}\right)\Delta x}{t_2 - t_1} = \frac{18.66 - 11.925}{180 - 120} = 0.1122 km/s = 404.1 km/h$$

$$c_B = \frac{\left|\left(l_{B,t_2} - l_{B,t_1}\right)\Delta x\right|}{t_2 - t_1} = \frac{|-7.860 + 4.725|}{180 - 120} = 0.0523 km/s = 188.3 km/h$$

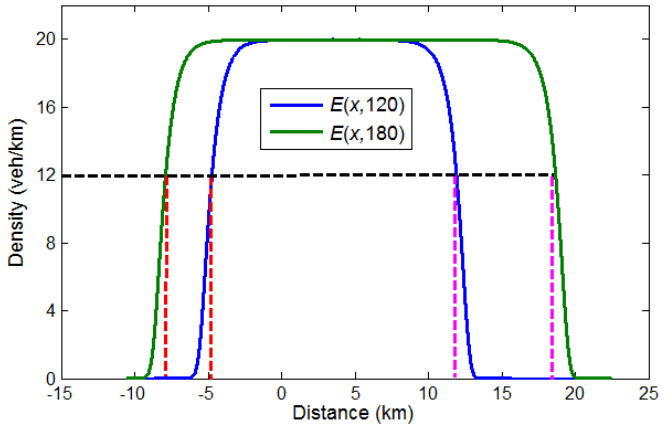

Fig 2.7: Density of information-excluded vehicles at $t = 120$ seconds and $t = 180$ seconds

2.5.2.2 Scenarios where the information packet can be propagated only locally

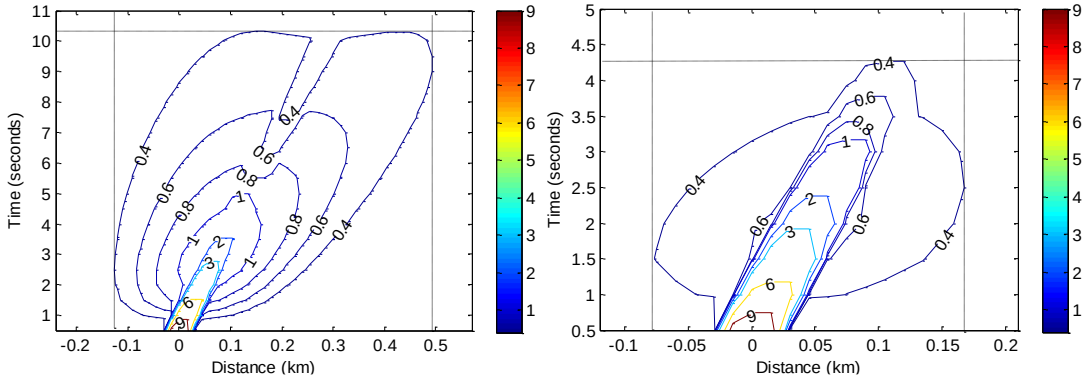

(a) **(b)**

Figure 2.8: Scenarios for which the information packets are propagated only locally: (a) Contour of density of information-relaying vehicle in space and time for $n_j = 15$ and $u_j = 0.66$; (b) Contour of density of information-relaying vehicle in space and time for $n_j = 15$ and $u_j = 1$.

As Theorem 4 indicates, the IFPW does not exist when the mean communication service rate is high enough such that $\gamma_j < 1$. In this case, the specific information packet in information class j can be propagated only locally. This property can be leveraged to send information packets in a small vicinity of where they are generated. The following example seeks to demonstrate how to control the propagation distance by leveraging communication service rate when information is propagated locally. Suppose the traffic flow density is 40 veh/km, the average arrival rate of information packets of information class j is 2 packets/second, and the number of assigned communication servers for information class j is 15. Let the density of information-relaying vehicles at location 0 and time 0 be 11 veh/km and 0 elsewhere. Figure 2.8(a) and Figure 2.8(b) show the spatiotemporal distribution of density of information-

relaying vehicles at $u = 0.66$ and $u = 1$, respectively. Note $\gamma_j < 1$ in both cases. Figure 2.8 illustrates that the density of information-relaying vehicles decreases to 0 in space and time. Recall only information-relaying vehicles can propagate the specific information packets of interest. This implies that the specific information packet can only be propagated locally. Vehicles far away from location 0 where the specific information packet is generated will not receive it. It can be noted that the density of information-relaying vehicles decreases to 0.4 (almost 0) at 500 meters and 165 meters downstream of location 0 at $u = 0.66$ and $u = 1$, respectively. This implies the information packets can be propagated further away under a lower communication service rate. Thereby, the mean communication service rate can also be leveraged to propagate information to different distances.

2.5.2.3 Integrated impacts of n_j and u_j on asymptotic IFPW speed and density of informed

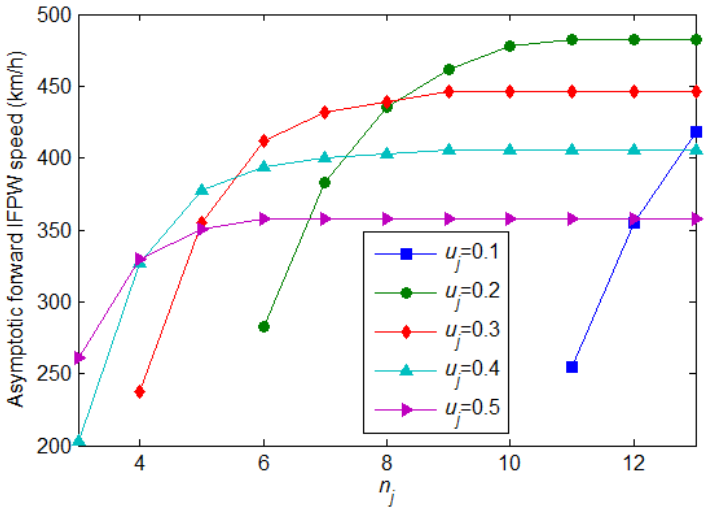

Figure 2.9: Impacts of n_j and u_j on asymptotic forward IFPW speed of an information packet of information class j

Suppose the traffic flow density is 50 veh/km, and the arrival rate of the information packets in information class j is 1 packet/second. To analyze the impacts of n_j and u_j on IFPW speed and density of informed vehicles, u_j is varied from 0.1 packets/second to 0.5 packets/second. According to M/M/n_j queuing theory, to enable propagation of the specific information packet of information class j, $\lambda_j/(n_j u_j)$ must be less than 1. Thereby, the minimum number of communication servers assigned to send information packets of information class j are 11, 6, 4, 3, 3 for $u_j = 0.1, 0.2, 0.3, 0.4, 0.5$, respectively. Figure 2.9 shows the asymptotic forward IFPW speed for various values of n_j and u_j. It shows that when u_j is fixed, the asymptotic forward IFPW speed increases monotonically with respect to n_j. This is

because as more communication servers are assigned to information class j, the mean waiting time of the specific information packet in the queue will reduce (see Figure 2.10). Thereby, it can be transmitted faster by the informed vehicles. Figure 2.9 also shows that for a fixed n_j, the IFPW speed decreases monotonically with respect to mean communication service rate u_j in most cases because an increase in mean communication service rate will reduce the transmission duration of the packet. However, in some cases (e.g., $n_j = 11, 12$, $u_j = 0.1, 0.2$.), increase in u_j may increase the forward IFPW speed. This is because for a fixed n_j, increase in u_j will reduce the mean waiting time in the queue (see Figure 2.10). Thereby, unlike that of the number of communication servers, the effect of mean communication service rate on the IFPW speed is more intricate. The proposed method in this study aids in determining the appropriate mean communication service rate for each information class to satisfy its application needs in terms of propagation performance.

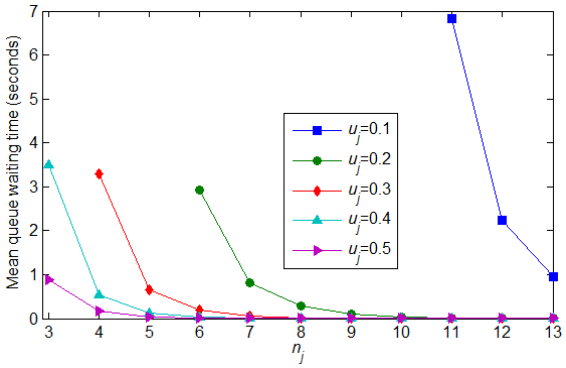

Figure 2.10: Mean waiting time of information packets in the queue

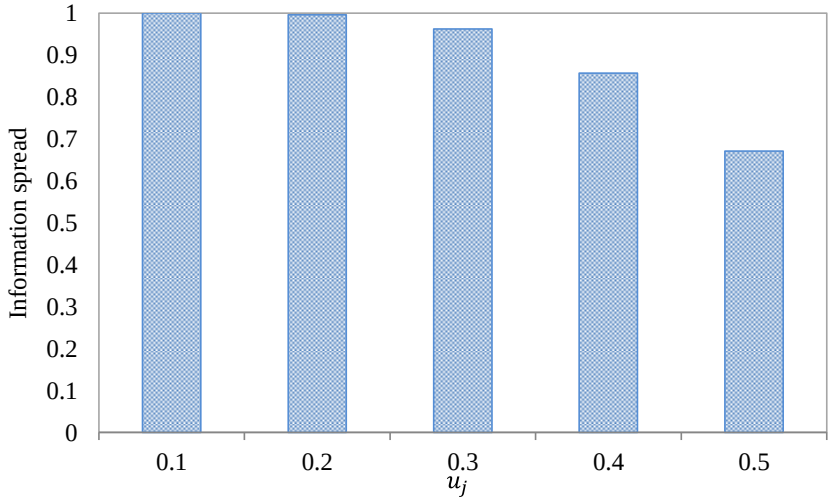

Figure 2.11: Information spread for different values of u_j

Figure 2.11 shows the information spread of the specific information of interest under different communication service rates. As the value of u_j increases, information spread decreases monotonically, implying that less number of vehicles will receive the specific information of interest. This is because an informed vehicle will exclude the specific information packet of interest from the communication servers faster under higher mean communication service rate. It is worth mentioning that the number of communication servers has no effect on information spread. Thereby, to design effective control strategies for propagating information packets in different classes, the mean communication service rate can be determined first to obtain the desired information spread. Then, the appropriate number of communication servers can be determined to be assigned to different information classes to control their propagation speed. Further, Figure 2.11 shows that the numerical solutions are almost identical to the analytical solutions.

2.5.2.4 Validate the analytical and numerical solutions using NS-3 simulation

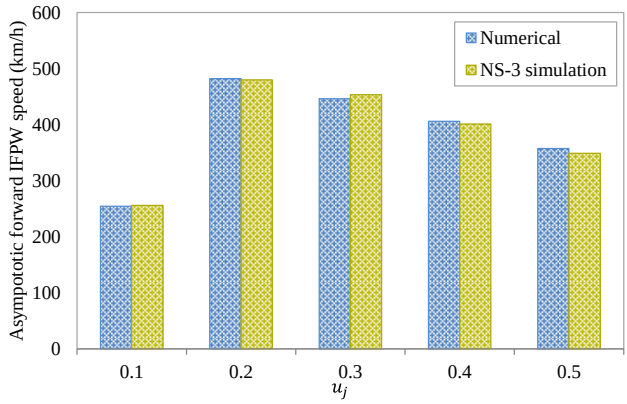

Figure 2.12: Comparison of numerical and NS-3 simulation results of asymptotic forward IFPW speed

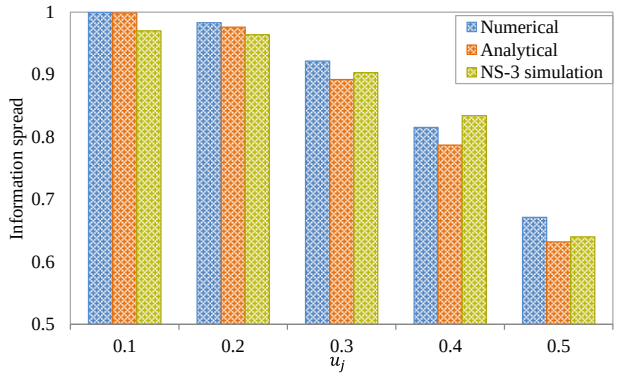

Figure 2.13: Comparison of numerical, analytical and NS-3 simulation results of information spread

This section uses NS-3 simulation to validate the performances of the analytical and numerical solutions by integrating the communication and traffic flow networks. Suppose the number of communication servers assigned to information class j is 12, and the information in information class j is propagated from the upstream traffic flow to the downstream traffic flow with an average arrival rate of 1 packet/second. Without loss of generality, suppose the traffic flow density is 50 veh/km and all vehicles travel at a uniform speed of 84 km/h. The other inputs for NS-3 parameters can be found in Table 2.2. Note that NS-3 simulation can record the time at which a vehicle is informed with the specific information of interest in information class j. Thereby, the method introduced in Section 2.4.2 can be applied to estimate the IFPW speed based on the NS-3 simulation results. The simulations are repeated 100 times to account for the stochasticity of communication failure. The average IPFW speed and the information spread will be used to validate the performances of analytical and numerical solutions. Figure 2.12 compares the numerical and NS-3 simulation results of the asymptotic forward IFPW speed under different communication service rates. It shows that the numerical solutions of the asymptotic forward IFPW speed are very close to those of the simulated results, with the maximum relative difference being less than 3%. Figure 2.13 compares the numerical, analytical and NS-3 simulation results of information spread under different communication service rates. It illustrates that the numerical and analytical results are almost identical while the NS-3 simulation results have very small differences from them. The small differences are mainly induced by stochastic communication failures between each pair of vehicles. The two figures indicate that the proposed method can accurately characterize the process of information flow propagation and can be used to control the propagation performance in terms of IFPW speed and information spread.

2.5.3 Control of multiclass information flow propagation under homogeneous and heterogeneous traffic conditions

2.5.3.1 Control of multiclass information flow propagation under homogeneous traffic conditions

This section analyzes the control of multiclass information propagation to meet application needs of various classes simultaneously. Recall that the queuing system for each information class is independent. Thereby, the number of communication servers and the mean communication service rate can be controlled for each information class to achieve desired propagation performance related to information spread (related to density of informed vehicles), time delay bounds (related to IFPW speed) and spatial coverage (related to existence of IFPW). Suppose traffic flow density is 50 veh/km and information from three information classes (labeled information class 1, 2 and 3) is propagated over the traffic stream. Let information class 1 contain “urgent” information (e.g., traffic accident blocks the freeway link fully). It is desirable for this information to reach all upstream and downstream vehicles with low latency. Information class 2 is constituted by less urgent

information; for example, routing information. It is delay-tolerant and is expected to reach a lower proportion of equipped vehicles compared to information class 1 to avoid congestion in other routes. Information class 3 contains information with limited impact area, which needs to be propagated locally, for example, information of sudden braking of a vehicle, lane merge information, etc. Suppose the mean arrival rate of information packets of information class 1, 2 and 3 are 0.3, 1 and 2 packets/second, respectively. According to Table 2.3, the total number of communication servers that can be assigned under traffic flow density 50 veh/km is 13. Let the number of communication servers assigned to information classes 1, 2 and 3 be 6, 4 and 3, respectively. The mean communication service rates are set correspondingly as $u_1 = 0.08$ packets/second, $u_2 = 0.5$ packets/second, and $u_3 = 1$ packets/second. Note that $\gamma_1 > 1, \gamma_2 > 1$, and $\gamma_3 < 1$. According to Theorem 4, the IFPW exists for propagation of information packets of information classes 1 and 2 while it does not exist for information packets of class 3.

Figure 2.14 compares the forward and backward IFPW speed of information classes 1 and 2. It shows that both forward and backward IFPW speeds of information class 1 are greater than those of information class 2. In addition, the proportion of vehicles (information spread) informed with the packets of information class 1 and information class 2 are 99.9% and 67.1%, respectively. Thereby, under the designed control strategy, packets from information class 1 can reach more number of vehicles with lower time delay compared to packets from information class 2. Figure 2.15 shows the contour of the density of information-relaying vehicles. It indicates that vehicles relaying the specific information packet of information class 3 decreases dramatically with space and time. The specific information packet is almost excluded by all vehicles beyond the locations 280 meters downstream and 120 meters upstream of its point of origin (i.e., location 0). Thereby, the information packets of class 3 are only propagated to a small area.

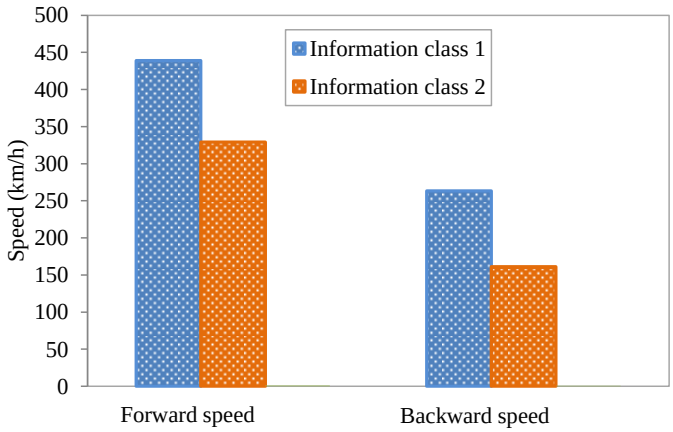

Figure 2.14: Comparison of forward and backward propagation speeds

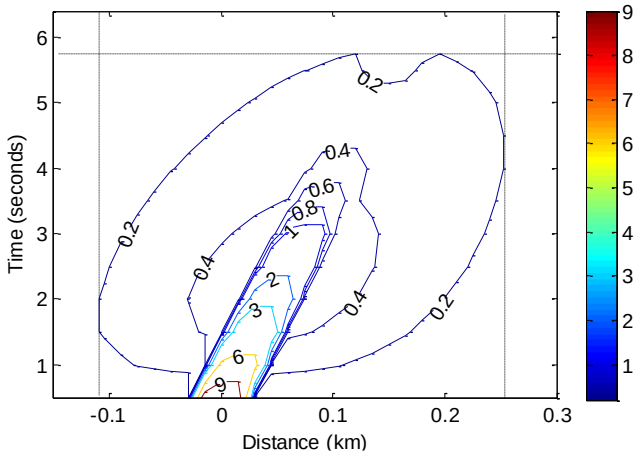

Figure 2.15: Contour of density of information-relaying vehicles of information class 3

2.5.3.2 Control of multiclass information flow propagation under heterogeneous conditions

This section address the control of information flow propagation under heterogeneous conditions. Similar to Kim et al. (2017), consider that a traffic accident happens at time 0 on a unidirectional highway with a traffic flow density of 50 veh./km. As illustrated by Figure 2.16, the incident occurs at location A. It reduces the link capacity by one third for 4 minutes before it is cleared. The congested traffic and the free flow traffic departing from the incident occurrence location are separated by Line AB. The occurrence and clearance of the incident induce two forward propagating traffic waves denoted by lines AD and BF, respectively. After the incident occurs, vehicles are jammed at the incident location, leading to a traffic wave propagating backward.

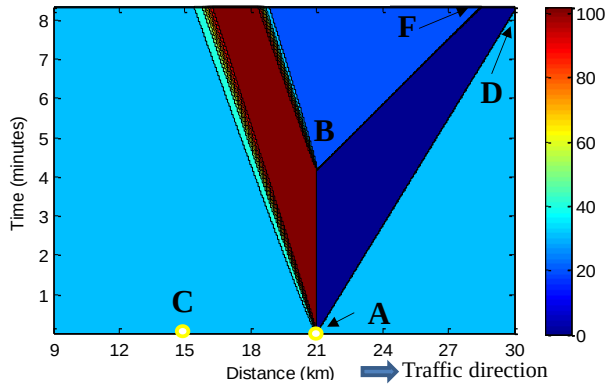

Figure 2.16: Contour of traffic density

Suppose information packets of three different information classes are generated at location C, and their arrival rates are identical. We label them information classes 1,

2, and 3. Information classes 1 and 2 contain routing information and are expected to reach the same number of equipped vehicles. However, information packet of class 2 is expected to be propagated faster than information packet of class 1 as it contains information related to the traffic accident, which requires more imminent response from the vehicles. Information class 3 contains information related to the level of traffic congestion induced by the traffic accident. Hence, information packets of class 3 are expected to be received by all vehicles in the impacted area.

To achieve these objectives, let the number of communication servers assigned for information classes 1, 2 and 3 be 3, 5 and 5, respectively. The mean communication service rates for the three information classes are $u_1 = 0.42$ packets/second, $u_2 = 0.42$ packets/second, and $u_3 = 0.25$ packets/second. The numerical solution method will be used to calculate the information propagation speed and the proportion of informed vehicles (information spread) for the three information classes.

Figure 2.17(a) and 2.17(b) compare the backward and forward IFPW speeds of information classes 1 and 2, respectively. They illustrate that information packets in both classes are propagated very fast in the uncongested area which is not impacted by the traffic accident (see stages a and a' in Figure 2.17(a) and 2.17(b), respectively). The propagation speed decreases significantly when the information packets arrive at the congested area induced by the traffic accident (stages b and b' in Figures 2.17(a) and 2.17(b), respectively). This is because higher traffic density of vehicles can increase communication interference, causing significant communication failures. The IFPW speed is recovered to the original value when the congested area is passed to catch up with the normal traffic (stages c and c' in Figure 2.17(a) and 2.17(b), respectively). It is important to note that information packets in information class 2 are propagated faster than those in information class 1. For example, the information packets of information class 1 take about 3 minutes and 4 minutes 15 seconds, respectively, to reach the points G and H located at 9 km and 30 km, respectively. In comparison, it only takes 2 minutes and 3 minutes 45 seconds for information packets of information class 2 to reach the two locations, respectively. These results indicate that under heterogeneous conditions, controlling the number of communication servers assigned to each information class can significantly impact the time delay of the information packets to reach the targeted locations. Figure 2.17(a) and 2.17(b) also reveal that the information spread (i.e., $P_{I_j}^*$) is the same in space and time. This implies that the number of communication servers only impacts the propagation speed, but not the asymptotic proportion of informed vehicles.

Figure 2.17(c) shows that $P_{I_3^*} = 0.996$, implying that almost all equipped vehicles can receive information packets of class 3. Note that the number of assigned communication servers for information classes 2 and 3 are identical. Figure 2.17(b) and Figure 2.17(c) indicate that smaller mean communication service rate will enable more number of vehicles to receive the specific information packet in corresponding information class. The proposed method in this study can aid transportation operators to determine the mean communication service rate and the number of communication

servers assigned to each information class to control the information propagation performance under both homogeneous and heterogeneous traffic conditions.

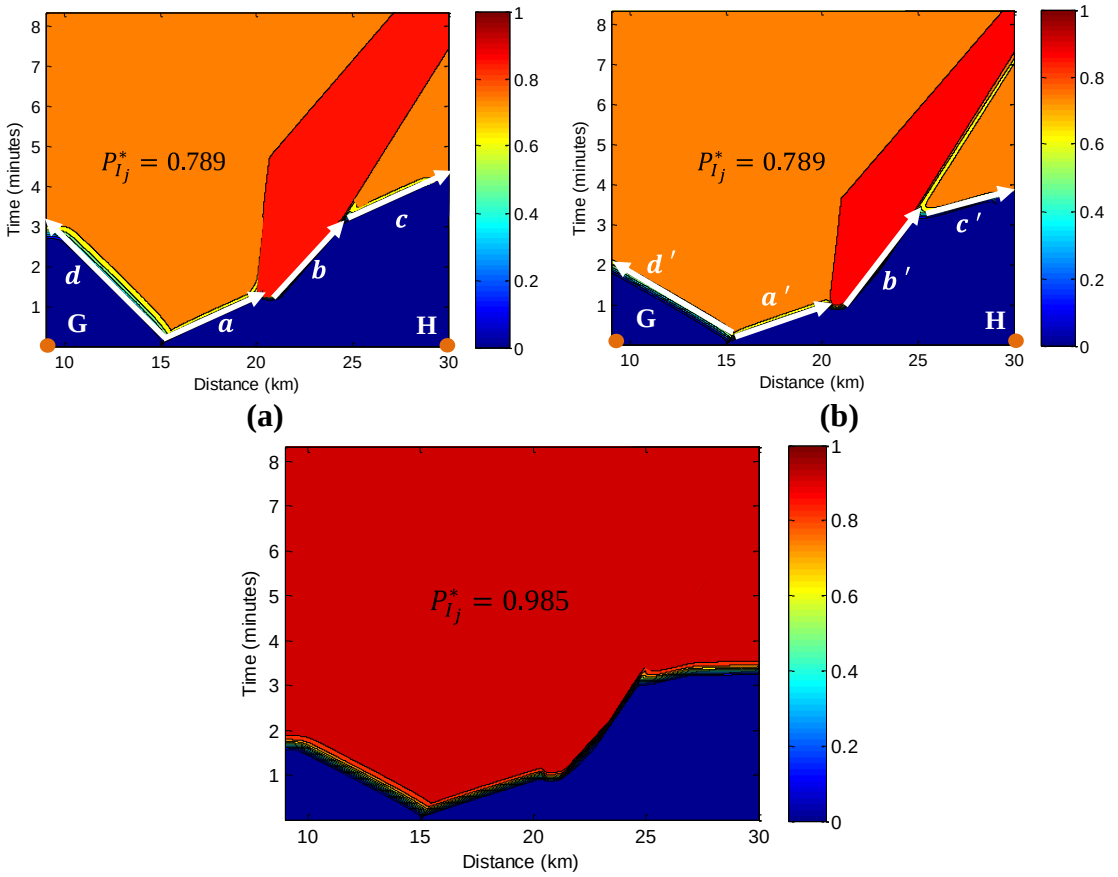

Figure 2.17: Contours of proportion of information-excluded vehicles of information packets of information classes 1, 2 and 3: (a) information class 1; (b) information class 2; (c) information class 3

3. Modelling and managing the integrated morning-evening commuting and parking patterns under the fully automated vehicle environment.

3.1 Introduction

Communication and automation technologies installed in connected and autonomous vehicles (CAVs) will significantly transform people's travel behavior in the future, mainly due to the following advantages. First, CAVs can enhance travel safety, and reduce traffic accidents caused by human errors (Assidiq et al., 2008). Second, CAVs can enhance roadway capacity by following each other closely. Studies suggest that highway capacity can be doubled if 60% of the vehicles are CAVs, and increased by 4 to 5 times if all vehicles are CAVs (Tientrakool et al., 2011). Third, CAVs require fewer inputs from human beings.

Hence, CAV users may have lower value of time (VOT) because they can spend the time during travel on other activities (van den Berg and Verhoef, 2016). Fourth, CAVs can improve energy efficiency by forming platoons. Studies show that CAVs can save 7%-15% of fuel consumption for light-duty CAVs and 15%-21% of fuel consumption for heavy truck CAVs by forming a CAV platoon (Shida et al., 2010; Shida and Nemoto, 2009; Bonnet and Fritz, 2000; Eben et al., 2013). CAVs will also lead to other benefits such as fewer parking spaces, reduced vehicle ownership, and reclamation of more green space. An overview of some of the advantages can be found in Fagnant and Kockelman (2015).

The aforementioned advantages can lead CAV users to have different route choice behaviors compared to human-driven vehicle (HDV) users. Here, HDVs are assumed to be not equipped with vehicle-to-vehicle (V2V) or vehicle-to-infrastructure (V2I) communication technologies that can enable seamless connectivity. The differential behaviors result in a mixed traffic flow pattern at the network level with the following three characteristics.

First, CAV flows can impact the route choices of HDV users. The travel time of mixed traffic flow is different from that of the single-class HDV flow due to the asymmetry in interactions involving HDVs and CAVs. For example, CAVs may follow HDVs using smaller headways, similar to how they would follow another CAV. By contrast, the driving behavior of HDVs can be different depending on whether they are following an HDV or a CAV. Hence, HDV drivers may perceive different travel times based on the CAV market penetration in the ambient traffic stream.

Second, travel cost in this mixed flow context includes the monetized travel time based on VOT, and the fuel consumption cost. Since VOT can be different for CAV and HDV users, the monetized travel time can also be different for them. Also, since route choice behaviors can be different for CAV and HDV users, fuel consumption costs can be different for them. Further, as CAVs can receive more accurate information on traffic conditions through seamless V2V and V2I connectivity (Ran et al., 2018, Ran et al., 2019), CAV users are more informed about shortest travel cost paths (which are not necessarily the shortest travel time paths).

Third, unlike HDVs, CAVs can have access to dedicated CAV facilities such as autonomous vehicle (AV) dedicated lanes. For example, some previous studies (Chen et al., 2016; Chen et al., 2017) propose the deployment of AV-dedicated lanes to foster CAV usage during the transition period from HDVs to CAVs to better exploit the advantages of CAVs. If AV-dedicated lanes exist in a traffic network, CAVs can use both AV-dedicated lanes and non-AV dedicated lanes (i.e., lanes can be accessed by both CAVs and HDVs) while HDVs can only use the non-AV dedicated lanes. Hence, CAVs can have a larger route choice set.

Levin and Boyles (2016) show that even if a small proportion of HDVs are replaced by CAVs, the redistributed network flows can reduce average travel time significantly. In summary, it is critical to estimate the network flows for effective transportation planning during the transition period when both CAVs and HDVs are in use.

To model the network flow under HDVs and CAVs, this study characterizes them as a mixed traffic flow. In transportation literature, such network flows are often estimated by formulating multiclass traffic assignment models, by extending the single-class traffic assignment model (such as the static user equilibrium (UE) model). These extensions can improve modeling realism by integrating the route choices of the users of different user classes using different disutility functions (Dafermos, 1972). Hence, static multiclass traffic assignment has been used to capture the heterogeneity in travel mode (Defermos, 1972; Florian, 1977; Chen et al., 2016; Levin and Boyles, 2015; Jiang et al., 2016), VOT (Yang and Huang, 1994; Nagurney and Dong, 2002), knowledge level of network conditions (Huang and Li, 2007; Huang and Lam, 2004), and risk-taking behavior (Shao et al., 2006; Lo et al., 2006).

Existing multiclass traffic assignment models are insufficient to estimate mixed traffic flows consisting of CAVs and HDVs for the following reasons. First, these models cannot accurately characterize the route choice behavior of HDV users. In particular, most multiclass traffic assignment studies adopt the perfect knowledge assumption and the static user equilibrium principle for route choices of HDV users (Chen et al., 2016; Levin and Boyles, 2015; Dafermos, 1972; Florian, 1977; Yang and Huang, 1994; Jiang et al., 2016). Some other studies (e.g., Huang and Lam, 2003; Shao et al., 2006; Huang and Li, 2007) adopt the logit-based stochastic user equilibrium (SUE) model to relax the perfect knowledge assumption of UE model for HDV users. Nonetheless, the SUE model suffers from the route overlap issue whereby the flows on routes with overlapping links are overestimated. This may deteriorate the estimation accuracy of mixed traffic flows significantly, raising issues of realism. Since the estimation of HDV flows significantly impacts the estimation of CAV flows, there is the need to more accurately characterize HDVs' route choices. Second, existing multiclass models ignore the asymmetry in driving interactions involving HDVs and CAVs, resulting in inaccurate travel time estimates which could affect flow allocations to routes. CAVs have lower reaction times and can respond to perturbations more quickly than HDVs. Further, CAVs can follow the vehicle in front of them more closely than HDVs, leading to increased link capacity. Thereby, the impact of one unit increase in CAV flow is different from that of a unit of HDV flow. Third, as discussed earlier, the route choice criteria of CAV users differ significantly from those of HDV users due to the reduced VOT, improved fuel economy, and the dedicated AV lanes. These new dimensions of routing criteria have not been considered in the literature, precluding holistic analyses of mixed traffic flows and the corresponding network equilibrium.

To more realistically characterize mixed traffic flows of CAVs and HDVs to support effective transportation planning in the emerging future, this study proposes a variational inequality-based multiclass traffic assignment model in which CAV users choose routes based on the UE principle and HDV users based on the cross nested-logit (CNL) model. The UE model characterizes the CAVs' capability to acquire accurate information on traffic conditions. The CNL model relaxes the strong knowledge-level assumption of the UE model and also overcomes the route overlap issue of logit-based SUE problem (Kitthamkesorn et al., 2016; Prashker and Bekhor, 1999). Remming (2001) illustrates the estimation effectiveness of the CNL model for HDV flows using the eastern Massachusetts

network. In our proposed model, the link cost functions integrate the difference in VOT and the asymmetry in interactions involving HDVs and CAVs, and the energy consumption savings through platooning in AV-dedicated lanes. Hence, the proposed multiclass traffic assignment model can enhance realism in characterizing mixed traffic flows.

Due to the complex analytical formulation of the CNL route choice model for HDVs, it is difficult to solve the proposed multiclass traffic assignment model efficiently using variational inequality-based algorithms such as projection-based algorithms (e.g., Nagurney, 2000; Nagurney and Dong, 2002; Jiang et al., 2016) or proximal point methods (e.g., Zhan and Ukkusuri, 2017). To address this problem, this study develops a new solution algorithm by integrating the self-regulated step size choice technique (Liu et al., 2009) into the concept of route swapping strategy (Smith, 1984). One advantage of the proposed algorithm is that, in each iteration, it finds the descent direction according to an analytical model to circumvent solving a computationally-intensive subproblem in the aforementioned algorithms. Another advantage is that the proposed algorithm updates the step size adaptively using information on the descent directions of the current iteration and the previous iteration. We provide rigorous analyses of the convergence of the solution algorithm. The proposed algorithm also resolves the convergence difficulty of the existing route-swapping-based algorithm (Huang and Lam, 2002).

To enhance applicability, this study further derives the analytical formula for the sensitivity analysis of the proposed model. In practice, planned (e.g., road maintenance, construction) or unexpected (e.g., accidents, facility failure, natural disasters) events can impact network flows significantly. Sensitivity analysis can help transportation decision-makers to estimate the impact of these events on network flows, and design better response and recovery strategies to reduce their negative effects. Besides, sensitivity analysis of the traffic assignment models can also be leveraged to design effective solution algorithms for continuous network design problems. There is limited literature for sensitivity analysis for multiclass traffic assignment models although extensive studies are available for single-class traffic assignment models (Yang and Bell, 2005; Tobin and Friesz, 1988; Clark and Watling, 2000). In particular, this study derives sufficient conditions for the existence of derivatives for HDV and CAV equilibrium link flows.

The contributions of the study are fourfold. First, this study finds a sufficient and necessary condition for the equilibrium state of the CNL model, and formulates a new equivalent variational inequality (VI) problem for it. In contrast to the equivalent mathematical programming problem for the CNL model developed by Prashker and Bekhor (1999), the variational inequality (VI) formulation of the CNL model contains only path flow variables. It facilitates developing the multiclass traffic assignment, solution algorithm, and sensitivity analysis method for mixed traffic flow of HDVs and CAVs. Second, a multiclass traffic assignment model is proposed where the routing behaviors of HDVs and CAVs follow the CNL and UE principles, respectively. The proposed model provides enhanced behavioral realism by integrating into the travel cost functions the impacts of heterogeneous VOT and asymmetry in interactions involving HDVs and CAVs. Thereby, this model enables planners to better estimate network flows to support effective transportation planning during the transition to a fully CAV future. Third, this study

develops a new solution algorithm based on the route-swapping concept to solve the proposed multiclass traffic assignment model efficiently. Comparison shows that the proposed algorithm has a convergence speed superior to that of the existing route-swapping-based algorithm (Huang and Lam, 2002), obtained by adaptively updating the step size in each iteration using a modified self-regulated step-size choice technique. Fourth, an analytical formula is derived for the sensitivity analysis of the proposed model, which enables planners to quickly estimate the perturbed traffic equilibrium and identify critical elements under planned or unexpected disruptive events. It can also be used to solve the continuous network design problem (e.g., to find optimal signal timing or tolling strategy to improve system performance under mixed traffic flows) with multiclass traffic flows.

The remainder of the paper is organized as follows. Section 2 introduces the CNL model and an equivalent VI problem to characterize the equilibrium state. Section 3 presents the proposed multiclass traffic assignment model where HDVs and CAVs choose routes according to the CNL model and UE principle, respectively. Section 4 develops the solution algorithm for the proposed model, and Section 5 discusses the results of numerical experiments for the proposed model and the performance of its solution algorithm. Section 6 introduces the sensitivity analysis method for the proposed multiclass traffic assignment model. Section 7 numerically applies the sensitivity analysis method to approximate the equilibrium link flow solutions of HDVs and CAVs. Section 8 concludes with the main findings, insights, and potential future research directions.

3.2 Cross-nested logit model and its equivalent VI problem

This section develops a VI-based traffic assignment model for HDV flows that assumes HDV drivers choose routes according to the CNL principle. In this section, all vehicles are assumed to be HDVs. To differentiate from the CAV flows in the multiclass traffic assignment model, this section contains a subscript H indicating HDVs. Consider a transportation network $G(\boldsymbol{N}_H, \boldsymbol{\Gamma}_H)$, where $\boldsymbol{N}_H$ represents the set of nodes and $\boldsymbol{\Gamma}_H$ represents the set of links that can be accessed by HDVs. Let W_H denote the set of origin-destination (OD) pairs for HDVs, and R_H^w denote the set of paths connecting OD pair $w \in W_H$. Denote $v_{a,H}$ and $t_{a,H}$ as the HDV flow and HDV travel cost on link $a \in \boldsymbol{\Gamma}_H$, respectively. Let $\mathbf{t}_H$ be the vector of HDV link travel costs and $\mathbf{v}_H$ be the vector of HDV link flows. The HDV flow on path k of OD pair w is denoted by $f_{k,H}^w$, $k \in R_H^w$. Let $\mathbf{f}_H$ be the vector of HDV flows of all paths in the network. Denote q_H^w as the demand of HDVs for OD pair w, and $\mathbf{q}_H$ as the vector of HDV traffic demand for all OD pairs. Let Δ_H and Λ_H denote the link-path and OD-path incidence matrices, respectively. Additional notation will be introduced when necessary.

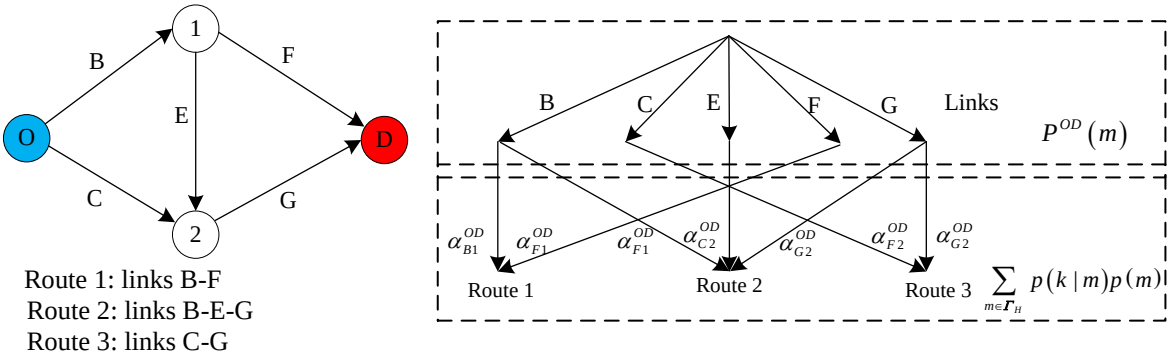

Figure 3.1: Illustration of the hierarchical structure of the CNL model

Vovsha (1997) derived the CNL model based on McFadden's (1981) generalized extreme value (GEV) function for mode choice split. Prashker and Bekhor (1999) extended it to characterize user's route choices. Figure 3.1 shows a small example to demonstrate how the CNL model overcomes the route overlap problem. It contains one OD pair and three routes. Route 2 overlaps with route 1 and route 3 through shared links B and G, respectively. As shown in Figure 1, the CNL model consists of two layers, where the upper layer contains all links in the network and the lower layer consists of all potential path choices. Each path in the CNL model is assigned to the upper nests (links) which are used by this path, and each nest in the upper layer groups all paths sharing the specific overlapped link. The CNL model introduces an inclusion coefficient ($\alpha_{m,k}^{w}, m \in \boldsymbol{\Gamma}_H$) for each path $k \in R_H^w$ and link m to denote the overlapping degree of this path with other paths in nest $m \in \boldsymbol{\Gamma}_H$, $\sum_{m\in\boldsymbol{\Gamma}_H} \alpha_{m,k}^{w} = 1$ (Prashker and Bekhor, 1999). Thereby, the CNL model accounts for the covariance between paths under each nest that addresses the route overlap problem. According to the CNL model, the probability of a user choosing path k of OD pair w (labelled as $p^w(k)$) can be written as the product of the marginal probability $p^w(m)$ and conditional probability $p^w(k|m)$:

$$p^w(k) = \sum_{m\in\boldsymbol{\Gamma}_H} p^w(k|m)p^w(m) \tag{3.1a}$$

where

$$p^w(k|m) = \frac{\left[\alpha_{m,k}^{w}\exp(-\theta c_{k,H}^{w})\right]^{1/u}}{\sum_{l\in R_H^w}\left[\alpha_{m,l}^{w}\exp(-\theta c_{l,H}^{w})\right]^{1/u}} \tag{3.1b}$$

$$p^w(m) = \frac{\left(\sum_{k\in R_H^w}\left[\alpha_{m,k}^{w}\exp(-\theta c_{k,H}^{w})\right]^{1/u}\right)^{u}}{\sum_{b\in\boldsymbol{\Gamma}_H}\left(\sum_{l\in R_H^w}\left[\alpha_{b,l}^{w}\exp(-\theta c_{l,H}^{w})\right]^{1/u}\right)^{u}} \tag{3.1c}$$

Here, u is the degree of nesting, $0 < u \leq 1$, θ is the dispersion parameter, and $c_{k,H}^{w}$ is the travel cost of path k of OD pair $w \in W_H$, which depends on the flows on links used by that

path. Cascetta et al. (1996) provide the following formulation for the inclusion coefficient ($\alpha_{m,k}^{w}, m \in \boldsymbol{\Gamma}_H$):

$$\alpha_{m,k}^{w} = \left(\frac{l_m}{l_k^w}\right)^{\gamma} \delta_{m,k}^{w} \tag{3.2}$$

where l_m and l_k^w are the length of link m and path k of OD pair w, respectively, and $\delta_{m,k}^{w} = 1$ if path k uses link m and 0 otherwise. Eq. (3.1) denotes that, as the degree of nesting tends to 0, the CNL model becomes the logit model. Note that the inclusion coefficients determined by Eq. (3.2) are independent of the link travel cost, which is a necessary condition to derive the CNL model from the GEV class. If the inclusion coefficient is proportional to link costs instead of link lengths, then $\alpha_{m,k}^{w}$ depends on traffic congestion. However, this will lead to a more complex analytical structure of the route-choice function rather than Eq. (3.1). Hence, this study analyzes the CNL model constructed using Eq. (3.1) derived based on the inclusion coefficients determined by Eq. (3.2).

According to Marzano and Papola (2008), for two arbitrary paths k_1, k_2 connecting OD pair w, the covariance of the two paths $Cov(k_1, k_2)$ can be expressed analytically as:

$$Cov(k_1, k_2) = \frac{\pi^2}{6\theta}(1-u^2)\sum\nolimits_{m\in\boldsymbol{\Gamma}_H}\left(\alpha_{m,k_1}^{w}\right)^{1/2}\left(\alpha_{m,k_2}^{w}\right)^{1/2}$$

This equation shows that the covariance of both paths increases with respect to both α_{m,k_1}^{w} and α_{m,k_2}^{w}, $m \in \boldsymbol{\Gamma}_H$. Prashker and Bekhor (1999) developed a CNL equivalent mathematical program to characterize users' route choices. However, it cannot be extended to model the route choices of mixed traffic flow due to the asymmetric impacts of HDVs and CAVs on link travel cost. Further, beyond path flows, the decision variables in the mathematical program are path flows belonging to different nests. Hence, this program contains a large number of decision variables, which scales the computational complexity for a large-size network. To model multiclass traffic assignment with mixed flow of CAVs and HDVs, this section develops an equivalent VI problem which contains only path flow variables.

In a large network, some paths are less likely to be used. Such paths are excluded from analysis in this study. Suppose R_H^w contains only paths that are likely to be used. To characterize the equilibrium condition of the CNL model, let $C_{k,H}^{w}$ be the generalized travel cost of path k for HDVs for OD pair w, formulated as:

$$C_{k,H}^{w} = c_{k,H}^{w} - \frac{u}{\theta}H_{k,H}^{w} + \frac{u}{\theta}ln\left(\frac{f_{k,H}^{w}}{q_H^w}\right) \tag{3.3}$$

where

$$H_{k,H}^{w} = ln\left[\sum_{m\in\Gamma_H}\left(\alpha_{m,k}^{w}\right)^{1/u}\left(\sum_{l\in R_H^w}\left[\alpha_{m,l}^{w}\exp(-\theta c_{l,H}^{w})\right]^{1/u}\right)^{u-1}\right] \tag{3.4}$$

The following Proposition provides the sufficient and necessary conditions for the equilibrium state of the CNL model. This proposition will be used to develop the equivalent VI-based traffic assignment model which will be embedded in the multiclass traffic assignment model in Section 3.

Proposition 1: The CNL path flows $\mathbf{f}_H^* = \left\{f_{k,H}^{w*}, \forall w \in W_H, \forall k \in R_H^w\right\}$ are at equilibrium if and only if the generalized travel cost of all paths for the corresponding OD pair is the same, i.e., $\mathbf{f}_H^*$ satisfies

$$C_{k,H}^{w}(\mathbf{f}_H^*) = \tau_H^w, \text{ for } \forall w \in W_H, \forall k \in R_H^w \tag{3.5}$$

where $\mathbf{f}_H^* \in \boldsymbol{\Omega}_{\mathbf{f}_H} = \{\mathbf{f}|\Lambda_H\mathbf{f}_H = \mathbf{q}_H, \mathbf{f}_H \geq 0\}$ and τ_H^w is a real value.

Proof: We first prove the sufficiency (the "if" part) condition. Based on Eq. (3.3), the probability that a path k is chosen by a traveler for an OD pair w is:

$$p^w(k) = \frac{f_{k,H}^{w}}{q_H^w} = \exp\left(\frac{\theta}{u}C_{k,H}^{w} - \frac{\theta}{u}c_{k,H}^{w} + H_{k,H}^{w}\right) \tag{3.6}$$

Note that the sum of the probabilities for all paths for OD pair w (i.e, R_H^w) is equal to 1. Thereby,

$$\sum_{j\in R_H^w} p^w(j) = 1 \tag{3.7}$$

Substituting Eq. (3.6) into Eq. (3.7) yields

$$\sum_{j\in R_H^w} p^w(j) = \sum_{j\in R_H^w}\exp\left(\frac{\theta}{u}C_{j,H}^{w} - \frac{\theta}{u}c_{j,H}^{w} + H_{j,H}^{w}\right) = 1$$

Based on Eq. (3.5), the generalized travel cost for all paths for an OD pair is the same. Thereby,

$$\exp\left(\frac{\theta}{u}C_{k,H}^{w}\right) = \exp\left(\frac{\theta}{u}\tau_H^w\right) = \frac{1}{\sum_{j\in R_H^w}\exp\left(-\frac{\theta}{u}c_{j,H}^{w} + H_{j,H}^{w}\right)} \tag{3.8}$$

Substituting Eq. (3.8) into Eq. (3.6), we have

$$p^w(k) = \frac{\exp\left(-\frac{\theta}{u}c_{k,H}^{w} + H_{k,H}^{w}\right)}{\sum_{j\in R_H^w}\exp\left(-\frac{\theta}{u}c_{j,H}^{w} + H_{j,H}^{w}\right)} \tag{3.9}$$

$$= \frac{\exp\left(-\frac{\theta}{u}c_{k,H}^{w} + ln\left[\sum_{m\in\boldsymbol{\Gamma}_H}\left(\alpha_{m,k}^{w}\right)^{1/u}\left(\sum_{l\in R_H^w}\left[\alpha_{m,l}^{w}\exp(-\theta c_{l,H}^{w})\right]^{1/u}\right)^{u-1}\right]\right)}{\sum_{j\in R_H^w}\exp\left(-\frac{\theta}{u}c_{j,H}^{w} + ln\left[\sum_{b\in\boldsymbol{\Gamma}_H}\left(\alpha_{b,j}^{w}\right)^{1/u}\left(\sum_{i\in R_H^w}\left[\alpha_{b,i}^{w}\exp(-\theta c_{i,H}^{w})\right]^{1/u}\right)^{u-1}\right]\right)}$$

$$= \frac{\exp\left(-\frac{\theta}{u}c_{k,H}^{w} + ln\left[\sum_{m\in\boldsymbol{\Gamma}_H}\left(\alpha_{m,k}^{w}\right)^{1/u}\left(\sum_{l\in R_H^w}\left[\alpha_{m,l}^{w}\exp(-\theta c_{l,H}^{w})\right]^{1/u}\right)^{u-1}\right]\right)}{\sum_{j\in R_H^w}\left(\sum_{b\in\boldsymbol{\Gamma}_H}\left(\alpha_{b,j}^{w}\exp(-\theta c_{j,H}^{w})\right)^{1/u}\left(\sum_{i\in R_H^w}\left[\alpha_{b,i}^{w}\exp(-\theta c_{i,H}^{w})\right]^{1/u}\right)^{u-1}\right)}$$

$$= \frac{\sum_{m\in\boldsymbol{\Gamma}_H}\left\{\left[\alpha_{m,k}^{w}\exp(-\theta c_{k,H}^{w})\right]^{1/u}\left(\sum_{l\in R_H^w}\left[\alpha_{m,l}^{w}\exp(-\theta c_{l,H}^{w})\right]^{1/u}\right)^{u-1}\right\}}{\sum_{b\in\boldsymbol{\Gamma}_H}\left(\sum_{i\in R_H^w}\left[\alpha_{b,i}^{w}\exp(-\theta c_{i,H}^{w})\right]^{1/u}\right)^{u}}$$

Eq. (3.10) is consistent with the CNL route choice model shown in Eq. (3.1). The proof of the "if" is done.

Next, we prove the necessity (the "only if" part) condition. Suppose $\mathbf{f}_H^* = \left\{f_{k,H}^{w*}, \forall w \in W_H, \forall k \in R_H^w\right\}$ is the equilibrium path flow for the CNL model. Then, $\mathbf{f}_H^*$ satisfies Eq. (3.1), or equivalently, Eq. (3.9). Note that $f_{k,H}^{w*}/q_H^w = p^w(k)$. According to Eq. (3.3) and Eq. (3.9), we have

$$C_{k,H}^{w} = c_{k,H}^{w} - \frac{u}{\theta}H_{k,H}^{w} + \frac{u}{\theta}ln\left(\frac{f_{k,H}^{w*}}{q_H^w}\right)$$

$$= c_{k,H}^{w} - \frac{u}{\theta}H_{k,H}^{w} + \frac{u}{\theta}ln\left(p^w(k)\right)$$

$$= c_{k,H}^{w} + \frac{u}{\theta}ln\left(\frac{p^w(k)}{\sum_{m\in\boldsymbol{\Gamma}_H}\left(\alpha_{m,k}^{w}\right)^{\frac{1}{u}}\left(\sum_{l\in R_H^w}\left[\alpha_{m,l}^{w}\exp\left(-\theta c_{l,H}^{w}\right)\right]^{1/u}\right)^{u-1}}\right)$$

$$= c_{k,H}^{w} + \frac{u}{\theta}ln\left(\frac{\exp\left(-\frac{\theta}{u}c_{k,H}^{w}\right)}{\sum_{b\in\boldsymbol{\Gamma}_H}\left(\sum_{i\in R_H^w}\left[\alpha_{b,i}^{w}\exp(-\theta c_{i,H}^{w})\right]^{1/u}\right)^{u}}\right)$$

$$= c_{k,H}^{w} - c_{k,H}^{w} + \frac{u}{\theta}ln\left(\frac{1}{\sum_{b\in\boldsymbol{\Gamma}_H}\left(\sum_{i\in R_H^w}\left[\alpha_{b,i}^{w}\exp(-\theta c_{i,H}^{w})\right]^{1/u}\right)^{u}}\right) \tag{3.10}$$

$$= -ln\left(\sum_{b\in\boldsymbol{\Gamma}_H}\left(\sum_{i\in R_H^w}\left[\alpha_{b,i}^{w}\exp(-\theta c_{i,H}^{w})\right]^{1/u}\right)^{u}\right)$$

Eq. (3.10) shows that for an arbitrary OD pair $w \in W_H$, the generalized travel costs of all paths for this OD pair are identical. This completes the proof. ■

According to Proposition 1, the CNL equilibrium state for HDVs can be expressed as follows. At equilibrium, no HDV user can unilaterally change his/her path to reduce the generalized travel cost. Eq. (3.3) also shows that if $u = 1$, $C_{k,H}^{w} = c_{k,H}^{w} + \frac{1}{\theta} ln\left(\frac{f_{k,H}^{w}}{q_H^w}\right)$, which is the generalized travel cost for logit-based SUE model (Guo and Huang, 2016). Thereby, the logit-based SUE condition is a special case of CNL equilibrium. Following Wie et al. (1995) and Nagurney (2000), the conditions in Proposition 1 can further be expressed by a finite-dimensional VI problem as follows:

$$\sum_{w \in W_H} \sum_{k \in R_H^w} C_{k,H}^{w}\left(f_{k,H}^{w} - f_{k,H}^{w*}\right) \geq 0 \tag{3.11}$$

where $\mathbf{f}_H^*, \mathbf{f}_H \in \boldsymbol{\Omega}_{\mathbf{f}_H}$.

Note that the VI-based CNL traffic assignment model (3.11) is developed upon the generalized travel path cost Eq. (3.3) and Proposition 1. It only incorporates the path flow variables, and is fundamentally different from the mathematical programming problem for CNL model developed by Prashker and Bekhor (1999). This model will be used to develop a multiclass traffic assignment model for mixed flows in which the impacts of HDVs and CAVs on link travel cost are asymmetric. The CNL equilibrium path flow solution can be obtained by solving the VI problem (3.11). The VI-based equivalent problem for CNL model enables solving the CNL equilibrium path flow using VI-based solution algorithm (e.g., projection method). It also facilitates developing the multiclass traffic assignment model for mixed traffic of HDVs and CAVs, designing corresponding solution algorithm and the sensitivity analysis method for the multiclass traffic assignment model. Note that the path flow solution of the CNL model is unique (Prashker and Bekhor, 1999) under the assumption that the link travel cost function is strictly monotonic on traffic flows. Thereby, the path flow solution to the VI problem (3.11) is also unique under the same assumption.

Note that for a large network the set of paths that are likely to be used by the travelers impact the equilibrium result of VI problem (3.11) and the convergence speed of the solution algorithm developed in Section 4 for the multiclass traffic assignment model. The approaches to finding the set of these paths can be categorized into two classes, deterministic and probabilistic approaches. Deterministic approaches assume travelers perceive the link attributes exactly and their preferences are deterministic. The probabilistic approaches are built on repeated shortest path search, where link impedances or individual preferences are randomly drawn from certain probability distributions (Haghani, et al., 2016). Deterministic approaches include the K-shortest paths approach (Lombard and Church, 1993; Hunt and Kornhauser, 1997), the labelling approach (Ben-Akiva et al., 1984), the link elimination approach (Azevedo et al., 1993), and the link penalty approach (De la Barra et al., 1993). The K-shortest paths approach finds the heterogeneous paths according to different measures of dissimilarity. The labelling approach generates paths based on the idea that travelers have different route choice objectives, each of which determines one optimum path. The link elimination approach and the link penalty approach generate disjoint paths by either removing the links or increasing the impedances of the links on the shortest path found in each iteration. For probabilistic approaches, Fiorenzo-

Catalano and Van der Zijpp (2001) applied Monte Carlo simulation to find the paths assuming traveler's perception error of the link impedance following a certain distribution. Chen and Ji (2006) proposed three stochastic models to find the paths that are likely to be used by travelers considering travel time uncertainty. This study will use the link penalty approach proposed by De la Barra et al (1993) to find the paths due to its ease of implementation and computational efficiency for path-based traffic assignment methods (Chen et al., 2012; Wang et al., 2018).

3.3 Multiclass traffic assignment model for mixed traffic flow of HDVs and CAVs

This section seeks to develop a static multiclass traffic assignment model to characterize the route choice behavior of travelers in mixed traffic flow consisting of HDVs and CAVs. Note that dynamic traffic assignment (DTA) models have been used to characterize the route choice behavior of CAVs and HDVs using cell transmission models (CTM) (Levin and Boyles, 2016) or link transmission models (LTM) (Melson et al., 2018). These DTA models can capture the traffic flow dynamics more accurately compared to static traffic assignment models. Thereby, they can be leveraged to analyze the effectiveness and efficiency of an operational strategy (e.g., dynamic transit lanes) to improve the traffic system. However, DTA models in a practical context involve simulation of the time-dependent traffic flow which is computationally extensive. Furthermore, they are characterized by inherent mathematical intractability (Peeta and Ziliaskopoulos, 2000). It is hard to design an efficient solution algorithm for a network design problem (e.g., optimal AV dedicated lane deployment etc.) constructed on a DTA model. Thereby, it has limitations in its ability to be leveraged to address needs arising in the transportation planning context. To address this problem, we will develop a static multiclass traffic assignment model in this section. Static traffic assignment is usually applied for network design problems (see e.g., Yang and Huang, 2004; Wang and Lo, 2010). Further, Section 6 will derive the sensitivity analysis method for the proposed multiclass traffic assignment model which can be applied to solve continuous network design problems constructed upon the static multiclass traffic assignment model efficiently. In addition, this study uses a CNL model to capture travelers' perception error of travel cost rather than the UE model used in previous studies (Levin and Boyles,2016; Melson et al., 2018).

3.3.1 Link travel cost functions for HDVs and CAVs

The transition period towards full autonomy will consist of mixed traffic of HDVs and CAVs. Let $\boldsymbol{\Gamma}_1$ be the set of AV-dedicated lanes in the network if such lanes are deployed. To analyze the attractiveness of AV-dedicated lanes and the impact of VOT, we assume that the link travel cost of both CAVs and HDVs consists of two parts: travel time and fuel consumption costs. Both travel time and fuel consumption are converted into equivalent monetary costs. This assumption is also used by Levin and Boyles (2015) to study the effects of AV ownership on trip, mode, and route choice. To determine the link travel times of CAVs and HDVs in the mixed flow, the Bureau of Public Roads (BPR) function is used. It is a strictly monotone function of traffic flows.

$$\bar{t}_a(v_{a,H}, v_{a,A}) = \frac{l_a}{s_a}\left[1 + \left(\frac{v_{a,H} + v_{a,A}}{Q_a}\right)^4\right], a \in \boldsymbol{\Gamma}_H \tag{3.12a}$$

$$\bar{t}_a(v_{a,A}) = \frac{l_a}{s_a}\left[1 + \left(\frac{v_{a,A}}{Q_{a,A}}\right)^4\right], a \in \boldsymbol{\Gamma}_1 \tag{3.12b}$$

where $\bar{t}_a(v_{a,H}, v_{a,A})$ is the link travel time of either a CAV or a HDV, and $\boldsymbol{\Gamma}_H$ is the set of regular links (i.e., links not dedicated to AVs) which can be used by both HDVs and CAVs. s_a is the free-flow speed of link a, Q_a is the capacity of link a with mixed traffic flow, $Q_{a,A}$ is the capacity of a link with pure CAV flow, and $v_{a,A}$ is the CAV flow on link a.

As discussed in Section 1, CAVs and HDVs have different driving behaviors in mixed traffic. In this study, we assume that CAVs can follow leading vehicles (either a CAV or HDV) with smaller headways than HDVs due to the reduced reaction times. Hence, the capacity of a regular link a (i.e., Q_a) is a function of the proportion of CAVs as the time headway of CAVs is smaller (Levin and Boyles, 2016). Let ω_H and ω_A ($\omega_A < \omega_H$) be the reaction times of HDVs and CAVs, respectively. Denote ς as the average vehicle length. According to Levin and Boyles (2016), if the reaction times for HDVs and CAVs are equal across the vehicles in the same class, the capacity of a regular link with mixed traffic flow can be formulated as

$$Q_a = s_a \frac{1}{s_a\left(\frac{v_{a,H}}{v_{a,H} + v_{a,A}}\omega_H + \frac{v_{a,A}}{v_{a,H} + v_{a,A}}\omega_A\right) + \varsigma}, \tag{3.13}$$

According to Eq. (3.13), if all vehicles in a regular link are HDVs, then

$$Q_{a,H} = N_a \cdot s_a \frac{1}{s_a\omega_H + \varsigma}, \tag{3.14}$$

where $Q_{a,H}$ denotes the link capacity for pure HDV flow, and N_a is the number of lanes on link a. According to Eq. (3.14),

$$\omega_H = \frac{1}{Q_{a,H}} - \frac{\varsigma}{s_a}, \tag{3.15}$$

Similarly,

$$\omega_A = \frac{1}{Q_{a,A}} - \frac{\varsigma}{s_a}, \tag{3.16}$$

where $Q_{a,A}$ denotes the link capacity for pure CAV flow. Submitting Eq. (3.15) and Eq. (3.16) into Eq. (3.13),

$$Q_a = \frac{1}{\frac{v_{a,H}}{v_{a,H}+v_{a,A}}\frac{1}{Q_{a,H}} + \frac{v_{a,A}}{v_{a,H}+v_{a,A}}\frac{1}{Q_{a,A}}} \tag{3.17}$$

Note $Q_{a,A} \geq Q_{a,H}$ as the reaction times of CAVs are no larger than those of HDVs (Levin and Boyles, 2016). From Eq. (3.12a) and Eq. (3.17), the increase in link travel time through a unit increase in CAV flow is no larger than that of a unit increase in HDV flow as link capacity can be improved due to increased proportion of CAVs. Thereby, the marginal effects of CAV and HDV flows on link travel time are asymmetric.

To quantify the benefits of energy savings from a CAV platoon on an AV-dedicated lane, the fuel consumption of a vehicle on a link will be estimated and incorporated into the link cost function. We assume all vehicles (either HDVs or CAVs) are light-duty gasoline vehicles. Based on field experiments, Zhang et al. (2014) show that the gasoline consumption rate (per vehicle-mile) of a vehicle is an exponential function of the average traffic speed. Thereby, the total fuel consumption of a vehicle driving on a regular link $a \in \boldsymbol{\Gamma}_H$ can be estimated as

$$E_a = \vartheta_1 \left(\frac{L_a}{\bar{t}_a(v_{a,H}, v_{a,A})} \right)^{-\vartheta_2} l_a, \tag{3.18}$$

where l_a is the length of link a, $l_a/\bar{t}_a(v_{a,H}, v_{a,A})$ is the average travel speed of a vehicle on regular link a, and $\vartheta_1 > 0$ and $0<\vartheta_2 < 1$ are positive coefficients that need to be estimated.

Compared to a regular link, AV-dedicated lanes not only reduce CAV travel times, but also enhance their fuel efficiency by allowing them to form platoons to minimize air resistance. To account for the reduced energy consumption due to platooning, a discount factor σ will be used with E_a to account for energy savings for a CAV on an AV-dedicated lane. Thereby, the link travel cost of HDVs and CAVs can be formulated as follows:

$$t_{a,z} = \bar{t}_a(v_{a,H}, v_{a,A}) \cdot VOT_z + \eta \cdot E_a, a \in \boldsymbol{\Gamma}_H, z \in \{HDV, CAV\} \tag{3.19a}$$

$$t_{a,A} = \bar{t}_a(v_{a,A}) \cdot VOT_A + \sigma \cdot \eta \cdot E_a, a \in \boldsymbol{\Gamma}_1 \tag{3.19b}$$

where z denotes vehicle class. VOT_H and VOT_A are the value of time for HDV users and CAV users, respectively. η is the price per unit of gasoline, and σ is the percentage fuel consumption savings due to platooning. Note that the link travel cost functions defined by Eq. (3.19a) and Eq. (3.19b) are strictly monotonic with respect to link flow of either HDVs or CAVs.

3.3.2 Multiclass traffic assignment model

Let W_A be the set of OD pairs and R_A^w be the set of routes connecting OD pair $w \in W_A$ for CAVs. The set R_A^w contains the set R_H^w as all paths for HDVs can be used by CAVs. Denote $c_{k,A}^w$ and $C_{k,A}^w$ as the travel cost of path k and generalized travel cost of path k

for CAVs for OD pair w, respectively. The vector of CAV travel costs and CAV flows of all links and are denoted by $\mathbf{t}_A$ and $\mathbf{v}_A$, respectively. Denote $f_{k,A}^w$ as the CAV flow of path k for OD pair w and $\mathbf{f}_A$ as the vector of CAV flows of all paths. Let q_A^w be the CAV demand for OD pair w, $\mathbf{q}_A$ be the vector of CAV demands of all OD pairs, and Δ_A and Λ_A be the link-path and OD-path matrices, respectively.

Unlike HDVs, CAVs can obtain information on traffic conditions through vehicle-to-infrastructure and vehicle-to-vehicle communications. Thereby, we assume that CAVs have perfect knowledge of traffic conditions and can always choose paths with the minimum travel cost for the corresponding OD pairs, implying a static UE at equilibrium. In this context, $C_{k,A}^w = c_{k,A}^w, \forall k \in R_A^w, \forall w \in W_A$. Suppose $\mathbf{f}_A^* = \left[f_{k,A}^{w*}, \forall k \in R_A^w, \forall w \in W_A\right]$ is the UE path flow solution for CAVs; then, the generalized path travel cost of CAVs must satisfy:

$$C_{k,A}^w = c_{k,A}^w = \begin{cases} \tau_A^w, \text{if } f_{k,A}^{w*} > 0 \\ \geq \tau_A^w, \text{if } f_{k,A}^{w*} = 0 \end{cases}, \forall k \in R_A^w, \forall w \in W_A, \tag{3.20}$$

where $\mathbf{\Omega}_{\mathbf{f}_A} = \{\mathbf{f}_A | \Lambda_A \mathbf{f}_A = \mathbf{q}_A, \mathbf{f}_A \geq 0\}$, and τ_A^w is the cost of the shortest routes for CAVs. Note that for notational convenience, the generalized route travel cost $C_{k,A}^w$ will be used hereafter to model the multiclass traffic assignment model instead of $c_{k,A}^w$ as they are identical for CAVs.

According to equilibrium conditions (3.5) and (3.20), it can be shown that the path flows $(\mathbf{f}_H^{T*}, \mathbf{f}_A^{T*})$ are the equilibrium state of the CNL model and UE model for HDVs and CAVs, respectively, if and only if they satisfy the following VI problem:

$$\sum_{w \in W_H} \sum_{k \in R_H^w} C_{k,H}^w(\mathbf{f}_H^*, \mathbf{f}_A^*)\left(f_{k,H}^w - f_{k,H}^{w*}\right) + \sum_{w \in W_A} \sum_{k \in R_A^w} C_{k,A}^w(\mathbf{f}_H^*, \mathbf{f}_A^*)\left(f_{k,A}^w - f_{k,A}^{w*}\right) \geq 0, \tag{3.21}$$

where $[\mathbf{f}_H^T, \mathbf{f}_A^T], [\mathbf{f}_H^{T*}, \mathbf{f}_A^{T*}] \in \mathbf{\Omega}_{\mathbf{f}} = \{[\mathbf{f}_H^T, \mathbf{f}_A^T] | \Lambda_H \mathbf{f}_H = \mathbf{q}_H;\ \Lambda_A \mathbf{f}_A = \mathbf{q}_A; \mathbf{f}_H \geq 0; \mathbf{f}_A \geq 0\}$. The superscript ^{T} denotes transpose. The VI problem (3.21) is a multiclass traffic assignment model that characterizes the equilibrium state of the route flow of HDVs and CAVs. The equivalence between VI problem (3.21) and the two equilibrium conditions in Eq. (3.5) and Eq. (3.20) can be shown using the method in Nagurney (2000). It is omitted here to avoid duplication. Let $\mathbf{C}_H$ and $\mathbf{C}_A$ be the vector of generalized costs of all paths for HDVs and CAVs, respectively. Denote $\mathbf{C}_H^*$ and $\mathbf{C}_A^*$ as the generalized costs of all paths for HDVs and CAVs at the equilibrium state $[\mathbf{f}_H^{T*}, \mathbf{f}_A^{T*}]$, respectively. The VI problem (3.21) can be written in vector form:

$$\mathbf{C}_H^*(\mathbf{f}_H - \mathbf{f}_H^*)^T + \mathbf{C}_A^*(\mathbf{f}_A - \mathbf{f}_A^*)^T \geq 0, \tag{3.22}$$

where $[\mathbf{f}_H^T, \mathbf{f}_A^T] \in \mathbf{\Omega}_{\mathbf{f}}$. Note $\sum_{w \in W_A} \sum_{k \in R_A^w} C_{k,A}^w(\mathbf{f}_H^*, \mathbf{f}_A^*)\left(f_{k,A}^w - f_{k,A}^{w*}\right) = \sum_{a \in \Gamma_A} t_{a,A}(\mathbf{f}_H^*, \mathbf{f}_A^*)\left(v_{a,A}^w - v_{a,A}^{w*}\right)$, where $\boldsymbol{\Gamma}_A$ is the set of links for CAVs, $v_{a,A}^{w*}$ is the equilibrium flow of CAVs on link a at the equilibrium state $(\mathbf{f}_H^{T*}, \mathbf{f}_A^{T*})$. The VI problem (3.21) can be reformulated as follows by defining it on path flows of HDVs and link flows of CAVs:

$$\sum_{w\in W_H}\sum_{k\in R_H^w} C_{k,H}^w(\mathbf{f}_H^*,\mathbf{f}_A^*)\left(f_{k,H}^w - f_{k,H}^{w*}\right) + \sum_{a\in \Gamma_A} t_{a,A}(\mathbf{f}_H^*,\mathbf{f}_A^*)\left(v_{a,A}^w - v_{a,A}^{w*}\right) \geq 0, \quad (3.23)$$

where $[\mathbf{f}_H^T, \mathbf{v}_A^T] \in \boldsymbol{\Omega}_\mathbf{v} = \{[\mathbf{f}_H^T, \mathbf{v}_A^T] | \Lambda_H \mathbf{f}_H = \mathbf{q}_H;\ \Lambda_A \mathbf{f}_A = \mathbf{q}_A; \Delta_A \mathbf{f}_A = \mathbf{v}_A; \mathbf{f}_H \geq 0; \mathbf{f}_A \geq 0\}$. Equivalently, the VI problem (3.23) can be written as

$$\mathbf{C}_H^*(\mathbf{f}_H - \mathbf{f}_H^*)^T + \mathbf{t}_A^*(\mathbf{v}_A - \mathbf{v}_A^*)^T \geq 0, \quad (3.24)$$

where $[\mathbf{f}_H^T, \mathbf{v}_A^T] \in \boldsymbol{\Omega}_\mathbf{v}$. $\mathbf{t}_A^*$ is the vector of link travel costs of CAVs at the equilibrium state $[\mathbf{f}_H^{T*}, \mathbf{f}_A^{T*}]$. The following proposition discusses the existence of path flow solutions of VI problem (3.21).

Proposition 2: The VI problem (3.21) has at least one path flow solution.

*Proof***:** As the link travel cost functions (Eq. (3.19)) for both CAVs and HDVs are continuous with respect to link flows of CAVs and HDVs, the generalized path cost for both HDVs $(C_{k,H}^w(\mathbf{f}_H, \mathbf{f}_A), \forall k, w)$ and CAVs $(C_{k,A}^w(\mathbf{f}_H, \mathbf{f}_A), \forall k, w)$ are continuous with respect to $\mathbf{f}_H$ and $\mathbf{f}_A$**.** Besides, the constraints in the feasible path flow set $\boldsymbol{\Omega}_\mathbf{f}$ are affine. Thereby, the feasible path flow set $\boldsymbol{\Omega}_\mathbf{f}$ is closed and convex. According to Theorem 1.4 in Nagurney (2013), VI problem (3.21) has at least one path flow solution. ■

Proposition 2 implies that there exists at least one solution to VI problem (3.23) or (3.24). Let $\mathbf{f} = [\mathbf{f}_H^T, \mathbf{f}_A^T]^T, = [\mathbf{C}_H^T, \mathbf{C}_A^T]^T$. Note that the generalized path travel cost vector $\mathbf{C}$ in VI problem (3.22) is asymmetric to path flow $\mathbf{f}$ as the link travel cost is asymmetric between HDVs and CAVs. Thereby, both the VI problems (3.21) and (3.23) may have multiple local solutions due to the asymmetric relationship (Nagurney, 2000). .

Proposition 3: If $VOT_H = VOT_A$, then the path travel cost of CAVs for an OD pair is no larger than the path travel cost of HDVs for the same OD pair.

Proof: Note that all HDV paths are also potential CAV paths. Thereby, $R_H^w \subset R_A^w$, for $\forall w \in (W_A \cap W_H)$. As CAVs choose the paths with minimum travel cost for an OD pair, the path travel cost of an arbitrary CAV must be no larger than the path travel cost of an arbitrary HDV for the same OD pair. ■

When the level of automation of CAVs is not high, the drivers need to monitor the vehicle frequently and be ready to take over when requested to do so. In this scenario, the VOT of CAV users is close to that of HDV users. Note when $VOT_H = VOT_A$, the travel costs of HDVs and CAVs for the same path are identical. Proposition 3 suggests that a large proportion of HDV demand and CAV demand will be distributed on the same paths with shortest travel cost in this case, which increases traffic congestion and reduces system performance. It will be shown in the numerical example that the system performance of HDVs will benefit from the condition $VOT_H > VOT_A$, where a large proportion of HDV demand and CAV demand for the same OD pair will be distributed on different paths to reduce the network congestion level.

3.4 RSRS-MSRA Solution algorithm

Many VI-based solution algorithms can be used to solve the proposed multiclass traffic assignment model, such as the projection method (Nagurney, 2000; Nagurney and Dong, 2002; Jiang et al., 2016), Tikhonov regularization method (Tikhonov, 1963), proximal point methods (Bauschke, 2004; Zhan and Ukkusuri, 2017), etc., provided that the corresponding convergence conditions are satisfied. However, these methods need to solve a subproblem in each iteration, which projects the decent direction onto the feasible set defined by the constraints. This is computationally expensive for the proposed multiclass traffic assignment model due to the presence of the complex generalized path travel cost function for HDVs (see Eq. (3.3)). To circumvent this issue, a route-swapping-based solution algorithm will be developed in this study to solve the multiclass traffic assignment model (3.21). At each iteration, this algorithm calculates the descent direction using a closed-form formulation to circumvent solving the subproblem in VI-based solution algorithms.

Route-swapping models are usually formulated to characterize the evolution of traffic flow based on drivers' knowledge of traffic conditions (Wang et al., 2016). They address whether and how the flow pattern evolves from a non-equilibrium state toward an equilibrium state. Depending on route choice assumptions, existing route-swapping models can converge to a stationary state equivalent to UE (Smith, 1984; Smith and Wisten, 1995; Huang and Lam, 2002; Peeta and Yang, 2003, Friesz et al., 1994) or logit-based SUE (Guo, 2013; Smith and Watling, 2016). This characteristic enables route-swapping models to obtain a feasible solution algorithm for network equilibrium problems. Huang and Lam (2002) develop a heuristic algorithm based on the projected route-swapping (PRS) dynamic system to solve a VI-based departure time choice equilibrium problem. For convenience, we label it PRS algorithm. At each iteration, the descent direction of the PRS algorithm is calculated using an analytical model that assumes flow will shift from the more costly paths to the least-cost path at a rate that is proportional to the flow on the more costly paths and the cost difference from the least-cost path. This algorithm is used to solve other VI-based traffic assignment problems (see e.g., Lam and Huang, 2003; Szeto and Lo, 2006). However, many studies report the slow convergence of the algorithm (Szeto and Lo, 2006; Ramadurai and Ukkusuri, 2010). This is partly because the PRS algorithm only shifts flows to the least-cost paths from all other paths, which can overestimate the flows on the least-cost paths. Hence, the PRS algorithm converges slowly when the solution is close to the optimum, where the cost difference between least-cost paths and non-least-cost paths is small. Thereby, the PRS algorithm may fail to find a descent direction when it is close to the optimal solution. The steps to solve the multiclass traffic assignment problem (3.21) using the PRS algorithm are summarized in Appendix A.

This study develops a new route-swapping-based solution algorithm to solve the multiclass traffic assignment problem (3.21). We will show that the proposed algorithm can solve (3.21) effectively and can converge much faster than the PRS algorithm. Let n denotes the iteration number. At iteration $n+1$, unlike the PRS algorithm, the path flows $\mathbf{f}_{n+1}$ of both HDVs and CAVs will be updated according to the following model,

which is a revised version of the route-swapping model proposed by Smith (1984) to incorporate multi-user classes,

$$\mathbf{f}_{n+1} = \mathbf{f}_n + \beta_n \mathbf{\Phi}(\mathbf{f}_n) = \begin{bmatrix} \mathbf{f}_{n,H} \\ \mathbf{f}_{n,A} \end{bmatrix} + \beta_n \begin{bmatrix} \mathbf{\Phi}_H(\mathbf{f}_n) \\ \mathbf{\Phi}_A(\mathbf{f}_n) \end{bmatrix} \tag{3.25}$$

where $\beta_n > 0$ is a step, $\mathbf{f}_{n,H}$ and $\mathbf{f}_{n,A}$ are vectors of path flows for HDVs and CAVs on iteration n, respectively. $\mathbf{\Phi}_H(\mathbf{f}_n) = \left(\Phi_{k,H}^w(\mathbf{f}_n), \forall k \in R_H^w, w \in W_H\right)$ and $\mathbf{\Phi}_A(\mathbf{f}_n) = \left(\Phi_{k,A}^w(\mathbf{f}_n), \forall k \in R_A^w, w \in W_A\right)$ are updated by:

$$\Phi_{k,H}^w(\mathbf{f}_n) = \sum_{g \in R_H^w} \left[f_{g,H}^w(n) \left(C_{g,H}^w(\mathbf{f}_n) - C_{k,H}^w(\mathbf{f}_n) \right)_+ - f_{k,H}^w(n) \left(C_{k,H}^w(\mathbf{f}_n) - C_{g,H}^w(\mathbf{f}_n) \right)_+ \right] \tag{3.26a}$$

$$\Phi_{k,A}^w(\mathbf{f}_n) = \sum_{g \in R_A^w} \left[f_{g,A}^w(n) \left(C_{g,A}^w(\mathbf{f}_n) - C_{k,A}^w(\mathbf{f}_n) \right)_+ - f_{k,A}^w(n) \left(C_{k,A}^w(\mathbf{f}_n) - C_{g,A}^w(\mathbf{f}_n) \right)_+ \right] \tag{3.26b}$$

where $f_{i,z}^w(n)$ is the flow of path i for vehicle class $z \in \{HDV, CAV\}$ for OD pair w in iteration n. $\left(C_{g,z}^w(\mathbf{f}_n) - C_{k,z}^w(\mathbf{f}_n)\right)_+ = C_{g,z}^w(\mathbf{f}_n) - C_{k,z}^w(\mathbf{f}_n)$ if $C_{g,z}^w(\mathbf{f}_n) > C_{k,z}^w(\mathbf{f}_n)$, otherwise $\left(C_{g,z}^w(\mathbf{f}_n) - C_{k,z}^w(\mathbf{f}_n)\right)_+ = 0$. $z \in \{HDV, CAV\}$.

For simplicity, we label Eq. (3.25) as the revised Smith's route-swapping (RSRS) algorithm. This algorithm finds the descent direction based on an analytical formulation $\mathbf{\Phi}(\mathbf{f}_n)$ to circumvent the subproblem in VI-based algorithms**.** In each iteration, the descent direction can be updated quickly based on the path flow and generalized path travel cost of the previous iteration. Unlike the PRS algorithm (see Appendix A), the RSRS algorithm can address this problem effectively. In each iteration, the RSRS algorithm swaps flow from a path not only to the least-cost paths, but also to other paths with a lower cost. Thereby, the RSRS algorithm can increase flows not only on paths with the least cost increase, but also on paths with costs close to the least value. This procedure prevents the overestimation of flow swaps to the least-cost paths, which impedes the efficiency of the PRS algorithm when the solution is close to the optimum. The following proposition describes the equivalence between the stationary point of Eq. (3.25) and the solution of the multiclass traffic assignment problem (3.21).

Proposition 4: If the path flows $\mathbf{f}_n$ determined by the RSRS algorithm converge, then they must converge to the pattern that simultaneously satisfies the CNL equilibrium conditions for HDVs and UE conditions for CAVs.

Proof: Suppose $\mathbf{f}_n$ is a stationary point for Eq. (3.25), $\mathbf{f}_n = \mathbf{f}_{n+1}$. Then, for arbitrary OD pair $w, w \in W_H$

$$
\begin{aligned}
0 &= \left(\mathbf{C}_H^w(\mathbf{f}_n)\right)^T \left(\mathbf{f}_{n+1,H}^w - \mathbf{f}_{n,H}^w\right) \\
&= \left(\mathbf{C}_H^w(\mathbf{f}_n)\right)^T \left(\mathbf{f}_{n,H}^w + \beta_n \mathbf{\Phi}_H^w(\mathbf{f}_n) - \mathbf{f}_{n,H}^w\right) \\
&= \beta_n \sum_{k \in R_H^w} C_{k,H}^w \sum_{g \in R_H^w} \Big[f_{g,H}^w(n) \left(C_{g,H}^w(\mathbf{f}_n) - C_{k,H}^w(\mathbf{f}_n)\right)_+ \\
&\qquad - f_{k,H}^w(n) \left(C_{k,H}^w(\mathbf{f}_n) - C_{g,H}^w(\mathbf{f}_n)\right)_+ \Big]
\end{aligned} \tag{3.27}
$$

where $\mathbf{f}_{n,H}^w$ is the vector of flow of all paths for OD pair $w \in W_H$ at iteration n. $\mathbf{C}_H^w(\mathbf{f}_n)$ is the vector of generalized costs of all paths for HDVs for OD pair $w \in W_H$ at iteration n. $\mathbf{\Phi}_H^w(\mathbf{f}_n) = \left(\Phi_{k,H}^w(\mathbf{f}_n), \forall k \in R_H^w\right)$. Let $|R_H^w|$ denote the number of paths for HDVs for OD pair $w, w \in W_H$. Without loss of generality, suppose $C_{1,H}^w(\mathbf{f}_n) \geq C_{2,H}^w(\mathbf{f}_n) \geq \cdots \geq C_{|R_H^w|,H}^w(\mathbf{f}_n)$. Then, Eq. (3.27) can be simplified as:

$$
\begin{aligned}
0 &= \left(\mathbf{C}_H^w(\mathbf{f}_n)\right)^T (\mathbf{f}_{n+1}^w - \mathbf{f}_n^w) \\
&= \beta_n \sum_{k=1}^{|R_H^w|} \sum_{g=k+1}^{|R_H^w|} f_{k,H}^w(n) \left(C_{k,H}^w(\mathbf{f}_n) - C_{g,H}^w(\mathbf{f}_n)\right)^2
\end{aligned} \tag{3.28}
$$

Eq. (3.28) holds only when it satisfies Eq. (3.5). Using the same method, it can be shown that the stationary path flows for HDVs and CAVs for all OD pairs obtained by Eq. (3.25) satisfy the CNL equilibrium condition and UE condition in Eq. (3.5) and Eq. (3.20), respectively. Proposition 4 is proved. ■

Note that $\beta_n > 0$. If the path flow $\mathbf{f}_n$ determined by the RSRS algorithm converges, it must converge to a path flow pattern satisfying $\{\mathbf{f}|: \mathbf{\Phi}(\mathbf{f}) = \mathbf{0}\}$. Let $\text{SOL}(\mathbf{\Omega_f}, \mathbf{C})$ be the solution set of VI problem (3.22). Proposition 4 indicates that $\{\mathbf{f}|: \mathbf{\Phi}(\mathbf{f}) = \mathbf{0}\} \subseteqq \text{SOL}(\mathbf{\Omega_f}, \mathbf{C})$. Also, an arbitrary equilibrium path flow solution in set $\text{SOL}(\mathbf{\Omega_f}, \mathbf{C})$ must belong to the set $\{\mathbf{f}|: \mathbf{\Phi}(\mathbf{f}) = \mathbf{0}\}$, because the generalized travel costs of all used paths for an OD pair are the same for both CAVs and HDVs at the equilibrium state. Therefore, $\text{SOL}(\mathbf{\Omega_f}, \mathbf{C}) \subseteqq \{\mathbf{f}|: \mathbf{\Phi}(\mathbf{f}) = \mathbf{0}\}$. This indicates that $\text{SOL}(\mathbf{\Omega_f}, \mathbf{C}) = \{\mathbf{f}|: \mathbf{\Phi}(\mathbf{f}) = \mathbf{0}\}$, that is, the solution set of the VI problem (3.22) and the set of the stationary points of the RSRS algorithm are identical.

The following theorem based on Mounce and Carey (2015) provides sufficient conditions for the convergence of the RSRS algorithm.

Theorem 5. Suppose the generalized path travel cost $\mathbf{C}(\mathbf{f})$ is monotonic in $\mathbf{\Omega_f}$. Then, the RSRS algorithm (3.42) converges to the CNL equilibrium state and UE state for HDVs and CAVs, respectively, if β_n satisfy $\lim_{n \to \infty} \beta_n = 0, \sum_{n=1}^{\infty} \beta_n = \infty$.

The proof of Theorem 5 can follow the same method proposed by Mounce and Carey (2015). We omit the proof here to avoid duplication. Note that the monotonicity of $\mathbf{C}(\mathbf{f})$

is not guaranteed by the VI problem (3.22). To analyze the convergence of the RSRS algorithm, define a local optimal solution as the solution that is optimal within a neighboring set of candidate solutions. The set of local optimal solutions to VI problem (3.22) contains all of the equilibrium points defined by VI problem (3.22).The following assumption will be made to show the convergence of the RSRS algorithm.

Assumption 1: The generalized path travel cost $\mathbf{C}(\mathbf{f})$ is monotonic in a small vicinity around a local optimal solution $\mathbf{f}^*$.

Assumption 1 implies that while the $\mathbf{C}(\mathbf{f})$ may not be monotonic in the feasible set $\boldsymbol{\Omega}_\mathbf{f}$, it can be monotonic in a small vicinity around a local optimal solution. Huang and Lam (2002) also made the same assumption to ensure the local stability of the PRS algorithm. It is also often used for designing solution algorithms for non-convex traffic assignment problems (e.g., Zhan and Ukkusuri, 2017; Shao et al., 2006).

To ensure the convergence of the RSRS algorithm, Mounce and Carey (2015) use predetermined step sizes ($\beta_n = 1/n$) to solve the UE problem. However, the RSRS algorithm converges slowly using these predetermined step sizes, especially for large-size network problems (Mounce and Carey, 2015). Huang and Lam (2002) propose another predetermined step size choice strategy. It assumes the step sizes are the same for a large number of consecutive iterations and non-increasing with respect to the iteration number. The step sizes proposed by Huang and Lam can be analytically formulated as $\beta_n = e_1 \frac{1}{\left[\frac{n}{e_2}+1\right]}$, where e_1 is a small positive value, and e_2 is the number of iterations for which the step sizes are the same. Notation $\left[\frac{n}{e_2}+1\right]$ represents the integer part of the value $\frac{n}{e_2}+1$. For example, $\beta_n = 10^{-4} \times \frac{1}{\left[\frac{n}{1000}+1\right]} = 10^{-4} \times \left(1^{(1\to 1000)}, 1/2^{(1001\to 2000)}, \cdots\right)$, the step size of which remains the same for every 1000 iterations. However, the PRS algorithm still converges slowly though it is better than that using $\beta_n = 1/n$ (Ramadurai and Ukkusuri, 2010). In summary, it is difficult to determine effective step sizes offline as small step sizes make the algorithm converge slowly while large step sizes can preclude it from converging.

To enhance the convergence efficiency of the RSRS algorithm, this study modifies the self-regulated average (SRA) method developed by of Liu et al. (2009) to determine the step size in each iteration based on the self-regulated average method. The SRA method can adaptively updates the step size in each iteration using information from both the current iteration and the previous iteration. The modified SRA (MSRA) method is shown in Eq. (3.29). In Eq. (3.29), the term $1/\chi_n$ represents the step size determination rule of the SRA method. If the norm descent direction in iteration n is larger than that in iteration $n-1$, implying that the RSRS algorithm tends to diverge, a large value of Υ_1 is used to shrink the current step size. The opposite case implies that the RSRS method tends to converge, and the SRA method attempts to apply a large step size at the current iteration by setting a small value of Υ_2. However, the SRA method cannot ensure the feasibility of path flows computed by the Eq. (3.25). The proposed MSRA method

introduces the term $1/h_n$ to address the feasibility issue. This term is proposed to ensure that the total flow swapped from an arbitrary path to other paths by the RSRS algorithm is not larger than the flow on this path. The selection of h_n is also adaptively determined by the maximum value of the summation of differences in the generalized costs of path pairs and the minimum generalized path cost for the corresponding OD pair.

$$\beta_n = \frac{1}{h_n} \cdot \frac{1}{\chi_n} \tag{3.29a}$$

$$\chi_n = \begin{cases} 2; if\ n = 1 \\ \chi_{n-1} + \Upsilon_1; if\ \|\boldsymbol{\Phi}(\mathbf{f}_n)\| \geq \|\boldsymbol{\Phi}(\mathbf{f}_{n-1})\|\ and\ n \geq 2 \\ \chi_{n-1} + \Upsilon_2; if\ \|\boldsymbol{\Phi}(\mathbf{f}_n)\| < \|\boldsymbol{\Phi}(\mathbf{f}_{n-1})\|;\ and\ n \geq 2 \end{cases} \tag{3.29b}$$

where $h_n = \max\left(h_{i,z}^w(n) \middle| h_{i,z}^w(n) = \sum_{j \in R_z^w \setminus i} \left(C_{j,z}^w(\mathbf{f}_n) - C_{i,z}^w(\mathbf{f}_n)\right)_+, i \in R_z^w; \forall w \in W_z, \forall z \in \{HAV, CAV\}\right)$; and Υ_1 and Υ_2 are predetermined values, $\Upsilon_1 > 1; \Upsilon_2 \in (0,1)$.

The following proposition is useful to show that the path flows computed by Eq. (3.25) in each iteration using the RSRA step size choice technique (Eq.(3.29)) are within the feasible path flow set $\boldsymbol{\Omega}_{\mathbf{f}}$.

Proposition 5: If the initial path flows are feasible, then at each iteration n, the path flow (i.e., $\mathbf{f}_{n+1}$) computed by Eq. (3.25) and Eq. (3.29) must be nonnegative. Further, if $f_{k,z}^w(n)$ $(k \in R_z^w; \forall w \in W_z, \forall z \in \{HAV, CAV\})$ is positive, then, $f_{k,z}^w(n+1)$ is positive.

Proof: According to Eq. (3.25) and Eq. (3.29)

$$f_{k,z}^w(n+1) = f_{k,z}^w(n) + \beta_n \Phi_{k,z}^w(\mathbf{f}_n)$$

$$= f_{k,z}^w(n) + \beta_n \sum_{g \in R_z^w} \left[f_{g,z}^w(n) \left(C_{g,z}^w(\mathbf{f}_n) - C_{k,z}^w(\mathbf{f}_n)\right)_+ - f_{k,z}^w(n) \left(C_{k,z}^w(\mathbf{f}_n) - C_{g,z}^w(\mathbf{f}_n)\right)_+ \right]$$

$$\geq f_{k,z}^w(n) - \beta_n \sum_{g \in R_z^w} f_{k,z}^w(n) \left(C_{k,z}^w(\mathbf{f}_n) - C_{g,z}^w(\mathbf{f}_n)\right)_+$$

$$= f_{k,z}^w(n) - \frac{1}{h_n} \cdot \frac{1}{\chi_n} \sum_{g \in R_z^w} f_{k,z}^w(n) \left(C_{k,z}^w(\mathbf{f}_n) - C_{g,z}^w(\mathbf{f}_n)\right)_+$$

According to the definition of h_n,

$$\frac{1}{h_n} \sum_{g \in R_z^w} \left(C_{k,z}^w(\mathbf{f}_n) - C_{g,z}^w(\mathbf{f}_n)\right)_+ \leq 1$$

Thereby,

$$f_{k,z}^{w}(n) - \frac{1}{h_n} \cdot \frac{1}{\chi_n} \sum_{g \in R_z^w} f_{k,z}^{w}(n) \left(C_{k,z}^{w}(\mathbf{f}_n) - C_{g,z}^{w}(\mathbf{f}_n) \right)_+$$

$$\geq f_{k,z}^{w}(n) - \frac{1}{\chi_n} f_{k,z}^{w}(n)$$

Note that the initial path flow is feasible. It is then nonnegative. As $\chi_n > 1$, for $\forall n$, then

$$f_{k,z}^{w}(n+1) = f_{k,z}^{w}(n) + \beta_n \Phi_{k,z}^{w}(\mathbf{f}_n) \geq f_{k,z}^{w}(n) - \frac{1}{\chi_n} f_{k,z}^{w}(n) \geq 0$$

The equality holds only if $f_{k,z}^{w}(n) = 0$. Proposition 5 is proved. ■

Note that at each iteration, the path flow computed by Eq. (3.25) must satisfy the equality constraints in $\mathbf{\Omega_f}$. According to Proposition 5, the path flows computed by Eq. (3.25) and Eq. (3.29) are nonnegative. Thereby, at each iteration, the path flows computed by the RSRS-MSRA algorithm must satisfy the path flow constraints in $\mathbf{\Omega_f}$. In addition, if the initial flow of a path for HDVs is positive, the flow on that path computed by the RSRS-MSRA algorithm at each iteration will be positive. This property is useful to derive the convergence of the RSRS-MSRA algorithm in the following proposition.

Let $dist(\mathbf{f}, \text{SOL}(\mathbf{\Omega_f}, \mathbf{C}))$ denote the Euclidean distance from $\mathbf{f}$ to the path flow solution set $\text{SOL}(\mathbf{\Omega_f}, \mathbf{C})$.The following proposition discusses the convergence of the RSRS algorithm with the step sizes provided by the MSRA method (Eq. (3.29), labeled the "RSRS-MSRA algorithm".

Proposition 6: If the initial flows of all paths for HDVs are positive, for arbitrary positive value ζ, the RSRS-MSRA algorithm converges to the set $\{\mathbf{f} \in \mathbf{\Omega_f} | dist(\mathbf{f}, \text{SOL}(\mathbf{\Omega_f}, \mathbf{C})) < \zeta\}$ given Assumption 1.

Proof: Let $\mathbf{f}_n$ be the path flow obtained using the RSRS-MSRA algorithm at each iteration n. Suppose the Proposition does not hold. Then, we have $dist(\mathbf{f}_n, \text{SOL}(\mathbf{\Omega_f}, \mathbf{C})) \geq \zeta$ for $n = 1,2,\cdots$. This implies that $\mathbf{f}_n, \forall n$ are not equilibrium. Hence, $h_n > 0$, $\forall n$. Let $\vartheta_{min} = min\{h_n, n = 1,2,\cdots\}$. Then $h_n \geq \vartheta_{min} > 0$.

Next, we show $h_n, \forall n$ has a finite upper bound. Note that the path flows computed by the RSRS-MSRA algorithm in each iteration must be in the feasible path flow set $\mathbf{\Omega_f}$. Thereby, in each iteration, the path flows computed by the RSRS-MSRA algorithm for each OD pair are bounded above and below by the corresponding OD demand and 0, respectively, for both CAVs and HDVs. This implies $\mathbf{f}_n$ $(\forall n)$ is bounded. According to Eq. (3.19b), the costs of all links are bounded. Note that as the travel cost of a path for CAVs is the sum of costs on all links used by that path, $C_{i,A}^{w}(\mathbf{f}_n)$ is bounded. This implies that $h_{i,A}^{w}(n) = \sum_{j \in R_A^w \backslash i} \left(C_{j,A}^{w}(\mathbf{f}_n) - C_{i,A}^{w}(\mathbf{f}_n) \right)_+, \forall i \in R_H^w; \forall w \in W_H$ is bounded. Now we will show $h_{i,H}^{w}(n) = \sum_{j \in R_A^w \backslash i} \left(C_{j,H}^{w}(\mathbf{f}_n) - C_{i,H}^{w}(\mathbf{f}_n) \right)_+$ is bounded. Note that $\mathbf{f}_n$ has an upper bound. According to Eq. (3.3), $C_{i,H}^{w}(\mathbf{f}_n), i \in R_H^w; \forall w \in W_H$ is bounded from

above. As the initial path flows for HDVs are positive, according to Proposition 5, the path flows for HDVs computed by the RSRS-MSRA algorithm at each iteration must be positive. Thereby, $C_{i,H}^{w}(\mathbf{f}_n), i \in R_H^w; \forall w \in W_H$ has a finite lower bound. This indicates $h_{i,H}^{w}(n) = \sum_{j \in R_z^w \setminus i}\left(C_{j,H}^{w}(\mathbf{f}_n) - C_{i,H}^{w}(\mathbf{f}_n)\right)_+$ is bounded. Thereby, h_n has a finite upper bound. Let $\vartheta_{max} = \{h_n, n = 1,2,\cdots\}$. Then, $h_n \le \vartheta_{max} < \infty$.

The above analysis shows that if Proposition 6 does not hold, there must exist ϑ_{max} and ϑ_{min} such that $\infty > \vartheta_{max} \ge h_n \ge \vartheta_{min} > 0$. According to Eq. (3.29b), $n \cdot \Upsilon_2 \le \chi_n \le 2 + (n-1) \cdot \Upsilon_1$. Then $\frac{1}{\vartheta_{max}}\frac{1}{n \cdot \Upsilon_2} \le \beta_n \le \frac{1}{\vartheta_{min}}\frac{1}{(n-1)\cdot\Upsilon_1+2}$. As both Υ_1 and Υ_2 are fixed positive values, $\lim_{n\to\infty} \beta_n \le \lim_{n\to\infty} \frac{1}{\vartheta_{min}}\frac{1}{(n-1)\cdot\Upsilon_1+2} \to 0$, and $\sum_{n=1}^{\infty} \beta_n \ge \sum_{n=1}^{\infty} \frac{1}{\vartheta_{max}}\frac{1}{n\cdot\Upsilon_2} \to \infty$. According to Theorem 5, the path flow determined by the RSRS-MSRA algorithm must eventually enter into the set $\{\mathbf{f} \in \mathbf{\Omega_f} | dist(\mathbf{f}, \mathrm{SOL}(\mathbf{\Omega_f}, \mathbf{C})) < \zeta\}$ under assumption 1. Proposition 6 is proved. ■

According to above discussion, the steps to implement the RSRS-MSRA algorithm are summarized as follows:

Step 1: *Initialization*. Let $n = 1$. Assign the OD demands of HDVs and CAVs uniformly to all paths for the corresponding OD pair. Denote the resulted path flows for HDVs and CAVs as $\mathbf{f}_{n,H}$ and $\mathbf{f}_{n,A}$, respectively.

Step 2: *Route flow update*. Update path flows for HDVs and CAVs ($f_{k,z}^{w}(n+1), \forall k, w, z \in \{HDV, CAV\}$) according to Eq. (3.25) and Eq. (3.29);

Step 3. *Convergence check*. If the convergence criterion is satisfied, then stop. Otherwise, let $n = n + 1$ and go to step 2. The convergence criterion will be discussed later in section 5.1.

Note that the RSRS-MSRA algorithm can only find one local optimal solution depending on the initial path flow pattern. Further, the RSRS-MSRA solution algorithm contains two parameter (i.e., Υ_1 and Υ_2) whose values should be determined in advance. While the solution algorithm can converge for any combinations of values of Υ_1 ($\Upsilon_1 > 1$) and Υ_2 ($\Upsilon_2 \in (0,1)$), our analysis shows that the solution algorithm converges much faster for most networks when $\Upsilon_1 \in [1,6]$ and $\Upsilon_2 \in (0.0001, 0.01)$. In addition, the RSRS-MSRA solution algorithm is developed upon path flows. To find the paths that are likely to be used for each OD pair, the link penalty approach developed by De La Barra et al. (1993) is used in this study. Note that only acyclic paths are considered.

3.5 Numerical analysis

3.5.1 Small numerical example to illustrate the details of the RSRS-MSRA algorithm

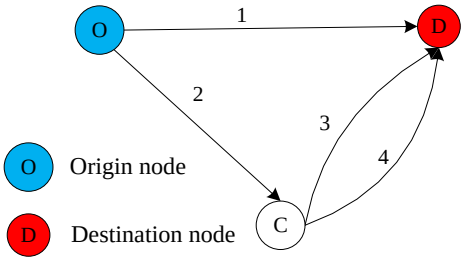

Figure 3.2: Network to illustrate the RSRS-MSRA solution algorithm

Table 3.1: Inputs for study network 1

Links	1	2	3	4
Link length (l_a) (mile)	5	2	3	3
Speed limit (s_a) (mile/h)	50	50	50	50
Capacity for HDVs ($Q_{a,H}$)	24	18	12	12
Capacity for CAVs ($Q_{a,A}$)	48	36	24	24

In this section, the small network shown in Figure 3.2 is used to illustrate the details of the RSRS-MSRA solution algorithm. It contains one OD pair and three routes connecting the origin and destination nodes for both HDVs and CAVs. The three paths are: path 1: link 1; path 2: links 2-3, and path 3: links 2-4. For simplicity, no AV dedicated lane is considered in this network. The OD demand for HDVs and CAVs are 21 and 9, respectively. The dispersion parameter and the nesting degree for both networks are $\theta = 0.5$ and $u = 0.5$, respectively. The parameters Υ_1 and Υ_2 are set as 4 and 0.001, respectively. The VOTs for HDVs and CAVs are set as 10 and 5, respectively. To estimate the gasoline consumption of a vehicle on link $a \in \boldsymbol{\Gamma}_H$, the following model (Zhang et al., 2014) which is calibrated using field data of 40 gasoline vehicles, will be used in this study:

$$E_a = 147.92\left(\frac{l_a}{\bar{t}_a(v_{a,H}, v_{a,A})}\right)^{-0.689}\frac{1.609 * l_a}{3.785} = 62.88\frac{(l_a)^{0.311}}{\bar{t}_a(v_{a,H}, v_{a,A})}$$

where 1.609 is the conversion rate of mile to kilometer, and 3.785 is conversion rate of gallon to liter. The travel cost for HDVs and CAVs on link $a, a \in \boldsymbol{\Gamma}_H$ is:

$$t_{a,z} = \bar{t}_a\left(v_{a,A}\right) \cdot VOT_z + 3 \cdot 53.69 \frac{(l_a)^{0.311}}{\bar{t}_a\left(v_{a,H}, v_{a,A}\right)}, a \in \boldsymbol{\Gamma}_H, z \in \{HAV, CAV\}$$

where the link travel time $\bar{t}_a\left(v_{a,H}, v_{a,A}\right)$ is from Eq. (3.12a).

To measure the solution quality, the convergence indicator (denoted as G) is formulated as follows:

$$G = \frac{\sum_{w \in W_H} \sum_{k \in R_H^w} f_{k,H}^w \left(C_{k,H}^w - C_{min,H}^w\right) + \sum_{w \in W_A} \sum_{k \in R_A^w} f_{k,A}^w \left(C_{k,A}^w - C_{min,A}^w\right)}{\sum_{w \in W_H} \sum_{k \in R_H^w} f_{k,H}^w C_{k,H}^w + \sum_{w \in W_A} \sum_{k \in R_A^w} f_{k,A}^w C_{k,A}^w}$$

where $C_{min,H}^w$ and $C_{min,A}^w$ are minimum generalized path costs for HDVs and CAVs, respectively, for OD pair w.

According to the RSRS-MSRA solution algorithm, the traffic demands for HDVs and CAVs are assigned uniformly initially to all paths of the OD pair. Thereby, we have

$$f_{1,H}(1) = 7; f_{2,H}(1) = 7; f_{3,H}(1) = 7;$$

$$f_{1,A}(1) = 3; f_{2,A}(1) = 3; f_{3,A}(1) = 3;$$

For simplicity, the notation for OD pair is omitted as the network in Figure 3.2 contains only one OD pair. According to Eq. (3.3) and Eq. (3.20), at iteration 1, the generalized travel costs of all paths for HDVs and CAVs are

$$C_{1,H}(1) = -0.503; \quad C_{2,H}(1) = -0.258; \quad C_{3,H}(1) = -0.258;$$

$$C_{1,A}(1) = 0.771; \quad C_{2,A}(1) = 0.918; \quad C_{3,A}(1) = 0.918;$$

According to Eq. (3.26)

$$\Phi_{1,H}^w(\mathbf{f}_1) = \sum_{g \in R_H^w} \Big[f_{g,H}^w(n) \left(C_{g,H}^w(\mathbf{f}_n) - C_{1,H}^w(\mathbf{f}_n)\right)_+ - f_{1,H}^w(n) \left(C_{1,H}^w(\mathbf{f}_n) - C_{g,H}^w(\mathbf{f}_n)\right)_+ \Big]$$

$$= 7 \Big\{ \left(\left(C_{2,H}^w(\mathbf{f}_n) - C_{1,H}^w(\mathbf{f}_n)\right)_+ - \left(C_{1,H}^w(\mathbf{f}_n) - C_{2,H}^w(\mathbf{f}_n)\right)_+ \right) + \left(\left(C_{3,H}^w(\mathbf{f}_n) - C_{1,H}^w(\mathbf{f}_n)\right)_+ - \left(C_{1,H}^w(\mathbf{f}_n) - C_{3,H}^w(\mathbf{f}_n)\right)_+ \right) \Big\}$$

$$= 7\{(0.245 - 0) + (0.245 - 0)\}$$

$$= 3.43$$

Similarly,

$$\Phi_{2,H}^w(\mathbf{f}_1) = -1.716; \quad \Phi_{3,H}^w(\mathbf{f}_1) = -1.716;$$

$$\Phi_{2,A}^{w}(\mathbf{f}_1) = 0.88; \quad \Phi_{2,A}^{w}(\mathbf{f}_1) = -0.44; \quad \Phi_{3,A}^{w}(\mathbf{f}_1) = -0.44;$$

According to Eq. (3.29a)

$$\beta_1 = \frac{1}{h_1} \cdot \frac{1}{\chi_1}$$

$$= \frac{1}{2} \frac{1}{\max\left(h_{i,z}^{w}(1) \middle| h_{i,z}^{w}(1) = \sum_{j \in R_z^w \setminus i} \left(C_{j,z}^{w}(\mathbf{f}_1) - C_{i,z}^{w}(\mathbf{f}_1)\right)_+, i \in R_z^w; \forall w \in W_z, \forall z \in \{HAV, CAV\}\right)}$$

$$= \frac{1}{2} \cdot \frac{1}{0.245}$$

$$= 2.04$$

Thereby, we can compute $\mathbf{f}_2$ as follows

$$f_{1,H}(2) = f_{1,H}(1) + \beta_1 \Phi_{1,H}^{w}(\mathbf{f}_1) = 7 + 2.04 * 3.43 = 14.0$$

$$f_{2,H}(2) = f_{2,H}(2) + \beta_1 \Phi_{2,H}^{w}(\mathbf{f}_1) = 7 - 2.04 * 1.716 = 3.5$$

$$f_{3,H}(2) = f_{3,H}(3) + \beta_1 \Phi_{3,H}^{w}(\mathbf{f}_1) = 7 - 2.04 * 1.716 = 3.5$$

$$f_{1,A}(2) = f_{1,A}(1) + \beta_1 \Phi_{1,A}^{w}(\mathbf{f}_1) = 3 + 2.04 * 0.88 = 4.795$$

$$f_{2,A}(2) = f_{2,A}(2) + \beta_1 \Phi_{2,A}^{w}(\mathbf{f}_1) = 3 - 2.04 * 0.44 = 2.102$$

$$f_{3,A}(2) = f_{3,A}(3) + \beta_1 \Phi_{3,A}^{w}(\mathbf{f}_1) = 3 - 2.04 * 0.44 = 2.102$$

Then, at iteration 2, the steps shown above can be repeated to obtain $\mathbf{f}_3$. The procedure stops when the value of the convergence criterion reaches the threshold value.

Figure 3.3 shows the convergence results for the RSRS-MSRA solution algorithm. The RSRS-MSRA solution algorithm takes about 150 iterations and 600 iterations to achieve the values of convergence indicator 10^{-4} and 10^{-8}, respectively. Thereby, it converges very fast for this small network. Note that paths 2 and 3 are symmetric, and their flows are identical. Figure 3.4 shows the evolution of flows of paths 1 and 2 for HDVs and CAVs. The path flows for HDVs are very close to the equilibrium state after only 20 iterations while those for CAVs converge after 100 iterations. These results further reinforce the effectiveness and efficiency of the proposed RSRS-MSRA solution algorithm.

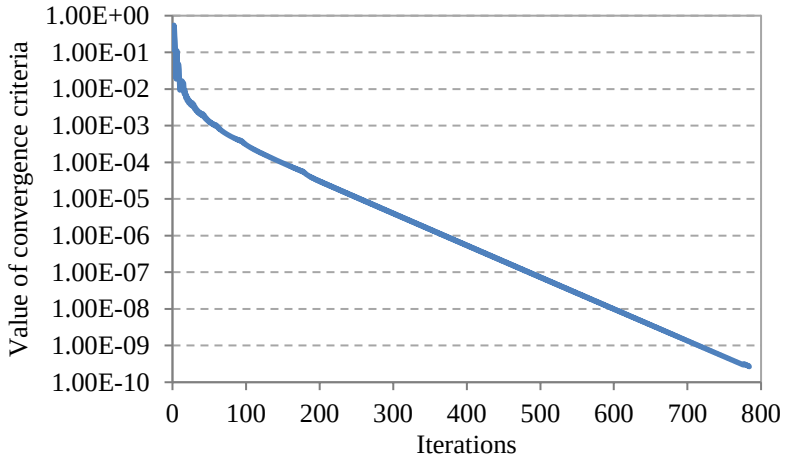

Figure 3.3: Convergence results for the RSRS-MSRA solution algorithm

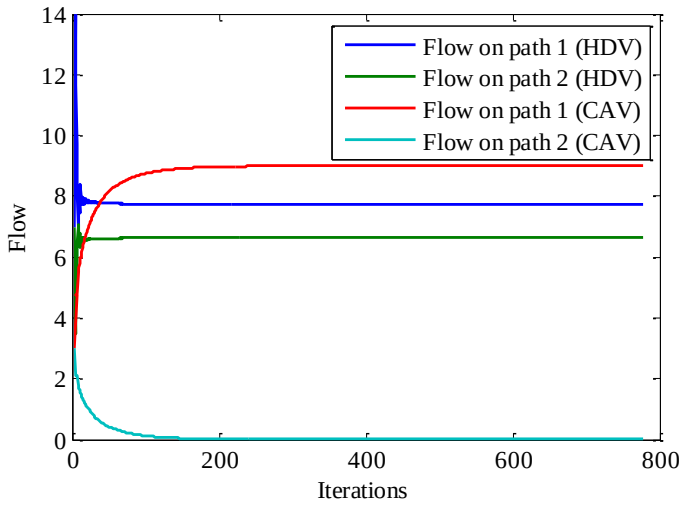

Figure 3.4: Evolution of path flows for HDVs and CAVs

3.5.2 Convergence performance of the RSRS-MSRA solution algorithm

To illustrate the convergence performance of the proposed RSRS-MSRA algorithm, the Nguyen-Dupuis, the Sioux Falls, and the Anaheim networks shown in Figure 3.5 are used. The Nguyen-Dupuis network is a small network with four OD pairs, i.e., W={1-2;1-3;4-2;4-3}. The OD demands for the four OD pairs are 1320, 990, 820, and 990, respectively. The other inputs for the network can be found in Table 3.1. The Sioux Falls network is a larger network consists of 24 nodes, 76 links and 552 O-D pairs. The inputs for the Sioux Falls network can be found in Leblanc (1973). The Anaheim network is a mid-size network consisting of 416 nodes, 914 links, and 1406 OD pairs.

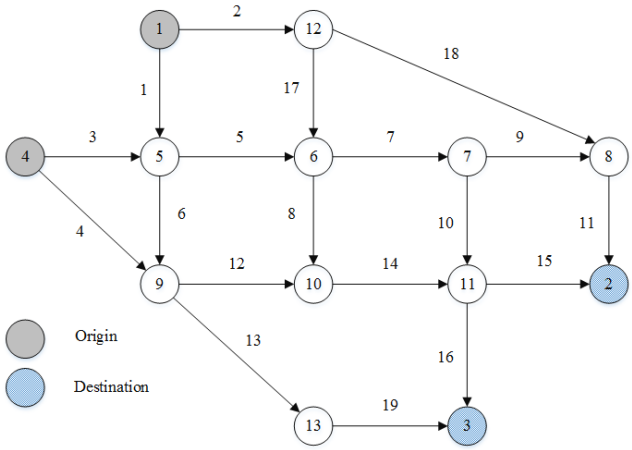

(a) Nguyen-Dupuis

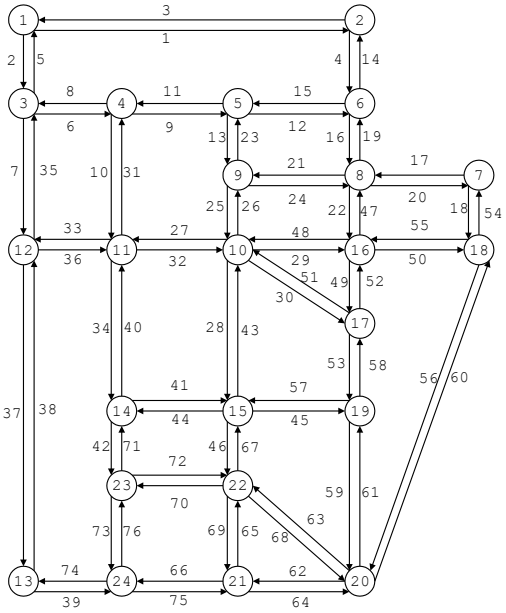

(b) Sioux Falls

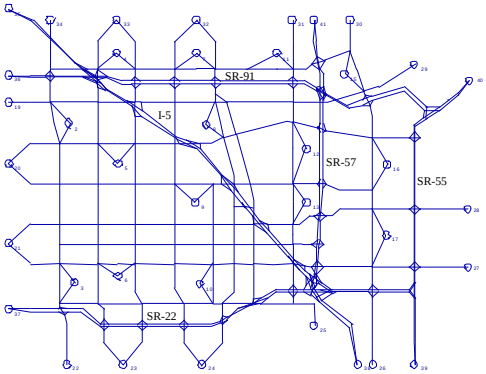

(c) Anaheim

Figure 3.5: Three test networks

Table 3.2: Inputs for Nguyen-Dupuis network

Link	l_a	Q_H	Q_A	Link	l_a	Q_H	Q_A
1	7	300	600	11	9	500	1000
2	9	200	400	12	10	550	1100
3	9	200	400	13	9	200	400
4	12	200	400	14	6	400	800
5	3	350	700	15	9	300	600
6	9	400	800	16	8	300	600
7	5	500	1000	17	7	200	400
8	13	250	500	18	14	300	600
9	5	250	500	19	11	200	400
10	9	300					

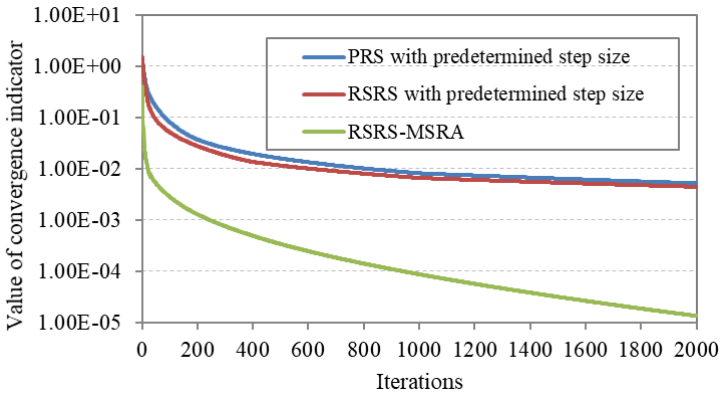

(a)

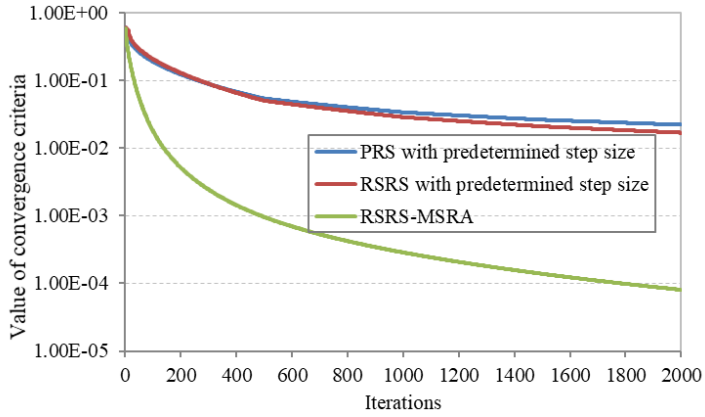

(b)

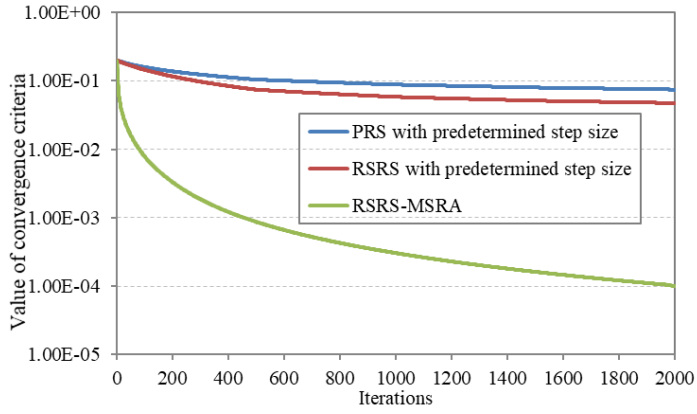

(c)

Figure 3.6: Convergence results for: (a) Nguyen-Dupuis network, (b) Sioux Falls network, and (c) Anaheim network

The CAV demand for each OD pair for the two networks is assumed to be 50%. The dispersion parameter and the nesting degree for the three networks are $\theta = 0.5, u = 0.5$. $Q_{a,A} = 2Q_{a,H}, \forall a \in \boldsymbol{\Gamma}_H$. The VOT for HDVs and CAVs is set as 10 and 5, respectively. The link penalty approach (De La Barra et al., 1993) is used to find the paths that are likely to be used for each OD pair. The number of paths for each OD pair (i.e., K) is set as 15. Thereby, 7920 and 21038 paths are found in total by the link penalty approach for the Sioux Falls and Anaheim networks, respectively. It is worth mentioning that there exist two OD pairs in the Anaheim network for which only two paths exist.

For comparison, the PRS and RSRS algorithm with predetermined step sizes proposed by Huang and Lam (2002) are also used to solve the multiclass traffic assignment model. The predetermined step sizes are set as $0.001 \times (1^{(1\rightarrow 499)}, 1/2^{(500\rightarrow 999)}, 1/3^{(1000\rightarrow 1499)} \cdots)$. These step sizes are carefully chosen as having the best convergence performance. For the RSRS-MSRA method, the two parameters γ_1 and γ_2 are set as 2 and 0.01, respectively. The three algorithms start from the same initial point. The experiments were coded in MATLAB and executed on a computer with an Intel Core i7-4790 3.60-GHz CPU with 8GB RAM. Figure 3.6 shows that the convergence performance of the RSRS algorithm with predetermined step sizes is better than that of the PRS algorithm with the same step sizes for all the three test networks. However, both algorithms performed very poorly in that the stop criterion cannot reach 0.001 for the three test networks after even 2000 iterations. The RSRS-MSRA algorithm substantially improves the convergence performance by adaptively choosing the step size in each iteration. As illustrated in Figure 6, the RSRS-MSRA algorithm takes about 1000 iterations for the Nguyen-Dupuis network, 1890 iterations for the Sioux Falls network, and 1990 iterations for the Anaheim network, to achieve a value of convergence indicator less than 0.0001. As the RSRS-MSRA algorithm updates the path flow in each iteration very efficiently, it only takes about 2.3 seconds, 230.5 and 438.7 seconds to achieve this convergence performance for the Nguyen-Dupuis, the Sioux Falls and the Anaheim networks, respectively.

Note that the RSRS-MSRA algorithm computes the equilibrium flow using a fixed path set generated by the link penalty approach. However, as the path flow is close to equilibrium state, the K-shortest paths provided by link penalty approach may no longer be the shortest. Furthermore, while a larger value of K increase the probability of the path set including all paths with the lowest cost in each iteration, it also increases the computational time of the RSRS-MSRA algorithm. Thereby, the value of K impacts both the equilibrium results and the convergence performance of the RSRS-MSRA algorithm. To analyze the sensitivity of the RSRS-MSRA algorithm to the value of K, this algorithm is tested under different values of K for the Sioux Falls network. The convergence criterion is taken as 0.0001. The equilibrium link flows for HDVs and CAVs computed by the RSRS-MSRA algorithm when $K = 40$ will be used as the baseline to test the accuracy of the equilibrium link flows computed when K is less than 40. Note that for the Sioux Falls network, 40 paths for each OD pair are sufficient to generate an equilibrium flow with high accuracy. Figure 3.7 shows the mean relative differences in link flows for HDVs and CAVs under different values of K compared to

the case with $K = 40$. The figure illustrates that large gaps exist between the equilibrium link flows when $K \leq 10$. The gaps reduce dramatically when K increases. When $K = 15$, the relative mean relative differences in link flows for both HDVs and CAVs are less than 4%. They reduce to 2.4% and 2.1%, respectively, when $K = 20$. It indicates that the RSRS-MSRA algorithm is sensitive to the value of K. However, the computational time increases significantly when K increase, due to the increased computational load of updating the path travel cost for both HDVs and CAVs. Figure 3.7 shows that the computational time for $K = 30$ is about 4 times more than that for $K = 6$. Hence, there is a tradeoff between the quality of the obtained results and the computational efficiency of the proposed RSRS-MSRA algorithm.

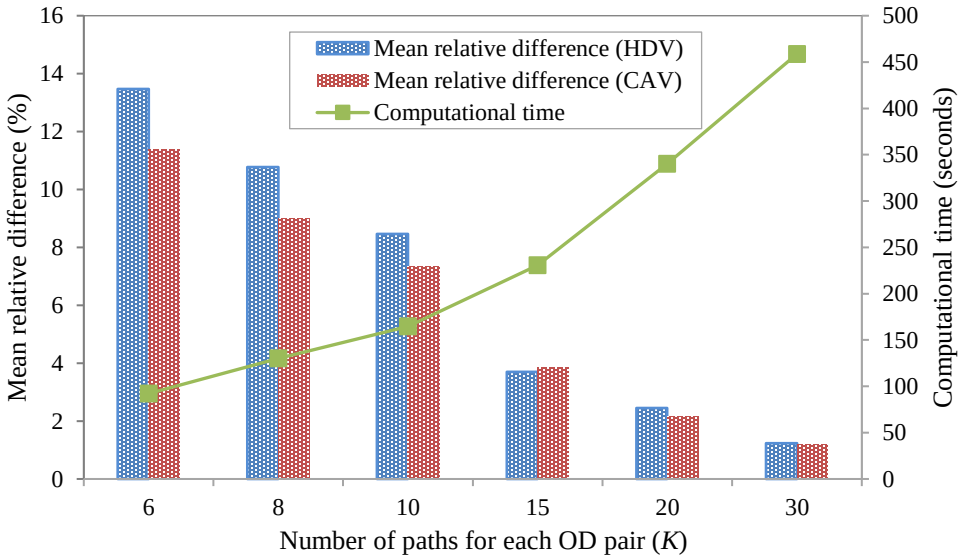

Figure 3.7: Mean relative differences in link flows of HDVs and CAVs under different values of K compared to those of $K = 40$, and corresponding computational times.

3.5.3 Impacts of CAVs on network performance

The Nguyen-Dupuis network is used to test the impacts of CAVs on network performance. Figure 3.8(a) compares the path costs for OD pair 1-3 (see Table 3.2) at the equilibrium state when the VOTs of HDVs and CAVs are 10 and 5, respectively. Then, the link cost functions for HDVs and CAVs are different. It indicates that the minimum-cost paths for HDVs and CAVs are different (i.e., path 3 for HDVs and path 6 for CAVs). A large proportion of HDVs and CAVs for OD pair 1-3 are distributed on different paths, which reduces the network congestion level. However, Proposition 3 indicates that when the VOTs of HDVs and CAVs are equal, the minimum-cost paths for HDVs and CAVs are identical, because the travel costs of HDVs and CAVs for the same path are identical. Then, a large number of HDVs and CAVs for an OD pair would use the same minimum-cost paths, potentially leading to increased traffic congestion. Figure 3.8(b) shows that as the VOT of CAVs increases, the total travel cost of HDVs also increases monotonically.

Table 3.3: Route-link incidence relationship for OD pair 1-3

Path ID	Node sequence
1	1-12-6-10-11-3
2	1-12-6-7-11-3
3	1-5-9-13-3
4	1-5-9-10-11-3
5	1-5-6-10-11-3
6	1-5-6-7-11-3

To analyze the impacts of the CAV market penetration rate, Figure 3.9 shows the average OD travel costs of HDVs and CAVs under different CAV market penetration rates. It suggests that even a small percentage of CAVs (e.g., 10%) can significantly reduce the OD travel cost of both HDVs and CAVs. In addition, the average OD travel cost of both CAVs and HDVs decreases monotonically as the market penetration rate of CAVs increases, because it can increase the link capacity to reduce travel cost.

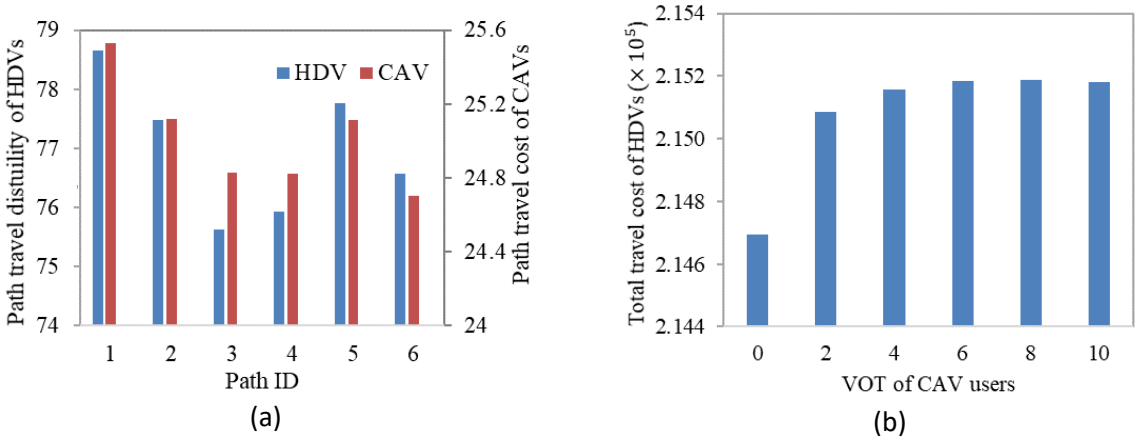

Figure 3.8: (a) Travel costs of paths for OD pair 1-4 for HDVs and CAVs, and (b) Total travel cost of HDVs under different VOTs for CAV users.

Suppose one of the lanes on link 7 is converted to an AV-dedicated lane. Figure 3.10(a) shows the total CAV flow on link 7 before and after the deployment of AV-dedicated lane. It indicates that the deployment of the AV-dedicated lane can attract more number of CAVs to link 7, especially when the market penetration rate of CAVs is low. To analyze the impact of the AV-dedicated lane on network performance, Figure 3.10(b) shows the ratio of the total travel costs (TTC) (i.e., the summation of travel costs of all CAV and HDV users in the network) after the deployment of the AV-dedicated lane and before the deployment. It suggests that the deployment of an AV-dedicated lane can reduce the network performance when the market penetration rate of CAVs is low as the usage of the AV-dedicated lane is low. Thereby, it is necessary to design an effective strategy to deploy an AV-dedicated lane optimally to improve the system performance under different CAV market penetration rates. The multiclass traffic assignment model and sensitivity analysis method proposed in this study can help to achieve this goal.

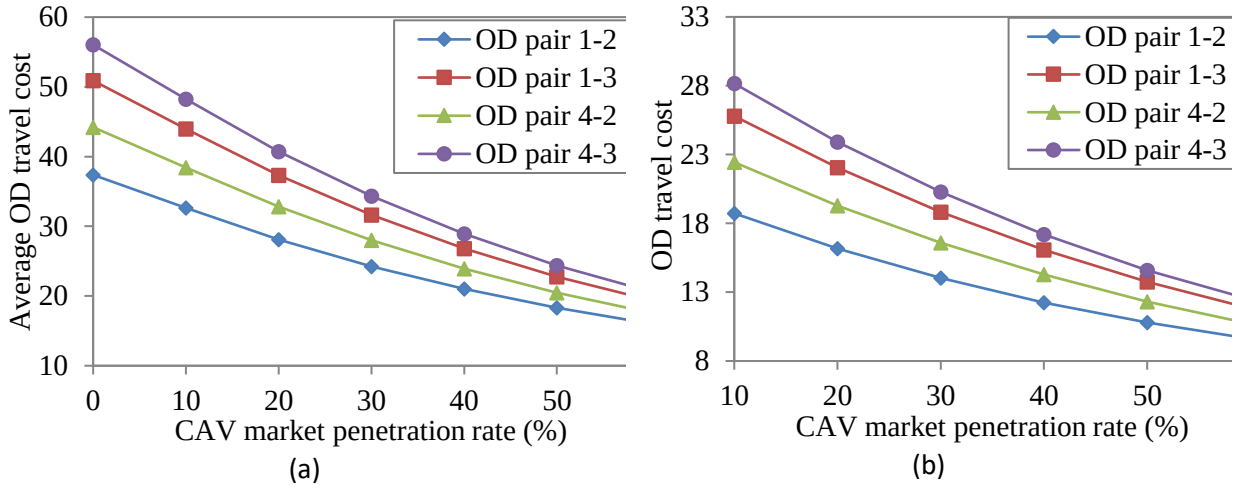

Figure 3.9: Average OD travel cost under different CAV penetration rates for: (a) HDVs, and (b) CAVs

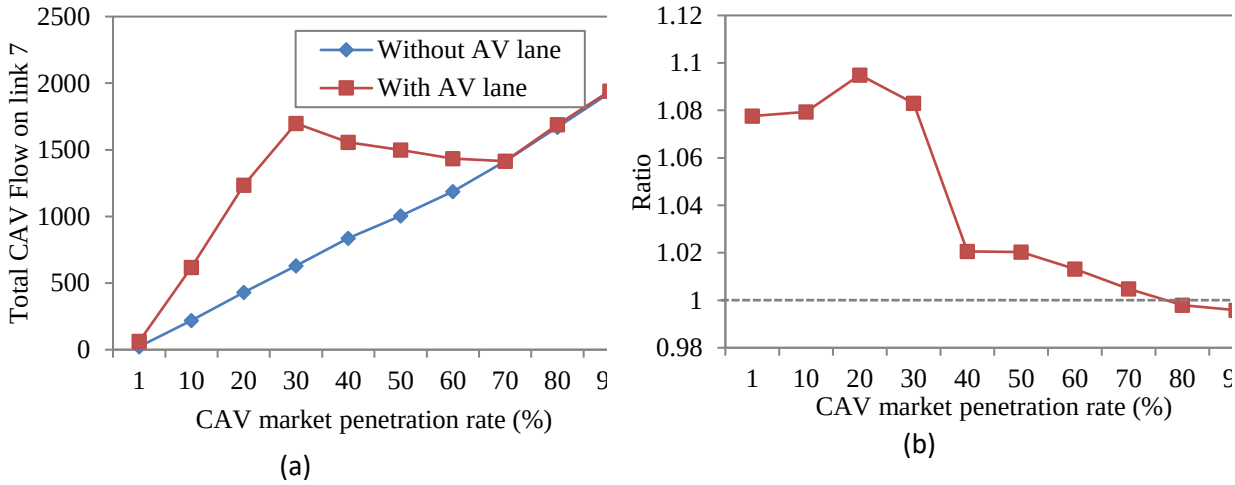

Figure 3.10: (a) Comparison of total CAV flow on link 7 before and after deployment of the AV-dedicated lane under different CAV market penetration rates, and (b) Ratio of total travel costs (TTC) after the deployment of AV-dedicated lane and before the deployment of AV-dedicated lane.

3.6 Sensitivity analysis

Planned (e.g., road maintenance, construction) or unexpected (e.g., accidents, facility failure, nature disasters) events can impact network flows significantly. When an event occurs, it is often difficult for planners and decision-makers to evaluate its impact on network performance (e.g., congestion, OD travel cost of CAVs) and to design effective strategies to mitigate negative effects. To address these issues, this study develops an analytical model for sensitivity analysis of the multiclass traffic assignment model. The sensitivity analysis determines the change in the objective function value for a unit change in the value of an explanatory variable. In literature, analytical formulations have been explored for sensitivity analysis of single-class traffic assignment models, including the

UE problem (Tobin and Friesz, 1988; Wang et al., 2016; Boyles et al., 2012; Jafari and Boyles, 2016), the logit-based and probit-based SUE models (Clark and Watling, 2000), the paired combinatorial logit model (Wang et al., 2018), and the elastic demand model (Yang, 1997). However, there are no studies that develop a sensitivity analysis method for multiclass traffic assignment model. The rest of this section derives the analytical model for sensitivity analysis of the proposed multiclass traffic assignment model (3.22) to obtain the gradients of equilibrium link flows of HDVs and CAVs with respect to perturbed parameters (e.g., link capacity, free-flow travel time, etc.). The analytical model can be used for applications such as: (i) constructing approximation methods to quickly estimate the perturbed mixed traffic equilibrium, (ii) identifying critical parameters (link capacity, signal splits) impacting network performance, (iii) risk analysis to provide insights on network performance reliability, (iv) analyzing impacts of traffic control methods on road network equilibrium, and (v) constructing solution algorithms for continuous network design problem (e.g., to find optimal signal timing or tolling strategy to improve the system performance under mixed traffic flow). This study explores the first application. Next, we will show the sufficient conditions for uniqueness of a local solution for link flows of HDVs and CAVs. The analytical model to obtain the gradients of the optimal link flow solution of HDVs and CAVs with respect to perturbed parameters is developed in Section 6.2.

3.6.1 Uniqueness of a local solution of link flows of HDVs and CAVs

The uniqueness of a local solution of link flows of HDVs and CAVs is a necessary condition for the existence of gradients of the equilibrium solution of link flows of HDVs and CAVs with respect to the perturbations (Facchinei and Pang, 2007). This section determines sufficient conditions for the uniqueness of a local solution of the VI problem (3.24). We will show that these sufficient conditions are mild, so that the local solution of path flows for HDVs and link flows for CAVs is unique in general.

Let $\boldsymbol{\nu} = [\mathbf{f}_H, \mathbf{v}_A]$, and $\tilde{\mathbf{C}} = [\mathbf{C}_H, \boldsymbol{t}_A]$. Denote $\boldsymbol{\nu}^*$as the solution to VI problem (3.24). Let SOL$(\boldsymbol{\Omega}_\mathbf{f}, \mathbf{C})$ and SOL$(\boldsymbol{\Omega}_\boldsymbol{\nu}, \tilde{\mathbf{C}})$ be the set of solutions of VI problems (3.22) and (3.24), respectively. Denote $\mathbf{f}^*$ ($\mathbf{f}^* \in$ SOL$(\boldsymbol{\Omega}_\mathbf{f}, \mathbf{C})$) and $\boldsymbol{\nu}^*$ ($\boldsymbol{\nu}^* \in$ SOL$(\boldsymbol{\Omega}_\boldsymbol{\nu}, \tilde{\mathbf{C}})$) as one of the solutions of VI problems (3.22) and (3.24), respectively. The following definition will be used to analyze whether $\mathbf{f}^*$ and $\boldsymbol{\nu}^*$ are locally unique.

Definition 3: Uniqueness of local solution (Facchinei and Pang, 2007). $\mathbf{f}^*$ is said to be a locally unique solution for VI problem (3.22) if there exists a neighborhood $\mathcal{H}_{\mathbf{f}^*}$ of $\mathbf{f}^*$ such that SOL$(\boldsymbol{\Omega}_\mathbf{f}, \mathbf{C}) \cap \mathcal{H}_{\mathbf{f}^*} = \mathbf{f}^*$; Similarly, $\boldsymbol{\nu}^*$ is said to be a locally unique solution for VI problem (3.24) if there exists a neighborhood $\mathcal{H}_{\boldsymbol{\nu}^*}$ of $\boldsymbol{\nu}^*$ such that SOL$\left(\boldsymbol{\Omega}_\boldsymbol{\nu}, \tilde{\mathbf{C}}\right) \cap \mathcal{H}_{\boldsymbol{\nu}^*} = \boldsymbol{\nu}^*$.

As CAVs choose paths according to the UE principle, any path flow solution $\mathbf{f}^*$ of the VI problem (3.22) may be locally non-unique because there may exist multiple equilibrium path flow solutions for CAVs in the neighborhood $\mathcal{H}_*$ of $\mathbf{f}^*$. According to Facchinei and Pang (2007), if Jacobian matrix of $\tilde{\mathbf{C}}$ with respect to $\boldsymbol{\nu}$ at the local optimal solution $\boldsymbol{\nu}^*$ (denoted as $\partial\tilde{\mathbf{C}}(\boldsymbol{\nu}^*)/\partial\boldsymbol{\nu}$) is positive definite, then $\boldsymbol{\nu}^*$ is a locally unique

solution for VI problem (3.24). In the following, we will analyze the sufficient conditions for $\partial\tilde{\mathbf{C}}(\mathbf{v}^*)/\partial\mathbf{v}$ being a positive definite matrix. Note

$$\frac{\partial\tilde{\mathbf{C}}(\mathbf{v}^*)}{\partial\mathbf{v}} = \begin{bmatrix} \frac{\partial \boldsymbol{C}_H^*}{\partial \mathbf{f}_H} & \frac{\partial \boldsymbol{C}_H^*}{\partial \mathbf{v}_A} \\ \frac{\partial \boldsymbol{t}_A^*}{\partial \mathbf{f}_H} & \frac{\partial \boldsymbol{t}_A^*}{\partial \mathbf{v}_A} \end{bmatrix}; \tag{3.30}$$

where

$$\frac{\partial \boldsymbol{t}_A^*}{\partial \mathbf{f}_H} = \nabla_{\mathbf{v}_H} \boldsymbol{t}_A^* \cdot \Delta_H \tag{3.31}$$

To characterize $\partial \boldsymbol{C}_H^*/\partial \mathbf{f}_H$ and $\partial \boldsymbol{C}_H^*/\partial \mathbf{v}_A$ analytically, let j be an arbitrary path for a HDV of an arbitrary OD pair w_1, $w_1 \in W_H$. According to Eq. (3.3)

$$\frac{dC_{k,H}^w}{df_{j,H}^{w_1}} = \frac{dc_{k,H}^w}{df_{j,H}^{w_1}} - \frac{u}{\theta}\frac{dH_{k,H}^w}{df_{j,H}^{w_1}} + \frac{u}{\theta}\frac{1}{f_{k,H}^w}\frac{df_{k,H}^w}{df_{j,H}^{w_1}} \tag{3.32}$$

where $df_k^w/df_j^{w_1} = 1$, if $w_1 = w$ and $k = j$. Otherwise, $df_k^w/df_j^{w_1} = 0$. According to Eq. (3.32)

$$\frac{dH_{k,H}}{df_{j,H}^{w_1}} = \frac{\sum_{m\in r_H}\left(\alpha_{m,k}^w\right)^{\frac{1}{u}}(u-1)\left(\sum_{l\in R_H^w}\left[\alpha_{m,l}^w \exp(-\theta c_{l,H}^w)\right]^{\frac{1}{u}}\right)^{u-2}}{\sum_{m\in r_H}\left(\alpha_{m,k}^w\right)^{1/u}\left(\sum_{l\in R_H^w}\left[\alpha_{m,l}^w \exp(-\theta c_{l,H}^w)\right]^{1/u}\right)^{u-1}} \sum_{l\in R_H^w}\left(-\frac{\theta}{u}\right)\left(\alpha_{m,l}^w\right)^{\frac{1}{u}}\exp\left(-\frac{\theta}{u}c_{l,H}^w\right)\frac{dc_{l,H}^w}{df_{j,H}^{w_1}}$$

Let

$$\rho_{k,l}^w = \frac{\sum_{m\in r_H}\left(\alpha_{m,k}^w\right)^{\frac{1}{u}}\left(\sum_{l\in R_H^w}\left[\alpha_{m,l}^w \exp(-\theta c_{l,H}^w)\right]^{\frac{1}{u}}\right)^{u-2}}{\sum_{m\in r_H}\left(\alpha_{m,k}^w\right)^{1/u}\left(\sum_{l\in R_H^w}\left[\alpha_{m,l}^w \exp(-\theta c_{l,H}^w)\right]^{1/u}\right)^{u-1}}\left(\alpha_{m,l}^w\right)^{\frac{1}{u}}\exp\left(-\frac{\theta}{u}c_{l,H}^w\right) \tag{3.33}$$

where $i \in R_H^w$. According to Eq. (3.33), $\rho_{k,l}^w \geq 0$ and

$$\sum_{l\in R_H^w}\rho_{k,l}^w = 1 \tag{3.34}$$

$$\frac{dH}{df_j^{w_1}} = \left(-\frac{\theta}{u}\right)(u-1)\begin{bmatrix}\rho_{k,1}^w & \rho_{k,2}^w & \cdots & \rho_{k,|R_H^w|}^w\end{bmatrix}\begin{bmatrix}\frac{dc_{1,H}^w}{df_{j,H}^{w_1}} & \frac{dc_{2,H}^w}{df_{j,H}^{w_1}} & \cdots & \frac{dc_{|R_H^w|,H}^w}{df_{j,H}^{w_1}}\end{bmatrix}^T \tag{3.35}$$

To characterize the matrix $\partial \boldsymbol{C}_H^*/\partial \mathbf{f}_H$ analytically, let $\boldsymbol{\rho}^w$ be a square matrix with dimension $|R_H^w|$,

$$\boldsymbol{\rho}^w = \begin{bmatrix} \rho^w_{1,1} & \rho^w_{1,2} & \cdots & \rho^w_{1,|R^w_H|} \\ \rho^w_{2,1} & \rho^w_{2,2} & \cdots & \rho^w_{2,|R^w_H|} \\ \vdots & \vdots & \vdots & \vdots \\ \rho^w_{|R^w_H|,1} & \rho^w_{|R^w_H|,2} & \cdots & \rho^w_{|R^w_H|,|R^w_H|} \end{bmatrix} \tag{3.36}$$

Let $\boldsymbol{\rho}$ be a diagonal block matrix with dimension equal to the number of paths for HDVs in the network:

$$\boldsymbol{\rho} = \begin{bmatrix} \boldsymbol{\rho^1} & 0 & 0 & 0 \\ 0 & \boldsymbol{\rho^2} & 0 & 0 \\ \vdots & \vdots & \vdots & \vdots \\ 0 & 0 & 0 & \boldsymbol{\rho}^{|W_H|} \end{bmatrix} \tag{3.37}$$

where $|W_H|$ is the number of OD pairs for HDVs in the network. According to Eq. (3.3), the gradient of $\mathbf{C}_H$ with respect to $\mathbf{f}_H$ at $\mathbf{f}^*$ is

$$\begin{aligned} \frac{\partial \boldsymbol{C}^*_H}{\partial \mathbf{f}_H} &= \nabla_{\mathbf{f}_H}\mathbf{c}^*_H - (1-u)\boldsymbol{\rho}^*\nabla_{\mathbf{f}_H}\mathbf{c}^*_H + \frac{u}{\theta} diag\left(\frac{\mathbf{1}}{\mathbf{f}^*_H}\right) \\ &= \Delta^T_H \cdot \nabla_{\mathbf{v}_H}\boldsymbol{t}^*_H \cdot \Delta_H - (1-u)\boldsymbol{\rho}^*\Delta^T_H \cdot \nabla_{\mathbf{v}_H}\boldsymbol{t}^*_H \cdot \Delta_H + \frac{u}{\theta} diag\left(\frac{\mathbf{1}}{\mathbf{f}^*_H}\right) \end{aligned} \tag{3.38}$$

where $\boldsymbol{\rho}^*$ denotes the value of matrix $\boldsymbol{\rho}$ at $\mathbf{f}^*$. Similarly,

$$\begin{aligned} \frac{\partial \boldsymbol{C}^*_H}{\partial \mathbf{v}} &= \nabla_{\mathbf{v}_A}\mathbf{c}^*_H - (1-u)\boldsymbol{\rho}^*\,\nabla_{\mathbf{v}_A}\mathbf{c}_H \\ &= \Delta^T_H \cdot \nabla_{\mathbf{v}_A}\boldsymbol{t}^*_H - (1-u)\boldsymbol{\rho}^*\Delta^T_H \cdot \nabla_{\mathbf{v}_A}\boldsymbol{t}^*_H \end{aligned} \tag{3.39}$$

Let $\mathbf{M}$ be a symmetric matrix defined as follows

$$\mathbf{M} = \frac{\partial \tilde{\mathbf{C}}(\mathbf{v}^*)}{\partial \mathbf{v}} + \left[\frac{\partial \tilde{\mathbf{C}}(\mathbf{v}^*)}{\partial \mathbf{v}}\right]^T = \begin{bmatrix} \mathbf{M}_1 + \frac{2u}{\theta} diag\left(\frac{1}{\mathbf{f}^*_H}\right) & \mathbf{M}_2 \\ \mathbf{M}_3 & 2\nabla_{\mathbf{v}_A}\boldsymbol{t}^*_A \end{bmatrix} \tag{3.40}$$

where

$$\mathbf{M}_1 = \nabla_{\mathbf{f}_H}\mathbf{c}^*_H + \left(\nabla_{\mathbf{f}_H}\mathbf{c}^*_H\right)^T - (1-u)\boldsymbol{\rho}^*\,\nabla_{\mathbf{f}_H}\mathbf{c}^*_H - \left[(1-u)\boldsymbol{\rho}^*\,\nabla_{\mathbf{f}_H}\mathbf{c}^*_H\right]^T \tag{3.41a}$$

$$\mathbf{M}_2 = \Delta^T_H \cdot \nabla_{\mathbf{v}_A}\boldsymbol{t}^*_H - (1-u)\boldsymbol{\rho}^*\Delta^T_H \cdot \nabla_{\mathbf{v}_A}\boldsymbol{t}^*_H + \left(\nabla_{\mathbf{v}_H}\boldsymbol{t}^*_A \cdot \Delta_H\right)^T \tag{3.41b}$$

$$\mathbf{M}_3 = \mathbf{M}^T_2 \tag{3.41c}$$

The following proposition will be used to show the sufficient conditions for uniqueness of a local solution of VI problem (3.24).

Proposition 7: $\mathbf{M}_1 + \frac{2u}{\theta} diag(\mathbf{f}_H) - \mathbf{M}_2\left(2\nabla_{\mathbf{v}_H}\boldsymbol{t}_A^*\right)^{-1}\mathbf{M}_3$ is a non-singular matrix if the matrix $\frac{\theta}{2u} diag(\mathbf{f}_H^*) \cdot \left(\mathbf{M}_2\left(2\nabla_{\mathbf{v}_H}\boldsymbol{t}_A^*\right)^{-1}\mathbf{M}_3 - \mathbf{M}_1\right)$ has no eigenvalue 1.

Proof: See Appendix B. ■

Proposition 8: If $\partial\mathbf{C}(\mathbf{f}^*)/\partial\mathbf{f}$ is positive semidefinite and the matrix $\frac{\theta}{2u} diag(\mathbf{f}_H^*)\left(\mathbf{M}_2\left(2\nabla_{\mathbf{v}_H}\boldsymbol{t}_A^*\right)^{-1}\mathbf{M}_3 - \mathbf{M}_1\right)$ has no eigenvalue 1, then $\partial\tilde{\mathbf{C}}(\mathbf{v}^*)/\partial\mathbf{v}$ is positive definite.

Proof: See Appendix C. ■

The two conditions are sufficient to show a solution of path flows for HDVs and link flows for CAVs is locally unique. Numerical test can be taken to identify whether the two conditions are satisfied at a local optimal solution $\mathbf{v}^*$ after it is obtained using the solution algorithm. However, it is important to know that the two conditions in Proposition 8 are not strong. First, the condition $\partial\mathbf{C}(\mathbf{f}^*)/\partial\mathbf{f}$ is positive semidefinite is sufficient to ensure $\mathbf{f}^*$ is a stationary optimal solution for VI problem (3.21), that is, $\mathbf{f}^*$ is not a saddle point (Facchinei and Pang, 2007). It can be satisfied by Assumption 1 in Section 4. To show the matrix $\frac{\theta}{2u} diag(\mathbf{f}_H^*)\left(\mathbf{M}_2\left(2\nabla_{\mathbf{v}_H}\boldsymbol{t}_A^*\right)^{-1}\mathbf{M}_3 - \mathbf{M}_1\right)$ has no eigenvalue 1 in general, we first investigate the conditions when $VOT_A = VOT_H$, and $Q_{a,H} = Q_{a,A}, \forall a \in \boldsymbol{\Gamma}_H$. Under these conditions, we have $\frac{\theta}{2u} diag(\mathbf{f}_H^*)\left(\mathbf{M}_2\left(2\nabla_{\mathbf{v}_H}\boldsymbol{t}_A^*\right)^{-1}\mathbf{M}_3 - \mathbf{M}_1\right) = \frac{\theta}{2u} diag(\mathbf{f}_H^*) \cdot \mathbf{0} = \mathbf{0}$. This implies that all eigenvalues of this matrix are 0 at $VOT_A = VOT_H$, and $Q_{a,H} = Q_{a,A}, \forall a \in \boldsymbol{\Gamma}_H$. Note that all the entries in the matrix vary continuously with respect to the values of VOT_A, and $Q_{a,H}, \forall a \in \boldsymbol{\Gamma}_H$. Thereby, when VOT_A, and $Q_{a,H}, \forall a \in \boldsymbol{\Gamma}_H$ change from the values $VOT_A = VOT_H$ and $Q_{a,H} = Q_{a,A}$, the eigenvalues of this matrix vary continuously in a neighbourhood of $\mathbf{0}$. This indicates the matrix $\frac{\theta}{2u} diag(\mathbf{f}_H^*) \cdot \left(\mathbf{M}_2\left(2\nabla_{\mathbf{v}_H}\boldsymbol{t}_A^*\right)^{-1}\mathbf{M}_3 - \mathbf{M}_1\right)$ having an eigenvalue 1 is a special case, and the likelihood of its occurrence is low for given values of VOT , and $Q_{a,H}, \forall a \in \boldsymbol{\Gamma}_H$ in a real-world network. Thereby, $\partial\tilde{\mathbf{C}}(\mathbf{v}^*)/\partial\mathbf{v}$ is positive definite at the equilibrium state in general. This indicates that while the solution of VI problems (3.22) is not locally unique, the solution of VI problem (3.24) is locally unique provided the conditions in Proposition 8 are satisfied. This property is a necessary condition for sensitivity analysis of the multiclass traffic assignment model in the next section. It is important to note that while the two conditions in Proposition 8 are not strong, numerical test is still needed to verify and ensure $\partial\tilde{\mathbf{C}}(\mathbf{v}^*)/\partial\mathbf{v}$ is positive definite.

3.6.2 Sensitivity analysis of the multiclass traffic assignment problem

This section presents an analytical model to determine the gradients of the equilibrium link flow of both CAVs and HDVs with respect to the perturbed parameters (e.g., signal splits, link capacity of pure CAVs and HDVs, value of time for CAVs and HDVs, etc). Let $\boldsymbol{\varepsilon}$ be a vector of perturbed parameters in the multiclass traffic assignment problem (3.22), and $\mathbf{f}^* = [\mathbf{f}_H^{T*}(\mathbf{0}), \mathbf{f}_A^{T*}(\mathbf{0})]$ be a local equilibrium path flow solution to the VI problem (3.22) at the unperturbed state (i.e., $\boldsymbol{\varepsilon} = \mathbf{0}$). The KKT conditions at $\mathbf{f}^*$ are

$$\mathbf{C}_H(\mathbf{f}^*, \mathbf{0}) - \boldsymbol{\pi}_H^* - \Lambda_H^T \boldsymbol{\mu}_H^* = \mathbf{0} \tag{3.42a}$$

$$\mathbf{C}_A(\mathbf{f}^*, \mathbf{0}) - \boldsymbol{\pi}_A^* - \Lambda_A \boldsymbol{\mu}_A^* = \mathbf{0} \tag{3.42b}$$

$$\begin{bmatrix} \Lambda_H & \\ & \Lambda_A \end{bmatrix} \begin{bmatrix} \mathbf{f}_H^* \\ \mathbf{f}_A^* \end{bmatrix} - \begin{bmatrix} \mathbf{q}_H(\mathbf{0}) \\ \mathbf{q}_A(\mathbf{0}) \end{bmatrix} = \mathbf{0} \tag{3.42c}$$

$$\boldsymbol{\pi}_H^* \mathbf{f}_H^* = \mathbf{0} \tag{3.42d}$$

$$\boldsymbol{\pi}_A^* \mathbf{f}_A^* = \mathbf{0} \tag{3.42e}$$

$$\mathbf{f}_A^* \geq \mathbf{0}; \mathbf{f}_H^* > \mathbf{0} \tag{3.42f}$$

$$\boldsymbol{\pi}_H^* \geq \mathbf{0}; \boldsymbol{\pi}_A^* \geq \mathbf{0} \tag{3.42g}$$

where $\boldsymbol{\mu}_H^*$ and $\boldsymbol{\mu}_A^*$ are vectors of Lagrange multipliers associated with the constraints $\Lambda_H \mathbf{f}_H = \mathbf{q}_H$ and $\Lambda_A \mathbf{f}_A = \mathbf{q}_A$, respectively. $\boldsymbol{\pi}_H^*$ and $\boldsymbol{\pi}_A^*$ are vectors of Lagrange multipliers associated with the nonnegative path flow constraints for HDVs and CAVs, respectively.

As discussed in Section 6.1, the path flow solution to VI problem (3.22) may not be locally unique. This precludes the existence of gradients for the path flow solution of VI problem (3.22) with respect to the perturbed parameters. To address this problem, a linear equation designed by Yang and Bell (2005) will be used in this study to obtain the path flow solution of CAVs that has the desired uniqueness. The method is developed upon the following assumption.

Assumption 2: The equilibrium path flow solution of CAVs of VI problem (3.22) at unperturbed state ($\boldsymbol{\varepsilon} = 0$) is not degenerate. That is, there exists a path flow solution such that the flow of equilibrated paths (i.e., paths with minimum travel cost for the corresponding OD pair) for CAVs is positive.

Assumption 2 is not strong in the sense that the degenerate points are isolated points when $\boldsymbol{\varepsilon}$ is nonzero. The likelihood of occurrence is low at the unperturbed state (i.e., $\boldsymbol{\varepsilon} = 0$) in the real network.

Let $\hat{R}_A$ be the set of equilibrated paths for CAVs at $[\mathbf{f}_H^*, \mathbf{f}_A^*]$, and $\hat{\mathbf{f}}_A^*$ be the flow vector for all equilibrated paths in set $\hat{R}_A$. Note that $\hat{\mathbf{f}}_A^*$ is not unique as $\mathbf{f}_A^*$ is not unique. Let $\begin{bmatrix} \hat{\Delta}_A \\ \hat{\Lambda} \end{bmatrix}$ be the link-path and OD-path matrix for paths in set $\hat{R}$. Denote $\begin{bmatrix} \bar{\Delta}_A \\ \bar{\Lambda}_A \end{bmatrix}$ as a full

column matrix constituted by column vectors in $\begin{bmatrix}\hat{\Delta}_A\\ \hat{\Lambda}_A\end{bmatrix}$ that has the same rank as $\begin{bmatrix}\hat{\Delta}_A\\ \hat{\Lambda}_A\end{bmatrix}$. Let $\bar{R}$ be the set of paths with link-path and OD-path matrix $\begin{bmatrix}\bar{\Delta}_A\\ \bar{\Lambda}_A\end{bmatrix}$. The paths in set $\bar{R}_A$ are labeled equilibrated and linearly independent (ELI) paths, and the equilibrated paths for CAVs not in set $\bar{R}_A$ are labeled equilibrated and linearly dependent (ELD) paths. Let $\bar{\mathbf{f}}_A$ and $\tilde{\mathbf{f}}_A$ be the vector of all ELI and ELD path flows for CAVs, respectively. According to Assumption 2, an equilibrium path flow solution exists for CAVs such that flow of all equilibrated paths is positive at $\boldsymbol{\varepsilon} = 0$. Let $\begin{bmatrix}\bar{\mathbf{f}}_A^*\\ \tilde{\mathbf{f}}_A^*\end{bmatrix}$ $(\bar{\mathbf{f}}_A^* > 0; \tilde{\mathbf{f}}_A^* > 0)$ be such a path flow solution for CAVs. Then

$$\begin{bmatrix}\hat{\Delta}_A\\ \hat{\Lambda}_A\end{bmatrix}\hat{\mathbf{f}}_A^* = \begin{bmatrix}\bar{\Delta}_A & \tilde{\Delta}_A\\ \bar{\Lambda}_A & \tilde{\Lambda}_A\end{bmatrix}\begin{bmatrix}\bar{\mathbf{f}}_A^*(\mathbf{0})\\ \tilde{\mathbf{f}}_A^*(\mathbf{0})\end{bmatrix} = \begin{bmatrix}\mathbf{v}_A(\mathbf{0})\\ \mathbf{d}_A(\mathbf{0})\end{bmatrix} \tag{3.43}$$

where $\begin{bmatrix}\tilde{\Delta}_A\\ \tilde{\Lambda}_A\end{bmatrix}$ is the link-path and OD-path matrix for all paths in $\tilde{\mathbf{f}}_A$. According to Eq. (3.43),

$$\begin{bmatrix}\bar{\Delta}_A\\ \bar{\Lambda}_A\end{bmatrix}\bar{\mathbf{f}}_A^*(\varepsilon) = \begin{bmatrix}\mathbf{v}_A(\varepsilon)\\ \mathbf{q}_A(\varepsilon)\end{bmatrix} - \begin{bmatrix}\tilde{\Delta}_A\\ \tilde{\Lambda}_A\end{bmatrix}\tilde{\mathbf{f}}_A^*(0) \tag{3.44}$$

When ε changes, only $\bar{\mathbf{f}}_A^*(\varepsilon)$ changes, and the flow of ELD paths for HDVs are fixed at $\tilde{\mathbf{f}}_A^*(0)$. As $\bar{\mathbf{f}}_A^*(0) > 0$, $\bar{\mathbf{f}}_A^*(\varepsilon) > 0$ for a small perturbation of $\boldsymbol{\varepsilon}$. Note that as $\begin{bmatrix}\bar{\Delta}_A\\ \bar{\Lambda}_A\end{bmatrix}$ is a full column matrix, $\bar{\mathbf{f}}_A^*(\varepsilon)$ is unique. Thereby, when $\boldsymbol{\varepsilon}$ varies for a sufficiently small value from 0, a unique path flow solution $\begin{bmatrix}\bar{\mathbf{f}}_A^*(\varepsilon)\\ \tilde{\mathbf{f}}_A^*(0)\end{bmatrix}$ can be found by Eq. (3.44). According to Assumption 2, the non-equilibrated paths will remain non-equilibrated for a small perturbation of $\boldsymbol{\varepsilon}$. Since the flows of HDVs are all positive, and $\bar{\mathbf{f}}_A^* > 0, \tilde{\mathbf{f}}_A^* > 0$, all the Lagrange multipliers in vector $\boldsymbol{\pi}_H^*$ and $\boldsymbol{\pi}_A^*$ are nonbinding. Thereby, Eq. (3.42) can be simplified as

$$\mathbf{C}_H(\mathbf{f}^*, 0) - \Lambda_H^T\boldsymbol{\mu}_H^*(0) = \mathbf{0} \tag{3.45a}$$

$$\bar{\mathbf{C}}_A(\mathbf{f}^*, 0) - \Lambda_A^T\boldsymbol{\mu}_A^*(0) = \mathbf{0} \tag{3.45b}$$

$$\begin{bmatrix}\Lambda_H & \\ & \bar{\Lambda}_A\end{bmatrix}\begin{bmatrix}\mathbf{f}_H^*(0)\\ \bar{\mathbf{f}}_A^*(0)\end{bmatrix} + \begin{bmatrix}0 & \\ & \tilde{\Lambda}_A\end{bmatrix}\begin{bmatrix}\mathbf{f}_H^*(0)\\ \tilde{\mathbf{f}}_A^*(0)\end{bmatrix} - \begin{bmatrix}\mathbf{q}_H(0)\\ \mathbf{q}_A(0)\end{bmatrix} = \mathbf{0} \tag{3.45c}$$

where $\bar{\mathbf{C}}_A(\mathbf{f}^*, 0)$ is the vector of generalized travel costs of all ELI paths for CAVs. As $\tilde{\mathbf{f}}_A^*(0)$ is fixed, the gradients of Eq. (3.45) with respect to the perturbed parameter $\boldsymbol{\varepsilon}$ are

$$\nabla_{\boldsymbol{\varepsilon}}\mathbf{C}_H(\mathbf{f}^*, 0) + \nabla_{\mathbf{f}_H}\mathbf{C}_H(\mathbf{f}^*, 0)\nabla_{\boldsymbol{\varepsilon}}\mathbf{f}_H^*(\mathbf{0}) + \nabla_{\bar{\mathbf{f}}_A}\mathbf{C}_H(\mathbf{f}^*, \mathbf{0})\nabla_{\boldsymbol{\varepsilon}}\bar{\mathbf{f}}^*(0) - \Lambda_H^T\nabla_{\boldsymbol{\varepsilon}}\boldsymbol{\mu}_H^*(0) = \mathbf{0} \tag{3.46a}$$

$$\nabla_{\boldsymbol{\varepsilon}}\bar{\mathbf{C}}_A(\mathbf{f}^*,0)+\nabla_{\mathbf{f}_H}\bar{\mathbf{C}}_A(\mathbf{f}^*,\mathbf{0})\nabla_{\boldsymbol{\varepsilon}}\mathbf{f}_H^*(0)+\nabla_{\bar{\mathbf{f}}_A}\bar{\mathbf{C}}_A(\mathbf{f}^*,0)\nabla_{\boldsymbol{\varepsilon}}\bar{\mathbf{f}}_A(\mathbf{0})-\bar{\Lambda}_A^T\nabla_{\boldsymbol{\varepsilon}}\boldsymbol{\mu}_A^*(0)=\mathbf{0} \quad (3.46b)$$

$$\begin{bmatrix}\Lambda_H & \\ & \bar{\Lambda}_A\end{bmatrix}\begin{bmatrix}\nabla_{\boldsymbol{\varepsilon}}\mathbf{f}_H^*(0)\\ \nabla_{\boldsymbol{\varepsilon}}\bar{\mathbf{f}}_A^*(0)\end{bmatrix}+\begin{bmatrix}0 & \\ & \tilde{\Lambda}_A\end{bmatrix}\begin{bmatrix}\nabla_{\boldsymbol{\varepsilon}}\mathbf{f}_H^*(0)\\ \nabla_{\boldsymbol{\varepsilon}}\tilde{\mathbf{f}}_A^*(0)\end{bmatrix}-\begin{bmatrix}\nabla_{\boldsymbol{\varepsilon}}\mathbf{q}_H(\mathbf{0})\\ \nabla_{\boldsymbol{\varepsilon}}\mathbf{q}_A(\mathbf{0})\end{bmatrix}=\mathbf{0} \quad (3.46c)$$

Note that $\nabla_{\boldsymbol{\varepsilon}}\tilde{\mathbf{f}}_A^*(0)\equiv 0$ as $\tilde{\mathbf{f}}_A$ is fixed. Thereby,

$$\begin{bmatrix}\nabla_{\boldsymbol{\varepsilon}}\mathbf{f}_H^*(0)\\ \nabla_{\boldsymbol{\varepsilon}}\bar{\mathbf{f}}_A^*(0)\\ \nabla_{\boldsymbol{\varepsilon}}\boldsymbol{\mu}_H^*(0)\\ \nabla_{\boldsymbol{\varepsilon}}\boldsymbol{\mu}_A^*(0)\end{bmatrix}=\left(\boldsymbol{J}_{\bar{\mathbf{f}}}^*\right)^{-1}(-\boldsymbol{J}_{\boldsymbol{\varepsilon}}^*) \quad (3.47)$$

where

$$\boldsymbol{J}_{\bar{\mathbf{f}}}^*=\begin{bmatrix}\nabla_{\mathbf{f}_H}\mathbf{C}_H(\mathbf{f}^*,\mathbf{0}) & \nabla_{\bar{\mathbf{f}}_A}\mathbf{C}_H(\mathbf{f}^*,\mathbf{0}) & \Lambda_H^T & \\ \nabla_{\mathbf{f}_H}\bar{\mathbf{C}}_A(\mathbf{f}^*,\mathbf{0}) & \nabla_{\bar{\mathbf{f}}_A}\bar{\mathbf{C}}_A(\mathbf{f}^*,\mathbf{0}) & & \bar{\Lambda}_A^T\\ \Lambda_H & & & \\ & \bar{\Lambda}_A & & \end{bmatrix} \quad (3.48)$$

$$\boldsymbol{J}_{\boldsymbol{\varepsilon}}^*=\begin{bmatrix}\nabla_{\boldsymbol{\varepsilon}}\mathbf{C}_H(\mathbf{f}^*,\mathbf{0})\\ \nabla_{\boldsymbol{\varepsilon}}\bar{\mathbf{C}}_A(\mathbf{f}^*,\mathbf{0})\\ \nabla_{\boldsymbol{\varepsilon}}\mathbf{q}_H(\mathbf{0})\\ \nabla_{\boldsymbol{\varepsilon}}\mathbf{q}_A(\mathbf{0})\end{bmatrix} \quad (3.49)$$

The analytical form of $\nabla_{\mathbf{f}_H}\mathbf{C}_H(\bar{\mathbf{f}}^*,\mathbf{0})$ can be found in Eq. (3.38). The analytical forms of $\nabla_{\bar{\mathbf{f}}_A}\mathbf{C}_H(\bar{\mathbf{f}}^*,\mathbf{0})$, $\nabla_{\mathbf{f}_H}\bar{\mathbf{C}}_A(\bar{\mathbf{f}}^*,\mathbf{0})$ and $\nabla_{\bar{\mathbf{f}}_A}\bar{\mathbf{C}}_A(\bar{\mathbf{f}}^*,\mathbf{0})$ are

$$\nabla_{\bar{\mathbf{f}}_A}\mathbf{C}_H(\mathbf{f}^*,\mathbf{0})=\Delta_H^T\cdot\nabla_{\mathbf{v}_A}\boldsymbol{t}_H^*\cdot\bar{\Delta}_A-(1-u)\boldsymbol{\rho}^*\Delta_H^T\cdot\nabla_{\mathbf{v}_A}\boldsymbol{t}_H^*\cdot\bar{\Delta}_A \quad (3.50a)$$

$$\nabla_{\mathbf{f}_H}\bar{\mathbf{C}}_A(\mathbf{f}^*,\mathbf{0})=\bar{\Delta}_A^T\cdot\nabla_{\mathbf{v}_H}\boldsymbol{t}_A^*\cdot\Delta_H \quad (3.50b)$$

$$\nabla_{\bar{\mathbf{f}}_A}\bar{\mathbf{C}}_A(\mathbf{f}^*,\mathbf{0})=\bar{\Delta}_A^T\cdot\nabla_{\mathbf{v}_A}\boldsymbol{t}_A^*\cdot\bar{\Delta}_A \quad (3.50c)$$

The following theorem constructed based on Corollary 3.2.5 in Fiacco (1983) provides the sufficient conditions for existence of gradients $\nabla_{\boldsymbol{\varepsilon}}\mathbf{f}_H^*(0)$, $\nabla_{\boldsymbol{\varepsilon}}\bar{\mathbf{f}}_A^*(0)$, $\nabla_{\boldsymbol{\varepsilon}}\boldsymbol{\mu}_H^*(0)$ and $\nabla_{\boldsymbol{\varepsilon}}\boldsymbol{\mu}_A^*(0)$ in Eq. (3.47).

Theorem 6: The gradients $\nabla_{\boldsymbol{\varepsilon}}\mathbf{f}_H^*(0)$, $\nabla_{\boldsymbol{\varepsilon}}\bar{\mathbf{f}}^*(0)$, $\nabla_{\boldsymbol{\varepsilon}}\boldsymbol{\mu}_H^*(0)$ and $\nabla_{\boldsymbol{\varepsilon}}\boldsymbol{\mu}_A^*(0)$ exist if $\boldsymbol{J}_{\bar{\mathbf{f}}}^*$ is invertible and the terms $\mathbf{C}_H(\mathbf{f}^*,\mathbf{0})$, $\mathbf{C}_A(\mathbf{f}^*,\mathbf{0})$, $\mathbf{q}_H(\mathbf{0})$ and $\mathbf{q}_A(\mathbf{0})$ are first-order differentiable with respect to $\boldsymbol{\varepsilon}$.

According to the link cost functions (Eq. (3.19)), $\mathbf{C}_H(\mathbf{f}^*,\mathbf{0})$, $\mathbf{C}_A(\mathbf{f}^*,\mathbf{0})$, $\mathbf{q}_H(\mathbf{0})$ and $\mathbf{q}_A(\mathbf{0})$ are first-order differentiable with respect to $\boldsymbol{\varepsilon}$. Thereby the derivatives in the left-hand side of Eq. (3.47) exists if $\boldsymbol{J}_{\bar{\mathbf{f}}}^*$ is invertible. The following proposition discusses the sufficient conditions for invertibility of $\boldsymbol{J}_{\bar{\mathbf{f}}}^*$.

Proposition 9: If matrix $\frac{\partial \tilde{\mathbf{C}}(\mathbf{v}^*)}{\partial \mathbf{v}} = \begin{bmatrix} \frac{\partial C_H^*}{\partial \mathbf{f}_H} & \frac{\partial C_H^*}{\partial \mathbf{v}_A} \\ \frac{\partial t_A^*}{\partial \mathbf{f}_H} & \frac{\partial t_A^*}{\partial \mathbf{v}_A} \end{bmatrix}$ is positive definite. Then $\boldsymbol{J}_{\bar{\mathbf{f}}}^*$ is invertible**.**

Proof: See Appendix D. ■

$\partial \tilde{\mathbf{C}}(\mathbf{v}^*)/\partial \mathbf{v}$ is positive definite is a sufficient condition to ensure that the solution $\mathbf{v}^*$ of VI problem (3.24) is locally unique. The two conditions for $\partial \tilde{\mathbf{C}}(\mathbf{v}^*)/\partial \mathbf{v}$ being a positive definite matrix are discussed in Proposition 8. Note that the two conditions are not strong. Thereby, $\boldsymbol{J}_{\bar{\mathbf{f}}}^*$ is invertible in general at the equilibrium state. It is important to note that if $\mathbf{v}^*$ is not locally unique, then the gradients in the left-hand side of Eq. (3.47) do not exist (Tobin, 1986). When applying the sensitivity analysis method in practice, rather than checking whether $\partial \tilde{\mathbf{C}}(\mathbf{v}^*)/\partial \mathbf{v}$ is positive definite, a simple way to check invertibility of matrix $\boldsymbol{J}_{\bar{\mathbf{f}}}^*$ is to determine whether it is a full rank matrix at the equilibrium state. According to Eq. (3.47)

$$\nabla_{\boldsymbol{\varepsilon}} \mathbf{v}_H^*(0) = \Delta_H \nabla_{\boldsymbol{\varepsilon}} \mathbf{f}_H^*(0) \tag{3.51a}$$

$$\nabla_{\boldsymbol{\varepsilon}} \mathbf{v}_A^*(0) = \bar{\Delta}_A \nabla_{\boldsymbol{\varepsilon}} \bar{\mathbf{f}}_A^*(0) \tag{3.51b}$$

Eq. (3.47) is derived based on the ELI path set $\bar{R}_A$ and the assumption of fixed flow of ELD paths when $\boldsymbol{\varepsilon}$ changes. Following the proof of Yang and Bell (2005), it can be shown that the gradients $\nabla_{\boldsymbol{\varepsilon}} \mathbf{v}_H^*(0)$ and $\nabla_{\boldsymbol{\varepsilon}} \mathbf{v}_A^*(0)$ are independent with respect to the ELI path set $\bar{R}_A$ and the corresponding flows of ELD paths. Thereby, the gradients $\nabla_{\boldsymbol{\varepsilon}} \mathbf{v}_H^*(0)$ and $\nabla_{\boldsymbol{\varepsilon}} \mathbf{v}_A^*(0)$ exist if the condition in Proposition 9 is satisfied. The perturbed equilibrium link flow for HDVs and CAVs can then be estimated using the first-order approximation (FOA) approach as follows:

$$\hat{\mathbf{v}}_H^* = \mathbf{v}_H^*(0) + \delta_{\boldsymbol{\varepsilon}} \times \nabla_{\boldsymbol{\varepsilon}} \mathbf{v}_H^*(0) \tag{3.52a}$$

$$\hat{\mathbf{v}}^* = \mathbf{v}^*(0) + \delta_{\boldsymbol{\varepsilon}} \times \nabla_{\boldsymbol{\varepsilon}} \mathbf{v}_A^*(0) \tag{3.52b}$$

where $\delta_{\boldsymbol{\varepsilon}}$ is the scale of perturbation.

3.7 Numerical examples for Sensitivity analysis

3.7.1 A small network

This section presents two examples to demonstrate the application of sensitivity analysis for the multiclass traffic assignment model. We use the first example, constructed on a small network shown in Figure 11, to illustrate the details of and insights into the sensitivity analysis process. It contains one OD pair, 5 regular links (i.e., links 1, 2, 3, 4 and 5) and one AV-dedicated lane (i.e., link 6). There are three paths for HDVs and four paths for CAVs. The paths for HDVs are represented by link chain as: path 1:{1,4}, path 2: {2,5} , path 3: {1,3,5}, and the additional path for only CAVs, i.e., path 4: {1,6,5}. The VOT for HDVs and CAVs is set as 10 and 5, respectively. The OD demand for HDVs and CAVs is 30 and 20, respectively. The dispersion parameter and degree of

nesting are $\theta = 1, u = 0.5$, respectively. The other inputs for this network can be found in Table 3.3. It is important to note that the capacity of the AV-dedicated lane (i.e., link 6) for HDVs is set to a very small value to prevent the HDVs from using the AV-dedicated lane.

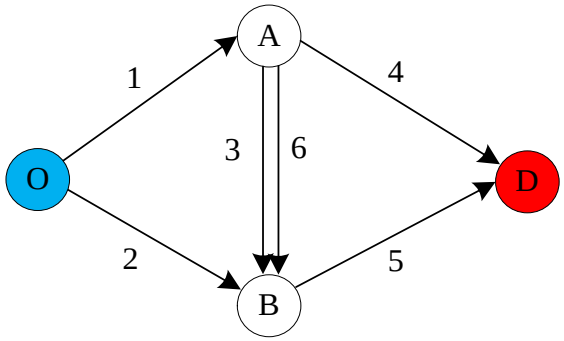

Figure 3.11: Network for demonstrating sensitivity analysis

Table 3.4: Inputs for the network in Figure 3.11

Links	1	2	3	4	5	6
Length of links (l_a)	4	7	1	5	2	1
Speed limit (s_a)	50	50	50	50	50	50
Capacity of HDVs ($Q_{a,H}$)	20	20	10	20	20	0.0001
Capacity of CAVs ($Q_{a,A}$)	40	40	20	20	40	60

The equilibrium path flow and link flow solutions for HDVs and CAVs are computed as

$$\mathbf{f}_H^* = [10.358 \quad 11.249 \quad 8.392]^T; \mathbf{f}_A^* = [6.304 \quad 9.834 \quad 0 \quad 3.861]^T;$$

$$\mathbf{v}_H^* = [18.751 \quad 11.249 \quad 8.392 \quad 10.358 \quad 19.642 \quad 0]^T;$$

$$\mathbf{v}_A^* = [10.166 \quad 9.834 \quad 0 \quad 6.304 \quad 13.696 \quad 3.861]^T$$

Note that path 3 is a non-equilibrated route for CAVs, and the link-path and OD-path incidence vector of the other three routes are linearly independent. Then, $\bar{\mathbf{f}}_A^* = [6.304 \quad 9.834 \quad 3.861]^T$, and

$$\bar{\Delta}_A = \begin{bmatrix} 1 & 0 & 1 \\ 0 & 1 & 0 \\ 0 & 0 & 0 \\ 1 & 0 & 0 \\ 0 & 1 & 1 \\ 0 & 0 & 1 \end{bmatrix}; \bar{\Lambda}_A = [1 \quad 1 \quad 1]; \Delta_H = \begin{bmatrix} 1 & 0 & 1 \\ 0 & 1 & 0 \\ 0 & 0 & 1 \\ 1 & 0 & 0 \\ 0 & 1 & 1 \\ 0 & 0 & 0 \end{bmatrix}; \Lambda_H = [1 \quad 1 \quad 1]$$

Suppose the OD demand for HDVs increases by 5. Then, $\varepsilon = q_H$, and

$$\boldsymbol{J}_{\boldsymbol{\varepsilon}}^{*} = [0 \quad 0 \quad 0 \quad 0 \quad 0 \quad 0 \quad 1 \quad 0]^{T} \tag{3.53}$$

To calculate $\boldsymbol{J}_{\bar{\mathbf{f}}}^{*}$, the matrix $\boldsymbol{\rho}^{*}$ is determined first using Eq. (3.37) as follows:

$$\boldsymbol{\rho}^{*} = \begin{bmatrix} 0.805 & 0 & 0.194 \\ 0 & 0.911 & 0.089 \\ 0.240 & 0.120 & 0.641 \end{bmatrix} \tag{3.54}$$

According to Eq. (3.38) and Eq. (3.50), the gradients of the generalized path travel costs for CAVs and HDVs with respect to path flows of both CAVs and HDVs are computed as:

$$\frac{\partial \boldsymbol{C}_{H}^{*}}{\partial \mathbf{f}_{H}} = \Delta_{H}^{T} \cdot \nabla_{\mathbf{v}_{H}} \boldsymbol{t}_{H}^{*} \cdot \Delta_{H} - (1-u)\boldsymbol{\rho}^{*} \Delta_{H}^{T} \cdot \nabla_{\mathbf{v}_{H}} \boldsymbol{t}_{H}^{*} \cdot \Delta_{H} + \frac{u}{\theta} diag\left(\frac{\mathbf{1}}{\bar{\mathbf{f}}_{H}^{*}}\right)$$
$$= \begin{bmatrix} 0.154 & -0.011 & 0.069 \\ -0.007 & 0.151 & 0.047 \\ 0.088 & 0.064 & 0.242 \end{bmatrix} \tag{3.55a}$$

$$\frac{\partial \boldsymbol{C}_{H}^{*}}{\partial \bar{\mathbf{f}}_{A}} = \Delta_{H}^{T} \cdot \nabla_{\mathbf{v}_{A}} \boldsymbol{t}_{H}^{*} \cdot \bar{\Delta}_{A} - (1-u)\boldsymbol{\rho}^{*} \Delta_{H}^{T} \cdot \nabla_{\mathbf{v}_{A}} \boldsymbol{t}_{H}^{*} \cdot \bar{\Delta}_{A}$$
$$= \begin{bmatrix} 0.053 & -0.005 & 0.036 \\ -0.004 & 0.053 & 0.024 \\ 0.044 & 0.032 & 0.081 \end{bmatrix} \tag{3.55b}$$

$$\frac{\partial \boldsymbol{C}_{A}^{*}}{\partial \mathbf{f}_{H}} = \bar{\Delta}_{A}^{T} \cdot \nabla_{\mathbf{v}_{H}} \boldsymbol{t}_{A}^{*} \cdot \Delta_{H} = \begin{bmatrix} 0.121 & 0 & 0.097 \\ 0 & 0.121 & 0.065 \\ 0.097 & 0.065 & 0.163 \end{bmatrix} \tag{3.55c}$$

$$\frac{\partial \boldsymbol{C}_{A}^{*}}{\partial \bar{\mathbf{f}}_{A}} = \bar{\Delta}_{A}^{T} \cdot \nabla_{\mathbf{v}_{A}} \boldsymbol{t}_{A}^{*} \cdot \bar{\Delta}_{A} = \begin{bmatrix} 0.061 & 0 & 0.049 \\ 0 & 0.061 & 0.033 \\ 0.049 & 0.033 & 0.081 \end{bmatrix} \tag{3.55d}$$

Substituting Eq. (3.55) into Eq. (3.48), we can compute the matrix $\boldsymbol{J}_{\bar{\mathbf{f}}}^{*}$. It can be verified that the matrix $\boldsymbol{J}_{\bar{\mathbf{f}}}^{*}$ is invertible as it is a full-rank square matrix. Thereby, the gradients $\nabla_{\boldsymbol{\varepsilon}} \mathbf{f}_{H}^{*}(0)$, $\nabla_{\boldsymbol{\varepsilon}} \bar{\mathbf{f}}_{A}^{*}(0)$, $\nabla_{\boldsymbol{\varepsilon}} \boldsymbol{\mu}_{H}(0)$, and $\nabla_{\boldsymbol{\varepsilon}} \boldsymbol{\mu}_{A}(0)$ exist. According to Eq. (3.47)

$$\begin{bmatrix} \nabla_{\boldsymbol{\varepsilon}} \mathbf{f}_{H}^{*}(0) \\ \nabla_{\boldsymbol{\varepsilon}} \bar{\mathbf{f}}_{A}^{*}(0) \\ \nabla_{\boldsymbol{\varepsilon}} \boldsymbol{\mu}_{H}(0) \\ \nabla_{\boldsymbol{\varepsilon}} \boldsymbol{\mu}_{A}(0) \end{bmatrix} = [0.381 \quad 0.407 \quad 0.212 \quad 0.710 \quad 0.456 \quad -1.166 \quad -0.062 \quad -0.053]^{T} \tag{3.56}$$

If the OD demand for HDVs is increased by 5, the perturbed equilibrium link flows of HDVs (denoted as $\hat{\mathbf{v}}_{H}^{*}(5)$) and CAVs (denoted as $\hat{\mathbf{v}}_{A}^{*}(5)$) can be estimated by the first-order approximation (FOA) method as follows:

$$\hat{\mathbf{v}}_{H}^{*}(5) = \mathbf{v}_{H}^{*}(0) + 5 \times \Delta_{H} \cdot \nabla_{\boldsymbol{\varepsilon}} \mathbf{f}_{H}^{*}(0) = [20.529 \quad 12.471 \quad 9.030 \quad 11.499 \quad 21.501 \quad 0]^{T}$$

$$\hat{\mathbf{v}}_A^*(5) = \mathbf{v}_A^*(0) + 5 \times \Delta_A \cdot \nabla_{\boldsymbol{\varepsilon}} \mathbf{f}_A^*(0) = [8.798 \quad 11.202 \quad 0 \quad 8.435 \quad 11.565 \quad 0.363]^T$$

The calculated equilibrium link flows of HDVs (denoted as $\mathbf{v}_H^*(5)$) and CAVs (denoted as $\mathbf{v}_A^*(5)$) at the perturbed state using the solution algorithm are

$$\mathbf{v}_H^*(5) = [20.514 \quad 12.486 \quad 8.996 \quad 11.518 \quad 21.482 \quad 0]^T$$

$$\mathbf{v}_A^*(5) = [8.964 \quad 11.036 \quad 0 \quad 8.181 \quad 11.819 \quad 0.784]^T$$

It can be seen that the estimated equilibrium link flows are very close to the calculated ones. Thereby, FOA approach can effectively estimate the perturbed solutions. It should be noted that the accuracy of the FOA approach decreases as the perturbation increases.

3.7.2 Sioux Falls network

The Sioux Falls network shown in Figure 3.5(b) is used to demonstrate the estimation performance of equilibrium flows of the FOA approach due to parametric perturbations in a larger network. The number of paths for each OD pair in the path set generated by the link penalty approach is set as 15. Assume the demand for both CAVs and HDVs for OD pairs 10-15,15-10,14-15,15-14, 19-15 and 15-19 are increased by 100%. Figure 3.12 shows the distribution of relative errors of estimated link flows for HDVs and CAVs. It illustrates that the FOA approach accurately estimates the HDV and CAV flows for most links with relative errors less than 0.2% and 2%, respectively. Further, the maximum relative errors of the estimated link flows for HDVs and CAVs are less than 1.2% and 10%, respectively. Thereby, the FOA approach accurately captures the flow variation due to the demand increase. Note that the estimation performance of CAV link flows is poorer than that of the HDV link flows. This is because CAVs choose routes based on the UE principle. They are more informed of traffic conditions than HDVs and are more sensitive to the network congestion due to increased demand. Thereby, the variation of link flows for CAVs is larger than that for HDVs, which reduces the estimation performance of the FOA approach.

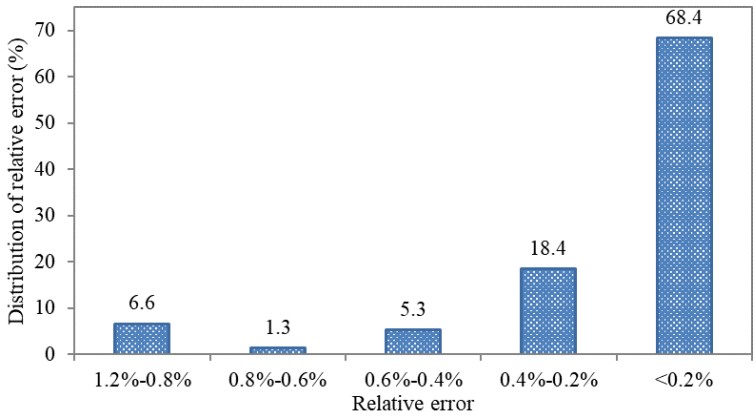

(a)

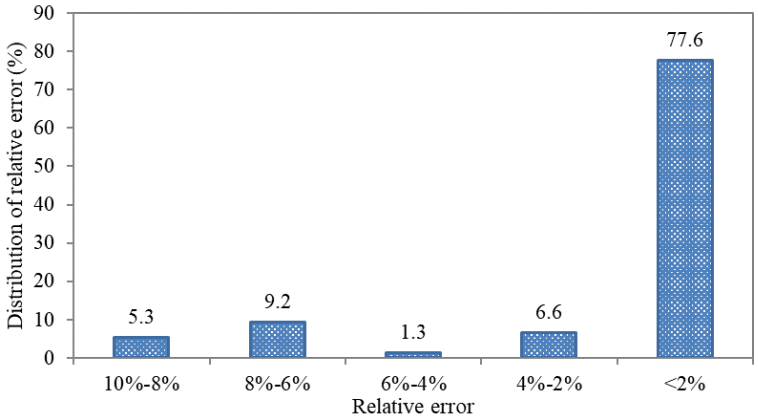

(b)

Figure 3.12: The distribution of relative errors of the estimated link flows for: (a) HDVs, and (b) CAVs.

4. Findings and Conclusions

The traffic information propagated in a V2V-based traffic system can be grouped into different classes based on application needs related to information spread, time delay bounds, and spatial coverage. To meet these needs of multiclass information under different traffic flow and communication environments, Chapter 2 proposes a queuing strategy for equipped vehicles to propagate the received information packets. The queuing strategy enables control for multiclass information propagation by leveraging two control parameters, the number of communication servers and the mean communication service rate. The spatiotemporal propagation of information in different information classes under the designed queuing strategy is characterized by a two-layer analytical model. The upper layer is an IDE system derived to model information dissemination under the designed queuing strategy, and a LWR model is used in the lower layer to describe the traffic flow dynamics. An analytical solution of asymptotic density of informed vehicles is developed under homogeneous traffic conditions. It helps to analyze the relationship between the density of informed vehicles and the two control parameters in the queuing strategy. In addition, the necessary conditions for existence of IFPW are derived. It describes the conditions under which the specific information packets will be propagated only locally. A numerical solution is proposed to solve the two-layer model to estimate the IFPW speed, which helps to estimate the time delay for an information packet to reach the target location.

Numerical experiments using the proposed model in Chapter 2 suggest that the mean communication service rate significantly impacts the asymptotic density of informed vehicles. Also, all else being equal, an increase in the number of communication servers assigned to an information class will increase the IFPW speed of the information packets in this information class. In addition, information will be propagated only locally under a high communication service rate because each information packet has little transmission duration. These findings provide valuable insights for controlling the propagation of multiclass information to achieve desired operational performance in a V2V-based traffic system. That is, they provide valuable tools to a traffic control center to target different information-based solutions for different traffic-related problems that arise regularly in urban areas. For example, they can be used to disseminate area-wide controlled information dissemination strategies to manage traffic conditions under a severe accident, and to simultaneously manage the impacts of a work zone by ensuring information (of a different class) is disseminated to vehicles in only a certain vicinity of it, thereby enabling vehicles to seamlessly receive and propagate multiclass information. Hence, this study can be leveraged to develop a new generation of information dissemination strategies focused on enabling specific V2V-based applications for traffic situations that arise on a daily basis.

This study proposes a multiclass traffic assignment model in which HDV and CAV users choose routes based on the CNL model and UE principle, respectively. The CNL model captures HDV users' perception uncertainty due to limited knowledge of traffic conditions while overcoming the route overlap issue of logit-based SUE. The UE model can characterize the CAV's capability for acquiring traffic information more accurately. In addition, the asymmetry in interactions involving HDVs and CAVs is analytically captured by the designed link travel cost functions. Thereby, the proposed multiclass traffic assignment model can enhance realism in characterizing mixed traffic flows. It can aid planners to quantitatively estimate the impacts of the VOT of CAV users, the CAV market penetrate rate, and the deployment of AV-dedicated lanes. A new route-swapping-

based solution algorithm, RSRS-MSRA, is developed to solve the multiclass traffic assignment model effectively. It converges much faster than the existing route-swapping-based algorithm (Huang and Lam, 2002) by adaptively determining the step size in each iteration. This solution algorithm can also be used to solve other path-based VI problems (e.g., Huang and Lam, 2004, Szeto and Lo, 2006; Ramadurai and Ukkusuri, 2010). The study also develops an analytical model for sensitivity analysis of the multiclass traffic assignment model.

The results in Chapter 3 suggest that when the VOT of CAV users is small, a large proportion of HDV and CAV demand will be distributed on different routes, which reduces the total travel cost of HDVs. The deployment of AV-dedicated lanes can attract more CAV flow than non-AV dedicated lanes. But changing an existing lane into an AV-dedicated lane may decrease system performance under a low CAV market penetration rate. In addition, the average OD travel cost of HDVs can be reduced significantly even with a relatively low CAV market penetration rate. The analytical model for sensitivity analysis of the multiclass traffic assignment model enables planners to quickly estimate the perturbed network flows due to expected or unexpected events. These insights can assist decision-makers to design effective planning and operational strategies that promote the benefits of CAVs and mitigate traffic congestion under mixed traffic flows during the transition to a fully autonomous and connected transportation system.

5. Recommendations

Chapter 2 can be extended in a few directions. First, analytical solutions of the IFPW speed can be derived to provide insights on the relationship between the two control parameters in the queuing strategy and the resulting IFPW speed of information packets in each information class. Second, this study only considers control of information flow propagation in a corridor. The performance of the proposed method on control of network-level information flow propagation needs to be investigated. Third, this study only investigates the effects on traffic flow dynamics on information flow propagation, the effects of information flow propagation on traffic flow dynamics are neglected. Analytical models will be developed to study the mutual interactions between traffic flow dynamics and information flow propagation. Fourth, this study assigns the received information packets into different queues according to the information classes they belong to. It assumes that the number of available communication servers is larger than the number of information classes. This assumption may not hold in scenarios of high traffic density, where the maximum number of information packets (i.e., N_max) an equipped vehicle can transmit in one-hop propagation is small due to information congestion (Wang et al., 2018). To address this, other queuing strategies such as preemptive priority and non-preemptive priority queuing systems will be developed to control the propagation of information of different information classes. Fifth, in this study, we only validate the effectiveness of the proposed model under homogeneous traffic flow conditions using NS-3 simulation. Due to the difficulty to simulate both the traffic flow dynamics and V2V communications in NS-3 simultaneously under heterogeneous traffic flow conditions (for example, when congestion occurs), we cannot validate the proposed method under heterogeneous traffic flow conditions. This will be addressed in future work.

Chapter 3 can be extended in a few directions. First, the study uses a fixed path set in the proposed RSRS-MSRA algorithm. However, if the path flows obtained using the solution algorithm are close to the equilibrium solution, the initial K-shortest paths may not be competitive. In future, the RSRS-MSRA algorithm can be extended by updating the set of paths at each iteration to solve the proposed multiclass traffic assignment. Second, we will leverage the sensitivity analysis method to identify critical parameters (link capacity, signal splits) that impact network performance, and perform risk analysis to generate insights on network performance reliability. Third, a continuous network design problem can be developed upon the multiclass traffic assignment model to determine the optimal signal timing and tolling strategies to maximize system performance under different CAV market penetration rates. Fourth, a combined modal split and multiclass traffic assignment model can be developed to simultaneously estimate the network flows and OD demand of both HDVs and CAVs by incorporating factors such as travel cost, price of vehicles, etc.

6. Synopsis of Performance indicators

6.1 Part I

The research from this was advanced. The research was presented at the Transportation Research Board 2020 Annual Meeting in Washington, DC. This project supported 1 student at the doctoral level.

6.2 Part II

Two (2) conference articles and 2 peer-reviewed journal articles were produced from this project. The outputs, outcomes, and impacts are described in Section 7 below.

7. OUTPUTS, OUTCOMES, AND IMPACTS

7.1 Outputs

- Wang, J., Peeta, S., Lu, L., & Li, T. (2019). Multiclass information flow propagation control under vehicle-to-vehicle communication environments. Transportation Research Part B: Methodological, 129, 96-121. https://www.sciencedirect.com/science/article/pii/S0191261518311767

- Wang, J., Peeta, S., & He, X. (2019). Multiclass traffic assignment model for mixed traffic flow of human-driven vehicles and connected and autonomous vehicles. Transportation Research Part B: Methodological, 126, 139-168. https://www.sciencedirect.com/science/article/pii/S0191261518309512

- Wang, J., Peeta, S., Lu, L., Li, T. (2020). Multiclass information flow propagation control under vehicle-to-vehicle communication environments. 99th Annual Meeting of Transportation Research Board (TRB), Washington, D.C, USA.

- Wang, J., Peeta, S., He, S., (2020). Multiclass traffic assignment model for mixed traffic flow of human-driven vehicles and connected and autonomous vehicles. 99th Annual Meeting of Transportation Research Board (TRB), Washington, D.C, USA

7.2 Outcomes

This research project enhances the understanding of the information propagation in a V2V-based traffic system and increase the awareness of the importance of the network impacts of CAVs during the transition period from HDVs to CAVs. Rigorous mathematical models are developed to enrich the body of knowledge in V2V information propagation dynamics and multiclass (HDV and CAV) traffic assignment. Specifically, a queuing strategy is proposed to address the potential conflicts and congestion of information propagation in the transportation context, which reveals the relationship between the density of informed vehicles and the two control parameters in the queuing strategy and can be used to estimate

the time delay for an information packet to reach the target location; and the multiclass traffic assignment model characterizes the CAV's capability for acquiring traffic information more accurately and the asymmetry in interactions involving HDVs and CAVs. It can aid planners to quantitatively estimate the impacts of the VOT of CAV users, the CAV market penetrate rate, and the deployment of AV-dedicated lanes. Therefore, this research can promote further research on the network-level CAV technology and support the development of necessary policies and regulation to potentially speed up the adoption of the CAV technology in the real world.

7.3 Impacts

The findings of this study provide valuable insights on the information propagation process in V2V-based traffic system and the network impacts of CAVs. The analytical information propagation models enable the traffic manager/operator to develop different information-based solutions for different traffic-related problems that arise regularly in urban areas. They can also be leveraged to develop a new generation of information dissemination strategies focused on enabling specific V2V-based applications for traffic situations that arise daily. While the proposed multiclass (HDV and CAV) traffic assignment model can enhance realism in characterizing mixed traffic flows and aids planners to quantitatively estimate the impacts of the VOT of CAV users, the CAV market penetrate rate, and the deployment of AV-dedicated lanes. Further, the insights can assist decision-makers to design effective planning and operational strategies that promote the benefits of CAVs and mitigate traffic congestion under mixed traffic flows during the transition to a fully autonomous and connected transportation system.

7.4 Tech Transfer

In the execution of the project titled Development of Dynamic Network Traffic Simulator for Mixed Traffic Flow under Connected and Autonomous Vehicles Technologies, the research team undertook a number of technology transfer activities. First, the research team published two articles in technical journals with a wide readership, high reputation, and high impact factor. The team also gave two presentations at the TRB annual meeting, a conference with over 14,000 attendees. Further, a number of tech transfer activities were undertaken as part of this project, such as communication with other universities through webinars and forums. The list below summarizes the tech transfer activities undertaken by the research team through the course of this project:

In 2019:
1. Technical paper in Transportation Research Part B: Methodological, 128, 271-301: A real-time deployable model predictive control-based cooperative platooning approach for connected and autonomous vehicles, by Wang, J., Gong, S., Peeta, S., & Lu, L.
2. Technical paper in Transportation Research Part B: Methodological, 126, 139-168: Multiclass traffic assignment model for mixed traffic flow of human-driven vehicles and connected and autonomous vehicles, by Wang, J., Peeta, S.*, & He, S.

In 2020:
1. Conference presentation at the 99th Annual Meeting of Transportation Research Board (TRB), Washington, D.C, USA: Multiclass information flow propagation control under vehicle-to-vehicle communication environments, by Wang, J., Peeta, S.*, Lu, L., & Li, T.
2. Conference presentation at the 99th Annual Meeting of Transportation Research Board (TRB), Washington, D.C, USA: Multiclass traffic assignment model for mixed traffic flow of human-driven vehicles and connected and autonomous vehicles, by Wang, J., Peeta, S.*, & He, S.

In 2021:
1. Presentation at the 2021 Master Forum of Transportation Engineering, Southeasten University, Nanjing, China: Information Flow Topologies and Propagation Modeling for Traffic Management and Control under Connected Vehicle Environments, Peeta, S.

8. References

Assidiq, A.A., Khalifa, O.O., Islam, M.R., Khan, S., 2008. Real time lane detection for autonomous vehicles. Proceedings of the International Conference on Computer and Communication Engineering, July, pp. 82-88, Kuala Lumpur, Malaysia.

Azevedo, J.A., Santos Costa, M.E.O., Silvestre Madera, J.J.E.R., Vieira Martins, E.Q., 1993. An algorithm for the ranking of shortest paths. European Journal of Operational Research, 69 (1), 97-106.

Bauschke, H.H., Matoušková, E., Reich, S., 2004. Projection and proximal point methods: convergence results and counterexamples. Nonlinear Analysis: Theory, Methods & Applications, 56 (5), 715-738.

Ben-Akiva M., Bergman M.J., Daly A.J., Ramaswamy R., 1984. Modelling inter urban route choice behaviour. Proceedings of the 9th International Symposium on Transportation and Traffic Theory, July, pp. 299-330, Utrecht, Netherlands.

Benin, J., Nowatkowski, M., Owen, H., 2012. Vehicular network simulation propagation loss model parameter standardization in ns-3 and beyond. 2012 Proceedings of IEEE Southeastcon, March, pp. 1-5, Florida, USA.

Bilstrup, K., Uhlemann, E., Ström, E., Bilstrup, U., 2009. On the ability of the 802.11 p MAC method and STDMA to support real-time vehicle-to-vehicle communication. EURASIP Journal on Wireless Communications and Networking. Article ID: 902414.

Bonnet, C., Fritz, H., 2000. Fuel consumption reduction in a platoon: Experimental results with two electronically coupled trucks at close spacing. Future Transportation Technology Conference & Exposition, August, pp. 1-9, California, USA.

Boyles, S.D., 2012. Bush-based sensitivity analysis for approximating subnetwork diversion. Transportation Research Part B: Methodological, 46 (1), 139-155.

Cascetta, E., Nuzzolo, A., Russo, F., Vitetta, A., 1996. A modified-logit route-choice model overcoming path overlapping problems: specification and some calibration results for interurban networks. Proceedings of International Symposium on Transportation and Traffic Theory, July, pp. 697-711, Lyon, France.

Catalano S.F., and Van der Zijpp N. A forecasting model for inland navigation based on route enumeration. In: *Proceedings of the European Transport Conference*, London, England 2001, 1-11, September.

Chen, Z., He, F., Yin, Y., Du, Y., 2017. Optimal design of autonomous vehicle zones in transportation networks. Transportation Research Part B: Methodological, 99, 44-61.

Chen, Z., He, F., Zhang, L., Yin, Y., 2016. Optimal deployment of autonomous vehicle lanes with endogenous market penetration. Transportation Research Part C: Emerging Technologies, 72, 143-156.

Chen, A, Ji, ZW. 2005. Path finding under uncertainty. Journal of Advanced Transportation, 39, 19–37

Chen, A., Zhou, Z., Xu, X. 2012. A self-adaptive gradient projection algorithm for the nonadditive traffic equilibrium problem. Computers & Operations Research, 39(2), 127–138.

Clark, S., Watling, D., 2000. Probit-based sensitivity analysis for general traffic networks. Transportation Research Record: Journal of the Transportation Research Board, 1733, 88-95.

De La Barra, T., Perez, B., Anez, J., 1993. Multidimensional path search and assignment. 21st PTRC Summer Annual Meeting, pp. 307-320, University of Manchester, United Kingdom.

Dafermos, S.C., 1972. The traffic assignment problem for multiclass-user transportation networks. Transportation science, 6 (1), 73-87.

Daganzo, C. F., 1995. A finite difference approximation of the kinematic wave model of traffic flow. Transportation Research Part B: Methodological, 29 (4), 261–276.

Dey, K.C., Rayamajhi, A., Chowdhury, M., Bhavsar, P., Martin, J., 2016. Vehicle-to-vehicle (V2V) and vehicle-to-infrastructure (V2I) communication in a heterogeneous wireless network–Performance evaluation. Transportation Research Part C: Emerging Technologies, 68, 168-184.

Du, L., Dao, H., 2015. Information dissemination delay in vehicle-to-vehicle communication networks in a traffic stream. IEEE Transactions on Intelligent Transportation Systems, 16 (1), 66-80.

Du, L., Gong, S., Wang, L., Li, X., 2016. Information-traffic coupled cell transmission model for information spreading dynamics over vehicular ad hoc network on road segments. Transportation Research Part C: Emerging Technologies, 73, 30-48.

Eben Li, S., Li, K., Wang, J., 2013. Economy-oriented vehicle adaptive cruise control with coordinating multiple objectives function. Vehicle System Dynamics, 51 (1), 1-17.

Fagnant, D.J., Kockelman, K., 2015. Preparing a nation for autonomous vehicles: opportunities, barriers and policy recommendations. Transportation Research Part A: Policy and Practice, 77, 167-181.

Facchinei, F., Pang, J.S., 2007. Finite-dimensional variational inequalities and complementarity problems. Springer Science & Business Media.

Fiacco, A.V., 1983. Introduction to sensitivity and stability analysis in nonlinear programming. London, UK: Academic Press.

Florian, M., 1977. A traffic equilibrium model of travel by car and public transit modes. Transportation Science, 11 (2), 166-179.

Friesz, T.L., Bernstein, D., Mehta, N.J., Tobin, R.L., Ganjalizadeh, S., 1994. Day-to-day dynamic network disequilibria and idealized traveler information systems. Operations Research, 42 (6), 1120-1136.

Gallier, J., 2011. Geometric methods and applications: for computer science and engineering (Vol. 38). Springer Science & Business Media.

Gross, D., Shortle, J. F., Thompson, J. M., Harris, C. M., 2008. Fundamentals of queuing theory, 4th Edition. John Wiley & Sons.

Guo, R.Y., Huang, H., 2016. A discrete dynamical system of formulating traffic assignment: Revisiting Smith's model. Transportation Research Part C: Emerging Technologies, 71, 122-142.

Guo, R.Y., Yang, H., Huang, H., 2013. A discrete rational adjustment process of link flows in traffic networks. Transportation Research Part C: Emerging Technologies, 34, 121-137.

Haghani, M., Shahhoseini, Z., Sarvi, M. 2016. Path sets size, model specification, or model estimation: Which one matters most in predicting stochastic user equilibrium traffic flow? Journal of Traffic and Transportation Engineering, 3(3), 181–191.

Hisham, A., Ström, E. G., Brännström, F., Yan, L., 2017. Scheduling and power control for V2V broadcast communications with adjacent channel interference. arXiv preprint, arXiv:1708.02444.

Hisham, A., Sun, W., Ström, E. G., Brännström, F., 2016. Power control for broadcast V2V communications with adjacent carrier interference effects. IEEE International Conference on Communication, May, pp.1-6, Kuala Lumpur, Malaysia.

Huang, H., Lam, W.H., 2002. Modeling and solving the dynamic user equilibrium route and departure time choice problem in network with queues. Transportation Research Part B: Methodological, 36 (3), 253-273.

Huang, H., Lam, W.H., 2003. A multi-class dynamic user equilibrium model for queuing networks with advanced traveler information systems. Journal of Mathematical Modelling and Algorithms, 2 (4), 349-377.

Huang, H., Li, Z., 2007. A multiclass, multicriteria logit-based traffic equilibrium assignment model under ATIS. European Journal of Operational Research, 176 (3), 1464-1477.

Hunt, D.T., Kornhauser, A.L., 1997. Assigning traffic over essentially-least-cost paths. Transportation Research Record, 1556, 1-7.

Jafari, E., Boyles, S.D., 2016. Improved bush-based methods for network contraction. Transportation Research Part B: Methodological, 83, 298-313.

Jiang, Y., Szeto, W.Y., Long, J., Han, K., 2016. Multi-class dynamic traffic assignment with physical queues: intersection-movement-based formulation and paradox. Transportmetrica A: Transport Science, 12 (10), 878-908.

Ji, X., Ban, X.J., Li, M., Zhang, J., Ran, B., 2017. Non-expected route choice model under risk on stochastic traffic networks. Networks and Spatial Economics, 17 (3), 777-807.
Kitthamkesorn, S., Chen, A., Xu, X., Ryu, S., 2016. Modeling mode and route similarities in network equilibrium problem with go-green modes. Networks and Spatial Economics, 16 (1), 33-60.
Kim, Y. H., Peeta, S., He, X., 2017. Modeling the information flow propagation wave under vehicle-to-vehicle communications. Transportation Research Part C: Emerging Technologies, 85, 377-395.
Kim, Y. H., Peeta, S., He, X., 2018. An analytical model to characterize the spatiotemporal propagation of information under vehicle-to-vehicle communications. IEEE Transactions on Intelligent Transportation Systems, 19 (1), 3-12.
Lam, W.H., Huang, H., 2003. Combined activity/travel choice models: time-dependent and dynamic versions. Networks and Spatial Economics, 3 (3), 323-347.
Leblanc, L.J., Abdulaal, M., 1982. Combined mode split-assignment and distribution-model split-assignment models with multiple groups of travelers. Transportation Science, 16 (4), 430-442.
Levin, M.W., Boyles, S.D., 2015. Effects of autonomous vehicle ownership on trip, mode, and route choice. Transportation Research Record: Journal of the Transportation Research Board, 2493, 29-38.
Levin, M.W., Boyles, S.D., 2016. A multiclass cell transmission model for shared human and autonomous vehicle roads. Transportation Research Part C: Emerging Technologies, 62, 103-116.
Li, M. Y., Graef, J. R., Wang, L., Karsai, J., 1999. Global dynamics of a SEIR model with varying total population size. Mathematical Biosciences, 160 (2), 191-213.
Li, M. Y., Muldowney, J. S., 1995. Global stability for the SEIR model in epidemiology. Mathematical biosciences, 125 (2), 155-164.
Li, Y.J., 2010. An overview of the DSRC/WAVE technology. In International Conference on Heterogeneous Networking for Quality, Reliability, Security and Robustness, November, pp. 544-558, Berlin, Germany.
Lighthill, M. J., Whitham, J. B., 1955. On kinematic waves. I: Flow movement in long river; II: A theory of traffic flow on long crowded roads. Proceedings of Royal Society A, 229 (1178), 281-345.
Liu, H.X., He, X., He, B., 2009. Method of successive weighted averages (MSWA) and self-regulated averaging schemes for solving stochastic user equilibrium problem. Networks and Spatial Economics, 9 (4), 485–503.
Lo, H.K., Luo, X.W., Siu, B.W., 2006. Degradable transport network: travel time budget of travelers with heterogeneous risk aversion. Transportation Research Part B: Methodological, 40 (9), 792-806.
Lombard, K., Church, R.L. 1993. The gateway shortest path problem: generating alternative routes for a corridor location problem. Geographical Systems, 1, 25-45.
Marzano, V., Papola, A. 2008. On the covariance structure of the cross-nested logit model. Transportation Research Part B: Methodological, 42 (2), 83–98.
Melson, C. L., Levin, M. W., Hammit, B. E., Boyles, S. D., 2018. Dynamic traffic assignment of cooperative adaptive cruise control. Transportation Research Part C: Emerging Technologies, 90, 114–133.
McFadden, D., 1981. Econometric models of probabilistic choice. Structural analysis of discrete data with econometric applications, MIT Press, Cambridge.
Mounce, R., Carey, M., 2014. On the convergence of the method of successive averages for calculating equilibrium in traffic networks. Transportation science, 49 (3), 535-542.
Nagurney, A., 2013. Network economics: A variational inequality approach (Vol.10). Springer Science & Business Media.
Nagurney, A., 2000. A multiclass, multicriteria traffic network equilibrium model. Mathematical and Computer Modelling, 32 (3-4), 393-411.
Nagurney, A., Dong, J., 2002. A multiclass, multicriteria traffic network equilibrium model with elastic demand. Transportation Research Part B: Methodological, 36 (5), 445-469.
Noori, H., Olyaei, B. B., 2013. A novel study on beaconing for VANET-based vehicle to vehicle communication: Probability of beacon delivery in realistic large-scale urban area using 802.11p.

2013 International Conference on Smart Communications in Network Technologies, June, pp. 1-6, Paris, France.
Peeta, S., Yang, T.H., 2003. Stability issues for dynamic traffic assignment. Automatica, 39 (1), 21-34.
Peeta, S., Ziliaskopoulos., 2001. Foundations of dynamic traffic assignment: the past, the present and the future. Networks and Spatial Economics, 1 (3-4), 233-266.
Prashker, J., Bekhor, S., 1999. Stochastic user-equilibrium formulations for extended-logit assignment models. Transportation Research Record: Journal of the Transportation Research Board, 1676, 145-152.
Ramadurai, G., Ukkusuri, S., 2010. Dynamic user equilibrium model for combined activity-travel choices using activity-travel supernetwork representation. Networks and Spatial Economics, 10 (2), 273-292.
Ramming, M.S., 2001. Network knowledge and route choice. Ph. D. Thesis, Massachusetts Institute of Technology.
Ran, B., Cheng, Y., Li, S., Ding, F., Jin, J., Chen, X., Zhang, Z., 2018. Connected automated vehicle highway systems and methods. U.S. Patent Application 15/628,331.
Ran, B., Cheng, Y., Li, S., Zhang, Z., Ding, F., Tan, H., Wu, Y., Dong, S., Ye, L., Li, X., Chen, T., 2019. Intelligent road infrastructure system (iris): systems and methods. U.S. Patent Application 16/135,916.
Richards, P. I., 1956. Shock waves on the highway. Operations Research, 4, 42-51.
Shao, H., Lam, W.H., Tam, M.L., 2006. A reliability-based stochastic traffic assignment model for network with multiple user classes under uncertainty in demand. Networks and Spatial Economics, 6 (3-4), 173-204.
Shida, M., Nemoto, Y., 2009. Development of a small-distance vehicle platooning system. 16th ITS World Congress and Exhibition on Intelligent Transport Systems and Services, September, Stockholm , Sweden.
Shida, M., Doi, T., Nemoto, Y., Tadakuma, K., 2010. A short-distance vehicle platooning system (second report): Evaluation of fuel savings by the developed cooperative control. In Proceedings of the 10th International Symposium on Advanced Vehicle Control, Auguest, pp. 719-723, Loughborough, UK.
Smith, M.J., 1984. The stability of a dynamic model of traffic assignment: an application of a method of Lyapunov. Transportation Science, 18 (3), 245–252.
Smith, M.J., Wisten, M.B., 1995. A continuous day-to-day traffic assignment model and the existence of a continuous dynamic user equilibrium. Annals of Operations Research, 60 (1), 59-79.
Smith, H. L., Wang, L., Li, M. Y., 2001. Global dynamics of an SEIR epidemic model with vertical transmission. SIAM Journal on Applied Mathematics, 62 (1), 58-69.
Smith, M.J., Watling, D.P., 2016. A route-swapping dynamical system and Lyapunov function for stochastic user equilibrium. Transportation Research Part B: Methodological, 85, 132-141.
Szeto, W.Y., Lo, H.K., 2006. Dynamic traffic assignment: Properties and extensions. Transportmetrica 2 (1), 31-52.
Talebpour, A., Mahmassani, H. S., Bustamante, F. E., 2016. Modeling driver behavior in a connected environment: Integrated microscopic simulation of traffic and mobile wireless telecommunication systems. Transportation Research Record: Journal of the Transportation Research Board, 2560, 75-86.
Tientrakool, P., Ho, Y.C., Maxemchuk, N.F., 2011, September. Highway capacity benefits from using vehicle-to-vehicle communication and sensors for collision avoidance. In Vehicular Technology Conference (VTC Fall), May, pp. 1-5, San Francisco, California, USA.
Tikhonov, A., 1963. Solution of incorrectly formulated problems and the regularization method. Soviet mathematics - doklady., 4, 1035-1038.
Tobin, R.L., 1986. Sensitivity analysis for variational inequalities. Journal of Optimization Theory and Applications, 48 (1), 191-204.
Tobin, R.L., Friesz, T.L., 1988. Sensitivity analysis for equilibrium network flow. Transportation Science, 22 (4), 242-250.

Torrent-Moreno, M., Mittag, J., Santi, P., Hartenstein, H., 2009. Vehicle-to-vehicle communication: Fair transmit power control for safety-critical information. IEEE Transactions on Vehicular Technology, 58(7), 3684-3703.

Van den Berg, V.A., Verhoef, E.T., 2016. Autonomous cars and dynamic bottleneck congestion: The effects on capacity, value of time and preference heterogeneity. Transportation Research Part B: Methodological, 94, 43-60.

Vovsha, P., 1997. The cross-nested logit model: application to mode choice in the Tel-Aviv metropolitan area. Presented at the 76th Transportation Research Board Annual Meeting, Washington, D.C.

Wang, D.Z., Lo, H.K., 2010. Global optimum of the linearized network design problem with equilibrium flows. Transportation Research Part B: Methodological, 44 (4), 482-492.

Wang, J., He, X., Peeta, S., 2016. Sensitivity analysis based approximation models for day-to-day link flow evolution process. Transportation Research Part B: Methodological, 92, 35-53.

Wang, J., Peeta, S., He, X., Zhao, J., 2018. Combined multinomial logit modal split and paired combinatorial logit traffic assignment model. Transportmetrica A: Transport Science. 14 (9), 737-760.

Wie, B.W., Tobin, R.L., Friesz, T.L., Bernstein, D., 1995. A discrete time, nested cost operator approach to the dynamic network user equilibrium problem. Transportation Science, 29 (1), 79-92.

Yang, H., 1997. Sensitivity analysis for the elastic-demand network equilibrium problem with applications. Transportation Research Part B: Methodological, 31 (1), 55-70.

Yang, H., Bell, M.G., 2005. Sensitivity analysis of network traffic equilibrium revisited: the corrected approach. In 4th IMA International Conference on Mathematics in Transport Institute of Mathematics and its Applications, September, London, United Kingdom.

Yang, H., Huang, H., 2004. The multi-class, multi-criteria traffic network equilibrium and systems optimum problem. Transportation Research Part B: Methodological, 38 (1), 1-15.

Yin, K., Wang, X., Zhang, Y., 2013. Vehicle-to-vehicle connectivity on two parallel roadways with a general headway distribution. Transportation Research Part C: Emerging Technologies 29, 84-96.

Yu, F., Biswas, S., 2007. A self-organizing MAC protocol for DSRC based vehicular ad hoc networks. In 27th International Conference on Distributed Computing Systems Workshops, June, pp. 1-6, Toronto, Canada.

Zhan, X., Ukkusuri, S.V., 2017. Multiclass, simultaneous route and departure time choice dynamic traffic assignment with an embedded spatial queuing model. Transportmetrica B: Transport Dynamics.

Zhang, J., Han, G., Qian, Y., 2016. Queuing theory based co-channel interference analysis approach for high-density wireless local area networks. Sensors, 16 (9), 1348.

Zhang, S., Wu, Y., Liu, H., Huang, R., Un, P., Zhou, Y., Fu, L., Hao, J., 2014. Real-world fuel consumption and CO2 (carbon dioxide) emissions by driving conditions for light-duty passenger vehicles in China. Energy, 69, 247-257.

9. Appendices

Appendix A: Steps to implement PRS algorithm

The PRS algorithm proposed by Huang and Lam (2002) adapted for the multiclass traffic assignment problem (3.21) is as follows.

Step 1: *Initialization*. Choose initial vectors of path flows $\mathbf{f}_{n,H}, \mathbf{f}_{n,A}$. Set the iteration index $n = 1$;

Step 2: *Generalized route travel cost update*. For both HDVs and CAVs, obtain the minimum travel cost for each OD pair and the corresponding path set by $C_{z,min}^{w} = min\{C_{k,z}^{w}(\mathbf{f}_{n,H}, \mathbf{f}_{n,A}): k \in R_z^w\}$, and

$$\tilde{R}_z^w = \{k | C_{k,z}^{w}(n) = C_{z,min}^{w}, k \in R_z^w\}, z \in \{HDV, CAV\}$$

Step 3: *Route flow update*. Update path flows for HDVs and CAVs ($f_{k,z}^{w}(n+1), \forall k, w, z \in \{HDV, CAV\}$) by

$$f_{k,z}^{w}(n+1) = f_{k,z}^{w}(n) + \beta_n f_{k,z}^{w}(n)\left[C_{k,z}^{w} - C_{z,min}^{w}\right], \quad k \in R_z^w \backslash \tilde{R}_z^w, z \in \{HDV, CAV\}$$

$$f_{k,z}^{w}(n+1) = f_{k,z}^{rs}(n) + \frac{\sum_{i \in R_z^w \backslash \tilde{R}_z^w} \beta_n f_{i,z}^{w}(n)\left[C_{i,z}^{w} - C_{z,min}^{w}\right]}{\left|\tilde{R}_z^w\right|}, k \in \tilde{R}_z^w, z \in \{HDV, CAV\}$$

where $\left|\tilde{R}_z^w\right|$ is the number of paths in set $\tilde{R}_z^w$, $f_{i,z}^{w}(n)$ is the flow on path *i* of OD pair *w* for vehicle class *z* in iteration *n*, and β_n is the step size of iteration *n*.

Step 4: *Convergence check*. If the convergence criterion is satisfied, then stop. Otherwise, let $n = n + 1$ and go to Step 2.

Appendix B: Proof of proposition 7

Proof. Suppose $\mathbf{M}_1 + \frac{2u}{\theta} diag(\mathbf{f}_H) - \mathbf{M}_2\left(2\nabla_{\mathbf{v}_H}\boldsymbol{t}_A^*\right)^{-1}\mathbf{M}_3$ is not a non-singular matrix, then there exists a nonzero vector $\boldsymbol{x}$ such that

$$\left(\mathbf{M}_1 + \frac{2u}{\theta} diag\left(\frac{1}{\mathbf{f}_H^*}\right) - \mathbf{M}_2\left(2\nabla_{\mathbf{v}_H}\boldsymbol{t}_A^*\right)^{-1}\mathbf{M}_3\right)\boldsymbol{x} = \mathbf{0} \tag{a1}$$

This implies

$$\frac{2u}{\theta} diag\left(\frac{1}{\mathbf{f}_H^*}\right)\boldsymbol{x} = \left(\mathbf{M}_2\left(2\nabla_{\mathbf{v}_H}\boldsymbol{t}_A^*\right)^{-1}\mathbf{M}_3 - \mathbf{M}_1\right)\boldsymbol{x} \tag{a2}$$

Note $\frac{2u}{\theta} diag\left(\frac{1}{\mathbf{f}_H^*}\right)$ is invertible; then

$$\boldsymbol{x} = \frac{\theta}{2u} diag(\mathbf{f}_H^*)\left(\mathbf{M}_2\left(2\nabla_{\mathbf{v}_H}\boldsymbol{t}_A^*\right)^{-1}\mathbf{M}_3 - \mathbf{M}_1\right)\boldsymbol{x} \tag{a3}$$

As $\frac{\theta}{2u} diag(\mathbf{f}_H^*)\left(\mathbf{M}_2\left(2\nabla_{\mathbf{v}_H}\boldsymbol{t}_A^*\right)^{-1}\mathbf{M}_3 - \mathbf{M}_1\right)$ has no eigenvalue 1, Eq. (a3) cannot hold. Proposition 7 is proved. ■

Appendix C Proof of Proposition 8

Proof. Note that

$$\frac{\partial \mathbf{C}(\mathbf{f}^*)}{\partial \mathbf{f}} = \begin{bmatrix}\mathbf{E}_H & \\ & \Delta_A^T\end{bmatrix}\frac{\partial \tilde{\mathbf{C}}(\boldsymbol{\nu}^*)}{\partial \boldsymbol{\nu}}\begin{bmatrix}\mathbf{E}_H & \\ & \Delta_A\end{bmatrix} \tag{a4}$$

where $\mathbf{E}_H$ is an identity matrix with dimension equal to the number of paths for HDVs in the network. As $\partial\mathbf{C}(\mathbf{f}^*)/\partial\mathbf{f}$ is positive semidefinite, both the matrices $\partial\tilde{\mathbf{C}}(\boldsymbol{\nu}^*)/\partial\boldsymbol{\nu}$ and $\mathbf{M}$ are positive semidefinite. According to Eq. (3.40), $\partial\tilde{\mathbf{C}}(\boldsymbol{\nu}^*)/\partial\boldsymbol{\nu}$ is positive definite if and only if $\mathbf{M}$ is positive definite. Note that $\mathbf{M}$ is a symmetric matrix and $\nabla_{\mathbf{v}_A}\boldsymbol{t}_A^*$ is a symmetric positive definite matrix. According to Proposition 16.2 in Gallier (2011), $\mathbf{M}_1 + \frac{2u}{\theta} diag\left(\frac{1}{\mathbf{f}_H^*}\right) - \mathbf{M}_2\left(2\nabla_{\mathbf{v}_H}\boldsymbol{t}_A^*\right)^{-1}\mathbf{M}_3$ is a symmetric positive semidefinite matrix, indicating that the eigenvalues of this matrix are nonnegative. Proposition 6 shows that $\mathbf{M}_1 + \frac{2u}{\theta} diag\left(\frac{1}{\mathbf{f}_H^*}\right) - \mathbf{M}_2\left(2\nabla_{\mathbf{v}_H}\boldsymbol{t}_A^*\right)^{-1}\mathbf{M}_3$ is a non-singular matrix. Thereby, $\mathbf{M}_1 + \frac{2u}{\theta} diag\left(\frac{1}{\mathbf{f}_H^*}\right) - \mathbf{M}_2\left(2\nabla_{\mathbf{v}_H}\boldsymbol{t}_A^*\right)^{-1}\mathbf{M}_3$ is positive definite. This implies both the matrices $\mathbf{M}$ and $\partial\tilde{\mathbf{C}}(\boldsymbol{\nu}^*)/\partial\boldsymbol{\nu}$ are positive definite. Proposition 8 is proved. ■

Appendix D: Proof of Proposition 9

Proof: Let $\boldsymbol{z} = [\boldsymbol{z}_1^T \quad \boldsymbol{z}_2^T \quad \boldsymbol{z}_3^T \quad \boldsymbol{z}_4^T]^T$. The dimensions of $\boldsymbol{z}_1^T$ and $\boldsymbol{z}_3^T$ are equal to the number of paths in $\mathbf{f}_H$, and the dimensions of $\boldsymbol{z}_2^T$ and $\boldsymbol{z}_4^T$ are equal to the number of paths in $\bar{\mathbf{f}}_A$. Proposition 9 will be proved by showing that the solution to the following equation is $\boldsymbol{z} = \mathbf{0}$.

$$\begin{bmatrix}\nabla_{\mathbf{f}_H}\mathbf{C}_H(\mathbf{f}^*,\mathbf{0}) & \nabla_{\bar{\mathbf{f}}_A}\mathbf{C}_H(\mathbf{f}^*,\mathbf{0}) & \Lambda_H^T & \\ \nabla_{\mathbf{f}_H}\bar{\mathbf{C}}_A(\mathbf{f}^*,\mathbf{0}) & \nabla_{\bar{\mathbf{f}}_A}\bar{\mathbf{C}}_A(\mathbf{f}^*,\mathbf{0}) & & \bar{\Lambda}_A^T \\ \Lambda_H & & & \\ & \bar{\Lambda}_A & & \end{bmatrix}\begin{bmatrix}\boldsymbol{z}_1 \\ \boldsymbol{z}_2 \\ \boldsymbol{z}_3 \\ \boldsymbol{z}_4\end{bmatrix} = \mathbf{0} \tag{a5}$$

According to Eq. (a5)

$$\nabla_{\mathbf{f}_H}\mathbf{C}_H(\mathbf{f}^*,\mathbf{0})\boldsymbol{z}_1 + \nabla_{\bar{\mathbf{f}}_A}\mathbf{C}_H(\mathbf{f}^*,\mathbf{0})\boldsymbol{z}_2 - \Lambda_H^T\boldsymbol{z}_3 = \mathbf{0} \tag{a6}$$

$$\nabla_{\mathbf{f}_H}\bar{\mathbf{C}}_A(\mathbf{f}^*,\mathbf{0})\boldsymbol{z}_1 + \nabla_{\bar{\mathbf{f}}_A}\bar{\mathbf{C}}_A(\mathbf{f}^*,\mathbf{0})\boldsymbol{z}_2 - \bar{\Lambda}_A^T\boldsymbol{z}_4 = \mathbf{0} \tag{a7}$$

$$\Lambda_H \boldsymbol{z}_1 = 0 \tag{a8}$$

$$\bar{\Lambda}_A \boldsymbol{z}_2 = 0 \tag{a9}$$

Multiplying Eq. (a6) and Eq. (a7) by $\boldsymbol{z}_1^T$ and $\boldsymbol{z}_2^T$ from left-hand side, respectively, we have

$$\boldsymbol{z}_1^T \nabla_{\mathbf{f}_H} \mathbf{C}_H(\mathbf{f}^*, \mathbf{0}) \boldsymbol{z}_1 + \boldsymbol{z}_1^T \nabla_{\bar{\mathbf{f}}_A} \mathbf{C}_H(\mathbf{f}^*, \mathbf{0}) \boldsymbol{z}_2 = \mathbf{0} \tag{a10}$$

$$\boldsymbol{z}_2^T \nabla_{\mathbf{f}_H} \bar{\mathbf{C}}_A(\mathbf{f}^*, \mathbf{0}) \boldsymbol{z}_1 + \boldsymbol{z}_2^T \nabla_{\bar{\mathbf{f}}_A} \bar{\mathbf{C}}_A(\mathbf{f}^*, \mathbf{0}) \boldsymbol{z}_2 = \mathbf{0} \tag{a11}$$

Equivalently, Eq. (a10) and Eq. (a11) can be written in a vector form

$$[\boldsymbol{z}_1^T \quad \boldsymbol{z}_2^T] \begin{bmatrix} \nabla_{\mathbf{f}_H} \mathbf{C}_H(\mathbf{f}^*, \mathbf{0}) & \nabla_{\bar{\mathbf{f}}_A} \mathbf{C}_H(\mathbf{f}^*, \mathbf{0}) \\ \nabla_{\mathbf{f}_H} \bar{\mathbf{C}}_A(\mathbf{f}^*, \mathbf{0}) & \nabla_{\bar{\mathbf{f}}_A} \bar{\mathbf{C}}_A(\mathbf{f}^*, \mathbf{0}) \end{bmatrix} \begin{bmatrix} \boldsymbol{z}_1 \\ \boldsymbol{z}_2 \end{bmatrix} = 0 \tag{a12}$$

Thereby,

$$[\boldsymbol{z}_1^T \quad \boldsymbol{z}_2^T] \begin{bmatrix} \mathbf{E}_H & \\ & \bar{\Delta}_A^T \end{bmatrix} \begin{bmatrix} \frac{\partial \boldsymbol{C}_H^*}{\partial \mathbf{f}_H} & \frac{\partial \boldsymbol{C}_H^*}{\partial \mathbf{v}_A} \\ \frac{\partial \boldsymbol{t}_A^*}{\partial \mathbf{f}_H} & \frac{\partial \boldsymbol{t}_A^*}{\partial \mathbf{v}_A} \end{bmatrix} \begin{bmatrix} \mathbf{E}_H & \\ & \bar{\Delta}_A \end{bmatrix} \begin{bmatrix} \boldsymbol{z}_1 \\ \boldsymbol{z}_2 \end{bmatrix} = 0 \tag{a13}$$

Note that the matrix $\begin{bmatrix} \frac{\partial \boldsymbol{C}_H^*}{\partial \mathbf{f}_H} & \frac{\partial \boldsymbol{C}_H^*}{\partial \mathbf{v}_A} \\ \frac{\partial \boldsymbol{t}_A^*}{\partial \mathbf{f}_H} & \frac{\partial \boldsymbol{t}_A^*}{\partial \mathbf{v}_A} \end{bmatrix}$ is positive definite. Eq. (a13) holds only when $\begin{bmatrix} \mathbf{E}_H & \\ & \bar{\Delta}_A \end{bmatrix} \begin{bmatrix} \boldsymbol{z}_1 \\ \boldsymbol{z}_2 \end{bmatrix} = \mathbf{0}$. This implies $\mathbf{E}_H \boldsymbol{z}_1 = 0$ and $\bar{\Delta}_A \boldsymbol{z}_2 = 0$. According to Eq. (9), this implies $\begin{bmatrix} \bar{\Delta}_A \\ \bar{\Lambda}_A \end{bmatrix} \boldsymbol{z}_2 = 0$. Note $\mathbf{E}_H \boldsymbol{z}_1 = 0$ only if $\boldsymbol{z}_1 = 0$. As $\begin{bmatrix} \bar{\Delta}_A \\ \bar{\Lambda}_A \end{bmatrix}$ is a full column matrix, $\begin{bmatrix} \bar{\Delta}_A \\ \bar{\Lambda}_A \end{bmatrix} \boldsymbol{z}_2 = 0$ only if $\boldsymbol{z}_2 = 0$. Thereby, Eq. (a13) holds only if $\boldsymbol{z}_1 = 0$ and $\boldsymbol{z}_2 = 0$. As both Λ_H^T and $\bar{\Lambda}_A^T$ are full column matrices, $\boldsymbol{z}_3 = 0$, and $\boldsymbol{z}_4 = 0$. The solution to Eq. (a5) is $[\boldsymbol{z}_1^T \quad \boldsymbol{z}_2^T \quad \boldsymbol{z}_3^T \quad \boldsymbol{z}_4^T] = \mathbf{0}$. $\boldsymbol{J}_{\bar{\mathbf{f}}}^*$ is invertible. Proposition 9 is proved. ■

Appendix E: Publication Abstracts

Development of Dynamic Network Traffic Simulator for Mixed Traffic Flow Under Connected and Autonomous Vehicles Technologies – Related Citations

Wang, J., Peeta, S., Lu, L., & Li, T. (2019). Multiclass information flow propagation control under vehicle-to-vehicle communication environments. Transportation Research Part B: Methodological, 129, 96-121.

Abstract

Most existing models for information flow propagation in a vehicle-to-vehicle (V2V) communications environment are descriptive. They lack capabilities to control information flow, which may preclude their ability to meet application needs, including the need to propagate different information types simultaneously to different target locations within corresponding time delay bounds. This study proposes a queuing-based modeling approach to control the propagation of information flow of multiple classes. Two control parameters associated with a vehicle, the number of communication servers and the mean communication service rate, are leveraged to control the propagation performance of different information classes. A two-layer model is developed to characterize the information flow propagation wave (IFPW) under the designed queuing strategy. The upper layer is formulated as integro-differential equations to characterize the spatiotemporal information dissemination due to V2V communication. The lower layer characterizes the traffic flow dynamics using the Lighthill–Whitham–Richards model. The analytical solution of the asymptotic density of informed vehicles and the necessary condition for existence of the IFPW are derived for homogeneous traffic conditions. Numerical experiments provide insights on the impact of the mean communication service rate on information spread and its spatial coverage. Further, a numerical solution method is developed to solve the two-layer model, which aids in estimating the impacts of the control parameters in the queuing strategy on the IFPW speed under homogenous and heterogeneous conditions. The proposed modeling approach enables controlling the propagation of information of different information classes to meet application needs, which can assist traffic managers to design effective and efficient traffic management and control strategies under V2V communications.

Wang, J., Peeta, S., & He, X. (2019). Multiclass traffic assignment model for mixed traffic flow of human-driven vehicles and connected and autonomous vehicles. Transportation Research Part B: Methodological, 126, 139-168.

Abstract

Compared to existing human-driven vehicles (HDVs), connected and autonomous vehicles (CAVs) offer users the potential for reduced value of time, enhanced quality of travel experience, and seamless situational awareness and connectivity. Hence, CAV users can differ in their route choice behavior compared to HDV users, leading to mixed traffic flows that can significantly deviate from the single-class HDV traffic pattern. However, due to the lack of quantitative models,

there is limited knowledge on the evolution of mixed traffic flows in a traffic network. To partly bridge this gap, this study proposes a multiclass traffic assignment model, where HDV users and CAV users follow different route choice principles, characterized by the cross-nested logit (CNL) model and user equilibrium (UE) model, respectively. The CNL model captures HDV users' uncertainty associated with limited knowledge of traffic conditions while overcoming the route overlap issue of logit-based stochastic user equilibrium. The UE model characterizes the CAV's capability for acquiring accurate information on traffic conditions. In addition, the multiclass model can capture the characteristics of mixed traffic flow such as the difference in value of time between HDVs and CAVs and the asymmetry in their driving interactions, thereby enhancing behavioral realism in the modeling. The study develops a new solution algorithm labeled RSRS-MSRA, in which a route-swapping based strategy is embedded with a self-regulated step size choice technique, to solve the proposed model efficiently. Sensitivity analysis of the proposed model is performed to gain insights into the effects of perturbations on the mixed traffic equilibrium, which facilitates the estimation of equilibrium traffic flow and identification of critical elements under expected or unexpected events. The study results can assist transportation decision-makers to design effective planning and operational strategies to leverage the advantages of CAVs and manage traffic congestion under mixed traffic flows.

Wang, J., Peeta, S., Lu, L., Li, T. (2020). Multiclass information flow propagation control under vehicle-to-vehicle communication environments. 99th Annual Meeting of Transportation Research Board (TRB), Washington, D.C, USA.

Abstract

Most existing models for information flow propagation in a vehicle-to-vehicle (V2V) communications environment are descriptive. They lack capabilities to control information flow, which may preclude their ability to meet application needs, including the need to propagate different information types simultaneously to different target locations within corresponding time delay bounds. This study proposes a queuing-based modeling approach to control the propagation of information flow of multiple classes. Two control parameters associated with a vehicle, the number of communication servers and the mean communication service rate, are leveraged to control the propagation performance of different information classes. A two-layer model is developed to characterize the information flow propagation wave (IFPW) under the designed queuing strategy. The upper layer is formulated as integro-differential equations to characterize the spatiotemporal information dissemination due to V2V communication. The lower layer characterizes the traffic flow dynamics using the Lighthill-Whitham-Richards model. The analytical solution of the asymptotic density of informed vehicles and the necessary condition for existence of the IFPW are derived for homogeneous traffic conditions. Further, a numerical solution method is developed to solve the two-layer model, which aids in estimating the impacts of the control parameters in the queuing strategy on the IFPW speed under homogenous and heterogeneous conditions. The proposed modeling approach enables controlling the propagation of information of different information classes to meet application needs, which can assist traffic

managers to design effective and efficient traffic management and control strategies under V2V communications.

Wang, J., Peeta, S., He, S., (2020). Multiclass traffic assignment model for mixed traffic flow of human-driven vehicles and connected and autonomous vehicles. 99th Annual Meeting of Transportation Research Board (TRB), Washington, D.C, USA.

Abstract

Compared to existing human-driven vehicles (HDVs), connected and autonomous vehicles (CAVs) offer users the potential for reduced value of time, enhanced quality of travel experience, and seamless situational awareness and connectivity. Hence, CAV users can differ in their route choice behavior compared to HDV users, leading to mixed traffic flows that can significantly deviate from the single-class HDV traffic pattern. However, due to the lack of quantitative models, there is limited knowledge on the evolution of mixed traffic flows in a traffic network. To partly bridge this gap, this study proposes a multiclass traffic assignment model, where HDV users and CAV users follow different route choice principles, characterized by the cross-nested logit (CNL) model and user equilibrium (UE) model, respectively. The CNL model captures HDV users' uncertainty associated with limited knowledge of traffic condition. The UE model characterizes the CAV's capability for acquiring accurate information on traffic conditions. In addition, the multiclass model can capture the characteristics of mixed traffic flow such as the difference in value of time between HDVs and CAVs and the asymmetry in their driving interactions, thereby enhancing behavioral realism in the modeling. The study develops a new solution algorithm labeled RSRS-MSRA, in which a route-swapping based strategy is embedded with a self-regulated step size choice technique, to solve the proposed model efficiently. The study results can assist transportation decision-makers to design effective planning and operational strategies to leverage the advantages of CAVs and manage traffic congestion under mixed traffic flows.